Electronic Supplementary Material (ESI) for Dalton Transactions.

Tuning spin-crossover transition temperatures in non-symmetrical homoleptic meridional/facial $[Fe(didentate)_3]^{2+}$ complexes: what for and who cares about it?

Neel Deorukhkar, Céline Besnard, Laure Guénée and Claude Piguet*

Supporting Information

(90 pages)

Appendix 1: Derivation of eq. 18.[61]

The general expression of the Curie law for a mixture containing high-spin and low spin complexes is

$$\chi_M T = x_{hs} \cdot \left(C_{hs} + T \cdot \mathrm{TIP}_{hs}\right) + x_{ls} \cdot \left(C_{ls} + T \cdot \mathrm{TIP}_{ls}\right) \quad (16)$$

The introduction of the mass balance depicted in eq. (A1-1) into eq. (19) gives eq. (A1-2)

$$x_{hs} + x_{ls} = 1 \quad (A1\text{-}1)$$

$$\chi_M T = x_{ls} \cdot \left(C_{ls} - C_{hs} + T \cdot \left(\mathrm{TIP}_{ls} - \mathrm{TIP}_{hs}\right)\right) + C_{hs} + T \cdot \mathrm{TIP}_{hs} \quad (A1\text{-}2)$$

Taking into account the spin crossover equilibria $K_{sco} = x_{hs}/x_{ls} = \left(1 - x_{ls}\right)/x_{ls}$ provides $x_{ls} = 1/\left(1 + K_{sco}\right)$. Introduction into eq, (A1-2) yields

$$\chi_M T = \frac{\left(C_{ls} - C_{hs} + T \cdot \left(\mathrm{TIP}_{ls} - \mathrm{TIP}_{hs}\right)\right)}{1 + K_{sco}} + C_{hs} + T \cdot \mathrm{TIP}_{hs} \quad (A1\text{-}3)$$

Finally, the introduction of the van't Hoff relationship $\Delta H_{sco} - T\Delta S_{sco} = -RT \ln\left(K_{sco}\right)$ yields

$$\chi_M T = \frac{\left(C_{ls} - C_{hs} + T \cdot \left(\mathrm{TIP}_{ls} - \mathrm{TIP}_{hs}\right)\right)}{1 + \exp\left(\frac{1}{R} \cdot \left(\Delta S_{sco} - \frac{\Delta H_{sco}}{T}\right)\right)} + C_{hs} + T \cdot \mathrm{TIP}_{hs} \quad (18)$$

In order to locate pertinent minima, the linear least-square fits of the magnetic data collected for $[Fe(\mathbf{L6})_3]^{2+}$ and $[Fe(\mathbf{L7})_3]^{2+}$ complexes in CD_3CN were initiated by setting C_{ls} = 0 $cm^3 \cdot K \cdot mol^{-1}$ and $TIP_{ls} = 351 \cdot 10^{-6}$ $cm^3 \cdot mol^{-1}$ found for $[Fe(\mathbf{bipy})_3]^{2+}$, and C_{hs} = 3.44 $cm^3 \cdot K \cdot mol^{-1}$ and $TIP_{hs} = 358 \cdot 10^{-6}$ $cm^3 \cdot mol^{-1}$ found for $[Fe(\mathbf{L2})_3]^{2+}$ while fitting ΔH_{SCO} and ΔS_{SCO}. Then, a second non-linear fitting process with the simultaneous optimization of five parameters (C_{ls} = 0 $cm^3 \cdot K \cdot mol^{-1}$) lead to the data collected in Table 3, entries 5-6.

Appendix 2: Derivation of eq. 20.[61]

For mononuclear homoleptic tris-diimine Fe^{II} complexes existing as a mixture of meridional and facial isomers, each displaying specific thermodynamic spin state equilibria but analogous (*i*. *e*. taken as identical) Curie constants ($C_{\mathbf{hs}}$ and $C_{\mathbf{ls}}$) and temperature-independent parameters (TIP_{hs} and TIP_{ls}), Eq. (16) transforms into

$$\chi_M T = \left(x_{hs}^{fac} + x_{hs}^{mer}\right)\cdot\left(C_{hs} + T\cdot TIP_{hs}\right) + \left(x_{ls}^{fac} + x_{ls}^{mer}\right)\cdot\left(C_{ls} + T\cdot TIP_{ls}\right) \tag{19}$$

The various mole fractions are correlated by mass balance (eq. A2-1) and by thermodynamic constants (eqs A2-2 to A2-4).

$$x_{hs}^{fac} + x_{ls}^{fac} + x_{hs}^{mer} + x_{ls}^{mer} = 1 \tag{A2-1}$$

$$K_{mer\rightarrow fac}^{\mathrm{Fe},\mathbf{Lk}} = \frac{x_{ls}^{fac} + x_{hs}^{fac}}{x_{ls}^{mer} + x_{hs}^{mer}} \tag{A2-2}$$

$$K_{SCO}^{fac\text{-}\mathrm{Fe}(\mathbf{Lk})_3} = \frac{x_{hs}^{fac}}{x_{ls}^{fac}} \tag{A2-3}$$

$$K_{SCO}^{mer\text{-}\mathrm{Fe}(\mathbf{Lk})_3} = \frac{x_{hs}^{mer}}{x_{ls}^{mer}} \tag{A2-4}$$

Straightforward mathematical manipulations yield

$$x_{ls}^{mer} = \frac{1}{\left(1 + K_{mer\rightarrow fac}^{\mathrm{Fe},\mathbf{Lk}}\right)\left(1 + K_{SCO}^{mer\text{-}\mathrm{Fe}(\mathbf{Lk})_3}\right)} \tag{A2-5}$$

$$x_{hs}^{mer} = \frac{K_{SCO}^{mer\text{-}\mathrm{Fe}(\mathbf{Lk})_3}}{\left(1 + K_{mer\rightarrow fac}^{\mathrm{Fe},\mathbf{Lk}}\right)\left(1 + K_{SCO}^{mer\text{-}\mathrm{Fe}(\mathbf{Lk})_3}\right)} \tag{A2-6}$$

$$x_{ls}^{fac} = \frac{K_{mer\rightarrow fac}^{\mathrm{Fe},\mathbf{Lk}}}{\left(1 + K_{mer\rightarrow fac}^{\mathrm{Fe},\mathbf{Lk}}\right)\left(1 + K_{SCO}^{fac\text{-}\mathrm{Fe}(\mathbf{Lk})_3}\right)} \tag{A2-7}$$

$$x_{hs}^{fac} = \frac{K_{SCO}^{fac\text{-}\mathrm{Fe}(\mathbf{Lk})_3}\cdot K_{mer\rightarrow fac}^{\mathrm{Fe},\mathbf{Lk}}}{\left(1 + K_{mer\rightarrow fac}^{\mathrm{Fe},\mathbf{Lk}}\right)\left(1 + K_{SCO}^{fac\text{-}\mathrm{Fe}(\mathbf{Lk})_3}\right)} \tag{A2-8}$$

Finally, the introduction of eqs (A2-5)-(A2-8) into eq. (22) yields

$$\chi_{\mathrm{M}}^{\mathrm{para}}T = \left(\frac{K_{\mathrm{SCO}}^{fac\text{-}\mathrm{Fe}(\mathbf{L}\boldsymbol{k})_3} \cdot K_{mer\rightarrow fac}^{\mathrm{Fe},\mathbf{L}\boldsymbol{k}}}{\left(1+K_{mer\rightarrow fac}^{\mathrm{Fe},\mathbf{L}\boldsymbol{k}}\right)\left(1+K_{\mathrm{SCO}}^{fac\text{-}\mathrm{Fe}(\mathbf{L}\boldsymbol{k})_3}\right)} + \frac{K_{\mathrm{SCO}}^{mer\text{-}\mathrm{Fe}(\mathbf{L}\boldsymbol{k})_3}}{\left(1+K_{mer\rightarrow fac}^{\mathrm{Fe},\mathbf{L}\boldsymbol{k}}\right)\left(1+K_{\mathrm{SCO}}^{mer\text{-}\mathrm{Fe}(\mathbf{L}\boldsymbol{k})_3}\right)} \right) \cdot \left(C_{\mathrm{hs}} + T \cdot \mathrm{TIP}_{\mathrm{hs}}\right) + \left(\frac{K_{mer\rightarrow fac}^{\mathrm{Fe},\mathbf{L}\boldsymbol{k}}}{\left(1+K_{mer\rightarrow fac}^{\mathrm{Fe},\mathbf{L}\boldsymbol{k}}\right)\left(1+K_{\mathrm{SCO}}^{fac\text{-}\mathrm{Fe}(\mathbf{L}\boldsymbol{k})_3}\right)} + \frac{1}{\left(1+K_{mer\rightarrow fac}^{\mathrm{Fe},\mathbf{L}\boldsymbol{k}}\right)\left(1+K_{\mathrm{SCO}}^{mer\text{-}\mathrm{Fe}(\mathbf{L}\boldsymbol{k})_3}\right)} \right) \cdot \left(C_{\mathrm{ls}} + T \cdot \mathrm{TIP}_{\mathrm{ls}}\right) \quad (20)$$

Eq. (20) was used for the fits of $\chi_{\mathrm{M}}^{\mathrm{para}}T$ products collected for $[\mathrm{Fe}(\mathbf{L6})_3]^{2+}$ in acetonitrile (Figure 7) with the help of the van't Hoff laws collected in eqs (A2-9)-(A2-11).

$$K_{mer\rightarrow fac}^{\mathrm{Fe},\mathbf{L}\boldsymbol{k}} = \exp\left(\frac{1}{R}\left(\Delta S_{mer\rightarrow fac}^{\mathrm{Fe},\mathbf{L}\boldsymbol{k}} - \frac{\Delta H_{mer\rightarrow fac}^{\mathrm{Fe},\mathbf{L}\boldsymbol{k}}}{T} \right) \right) \quad (A2\text{-}9)$$

$$K_{\mathrm{SCO}}^{fac\text{-}\mathrm{Fe}(\mathbf{L}\boldsymbol{k})_3} = \exp\left(\frac{1}{R}\left(\Delta S_{\mathrm{SCO}}^{fac\text{-}\mathrm{Fe}(\mathbf{L}\boldsymbol{k})_3} - \frac{\Delta H_{\mathrm{SCO}}^{fac\text{-}\mathrm{Fe}(\mathbf{L}\boldsymbol{k})_3}}{T} \right) \right) \quad (A2\text{-}10)$$

$$K_{\mathrm{SCO}}^{mer\text{-}\mathrm{Fe}(\mathbf{L}\boldsymbol{k})_3} = \exp\left(\frac{1}{R}\left(\Delta S_{\mathrm{SCO}}^{mer\text{-}\mathrm{Fe}(\mathbf{L}\boldsymbol{k})_3} - \frac{\Delta H_{\mathrm{SCO}}^{mer\text{-}\mathrm{Fe}(\mathbf{L}\boldsymbol{k})_3}}{T} \right) \right) \quad (A2\text{-}11)$$

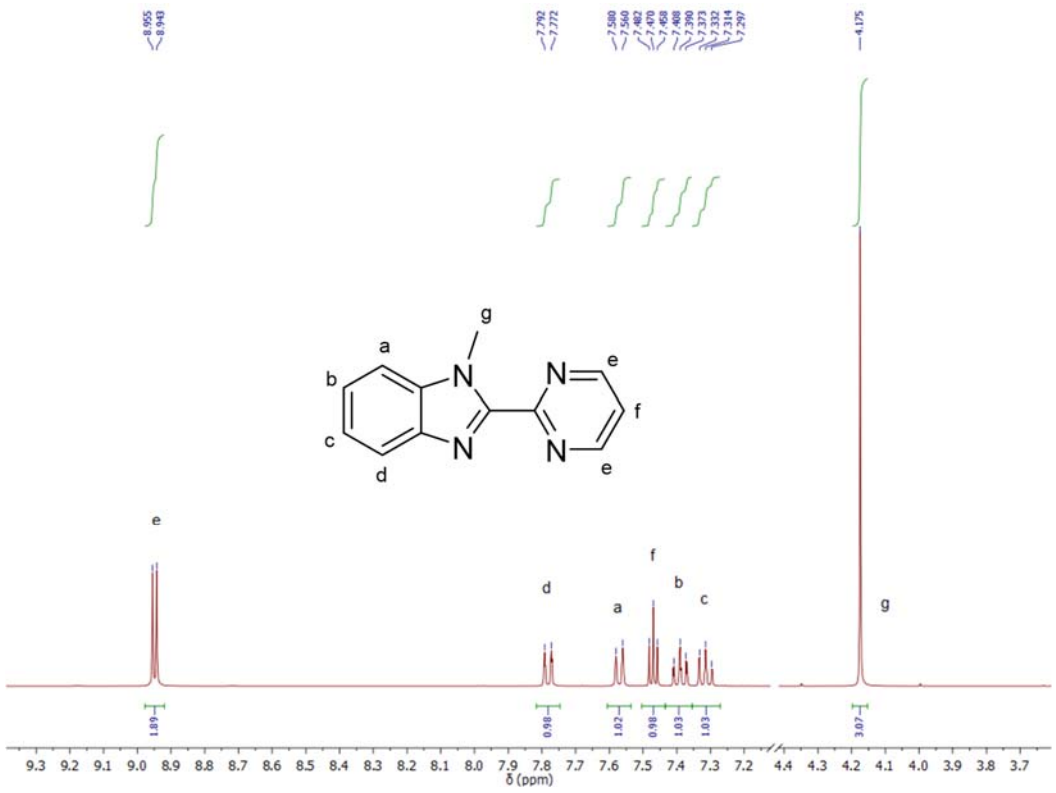

Figure S1 ^{1}H-NMR of the ligand 1-methyl-2-(pyrimidin-2-yl)-1H-benzo[d]imidazole (**L6**, CD_3CN, 298 K).

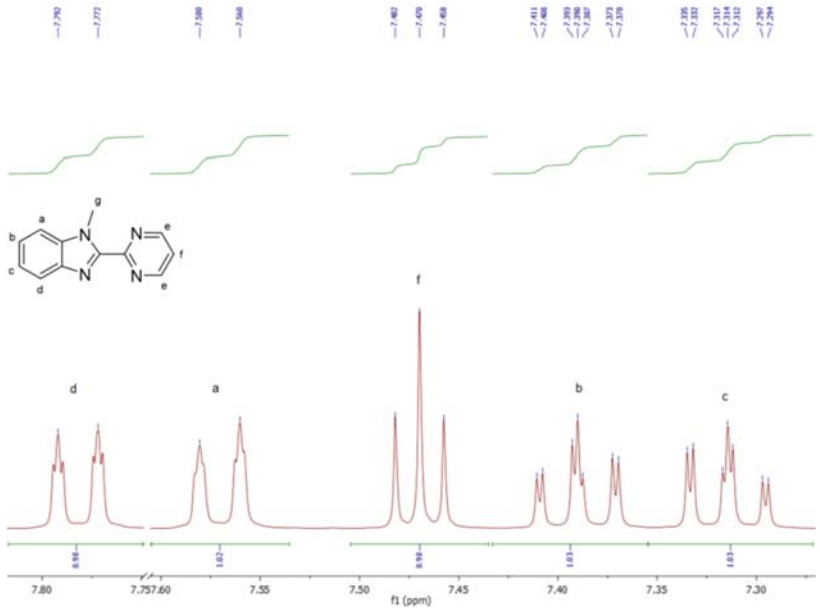

Figure S2 ^{1}H-NMR of the ligand 1-methyl-2-(pyrimidin-2-yl)-1H-benzo[d]imidazole (**L6**, CD_3CN, 298 K) highlighting the aromatic part.

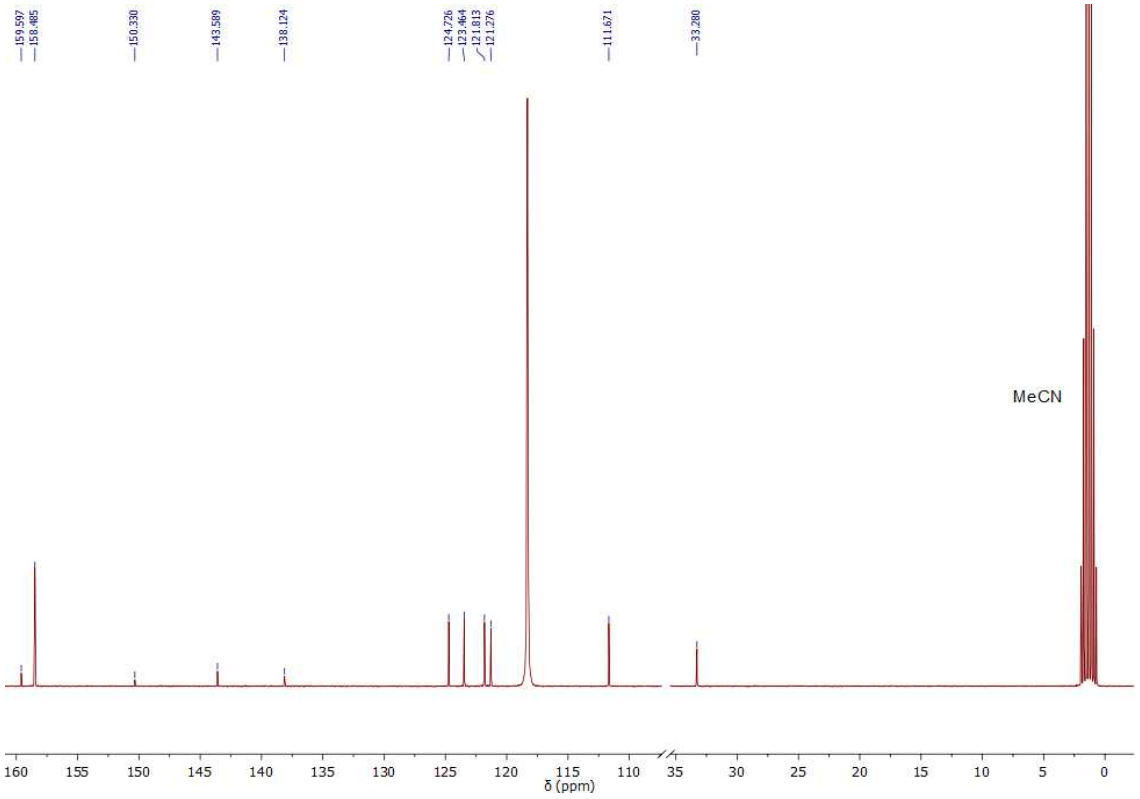

Figure S3 ^{13}C-NMR of the ligand 1-methyl-2-(pyrimidin-2-yl)-1H-benzo[d]imidazole (**L6**, CD_3CN, 298 K).

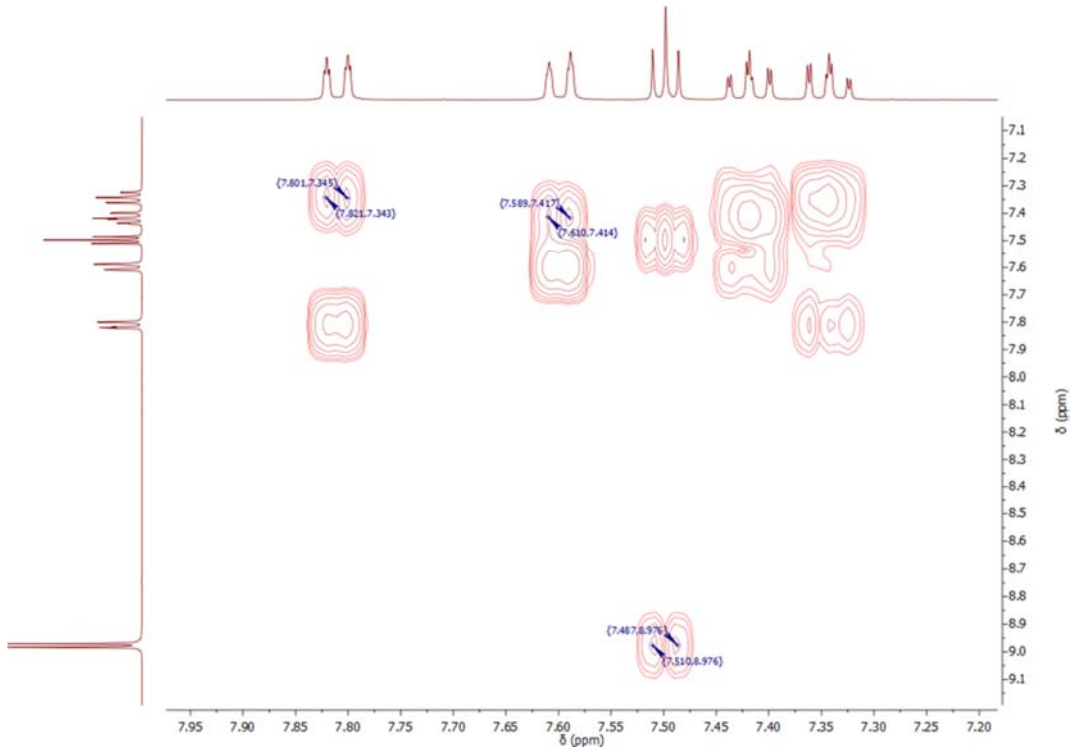

Figure S4 2D-{^{1}H,^{1}H}-COSY NMR of the ligand 1-methyl-2-(pyrimidin-2-yl)-1H-benzo[d]imidazole (**L6**, CD_3CN, 298 K).

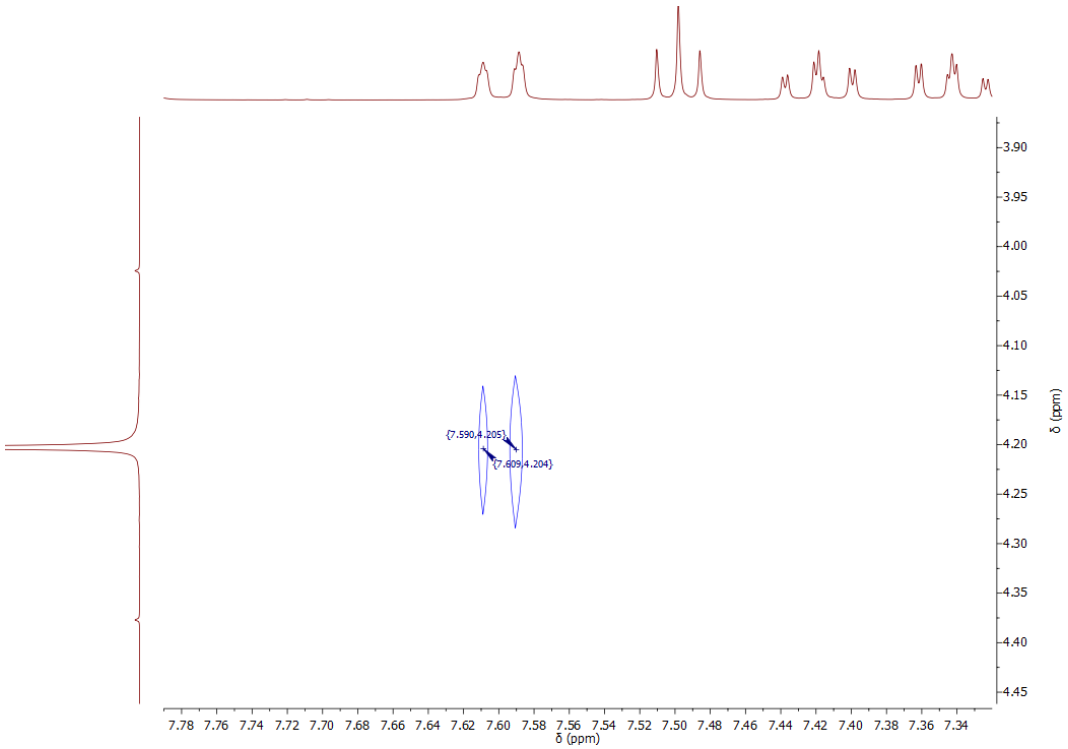

Figure S5 2D-{^{1}H,^{1}H}-NOESY NMR of the ligand 1-methyl-2-(pyrimidin-2-yl)-1H-benzo[d]imidazole ((**L6**, CD_3CN, 298 K).

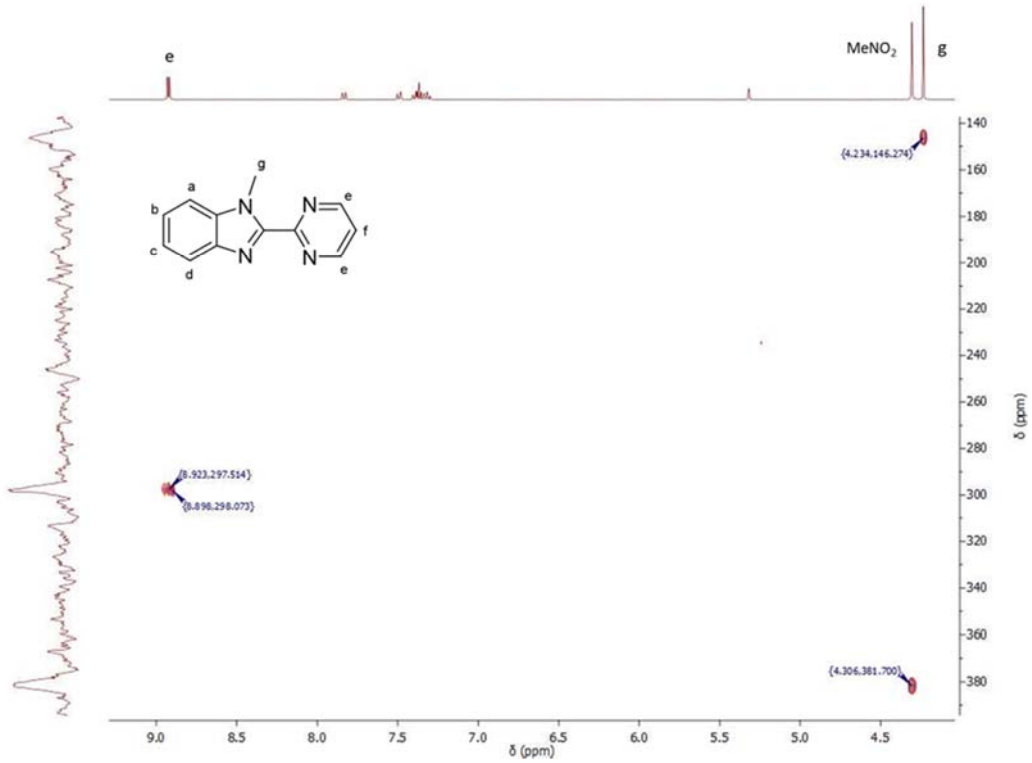

Figure S6 2D-{^{1}H-^{15}N}-HMBC NMR of the ligand 1-methyl-2-(pyrimidin-2-yl)-1H-benzo[d]imidazole (**L6**, CD_2Cl_2, 298 K).

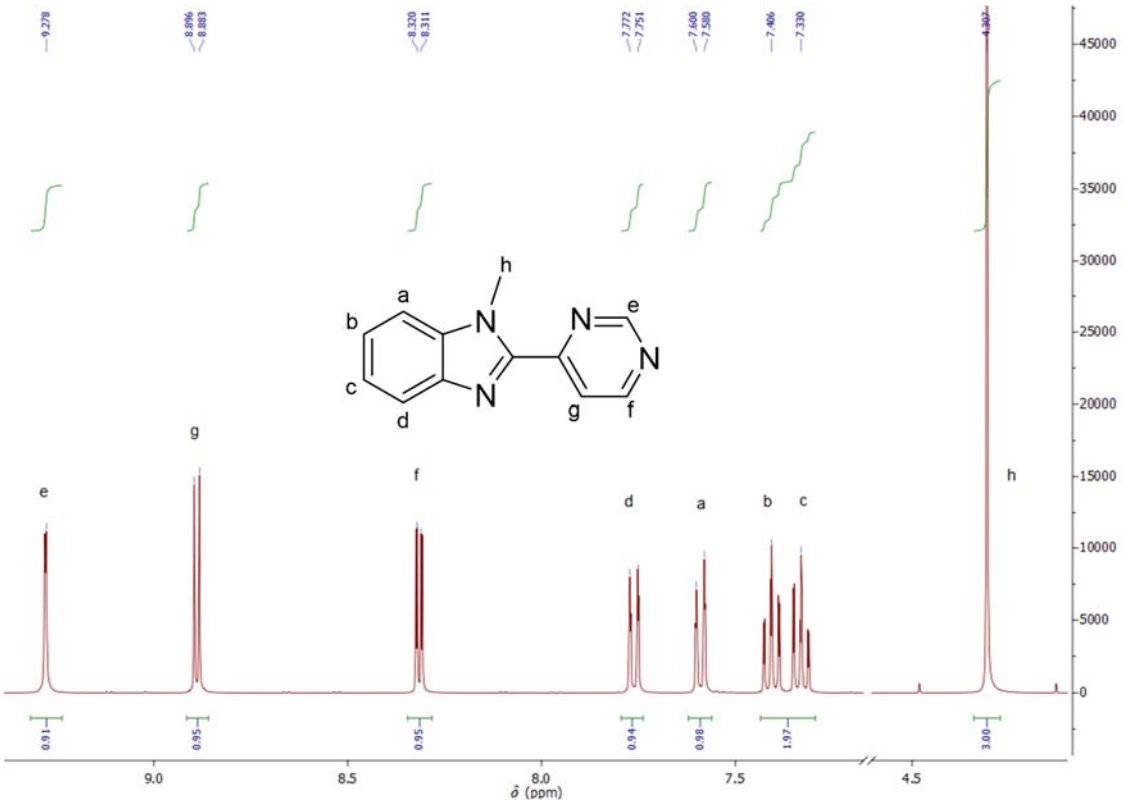

Figure S7 ^{1}H-NMR of the ligand 1-methyl-2-(pyrimidin-4-yl)-1H-benzo[d]imidazole (**L7**, CD_3CN, 298 K).

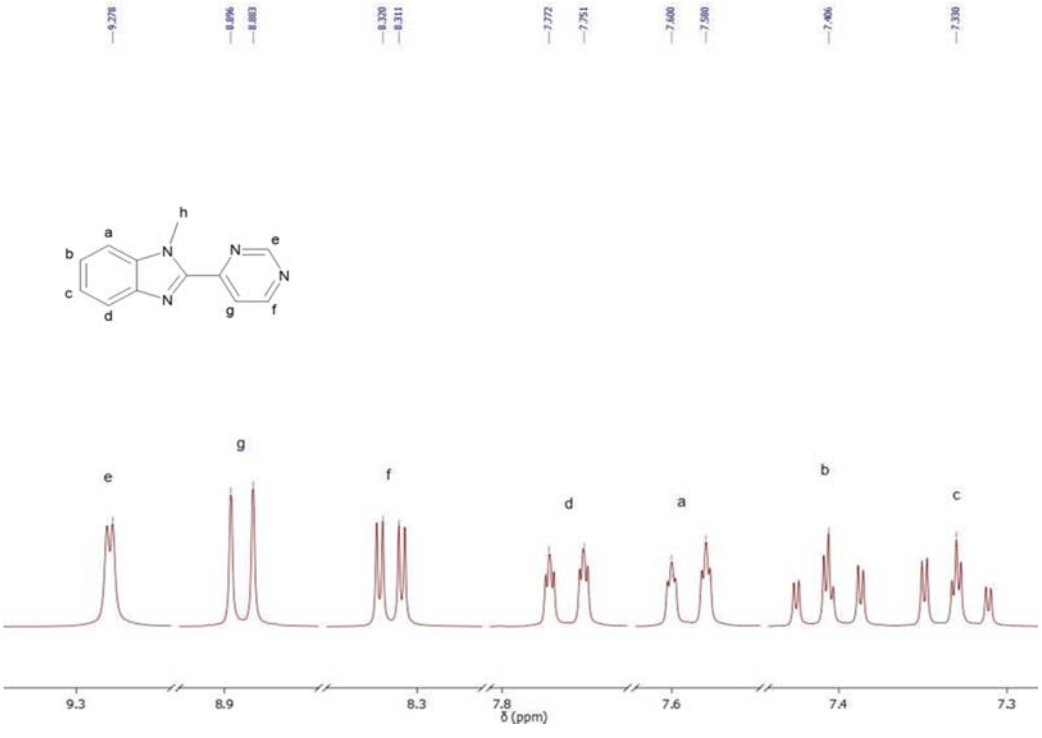

Figure S8 ^{1}H-NMR of the ligand 1-methyl-2-(pyrimidin-4-yl)-1H-benzo[d]imidazole (**L7**, CD_3CN, 298 K) highlighting the aromatic part.

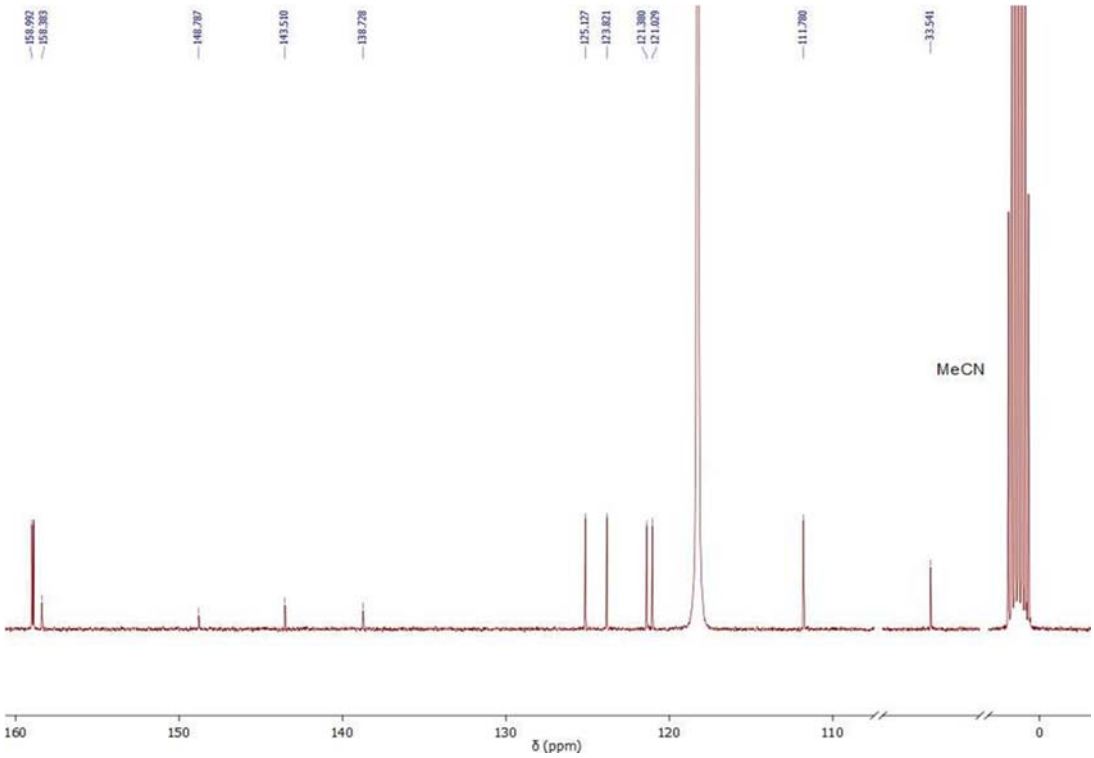

Figure S9 ^{13}C-NMR of the ligand 1-methyl-2-(pyrimidin-4-yl)-1H-benzo[d]imidazole (**L7**, CD_3CN, 298 K).

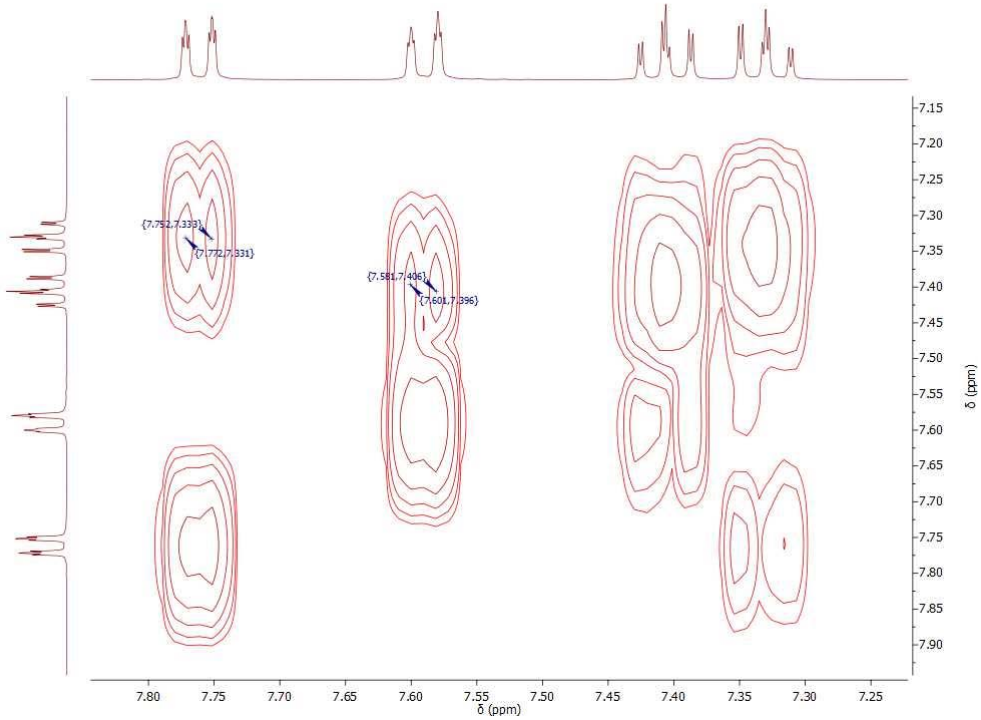

Figure S10 2D-{^{1}H,^{1}H}-COSY NMR of the ligand 1-methyl-2-(pyrimidin-2-yl)-1H-benzo[d]imidazole (**L7**, CD_3CN, 298 K).

.

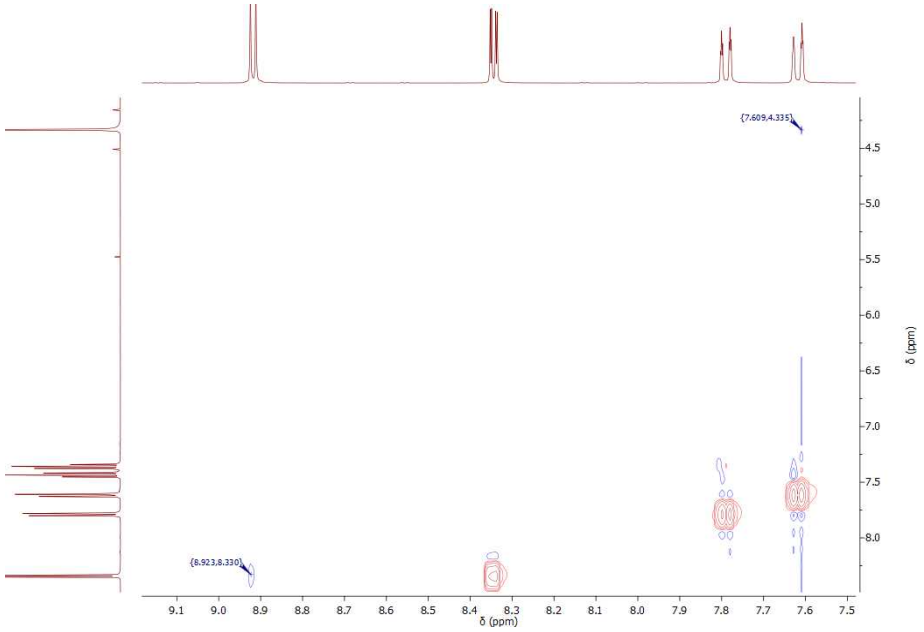

Figure S11 2D-{^{1}H,^{1}H}-NOESY NMR of the ligand 1-methyl-2-(pyrimidin-4-yl)-1H-benzo[d]imidazole ((**L7**, CD_3CN, 298 K).

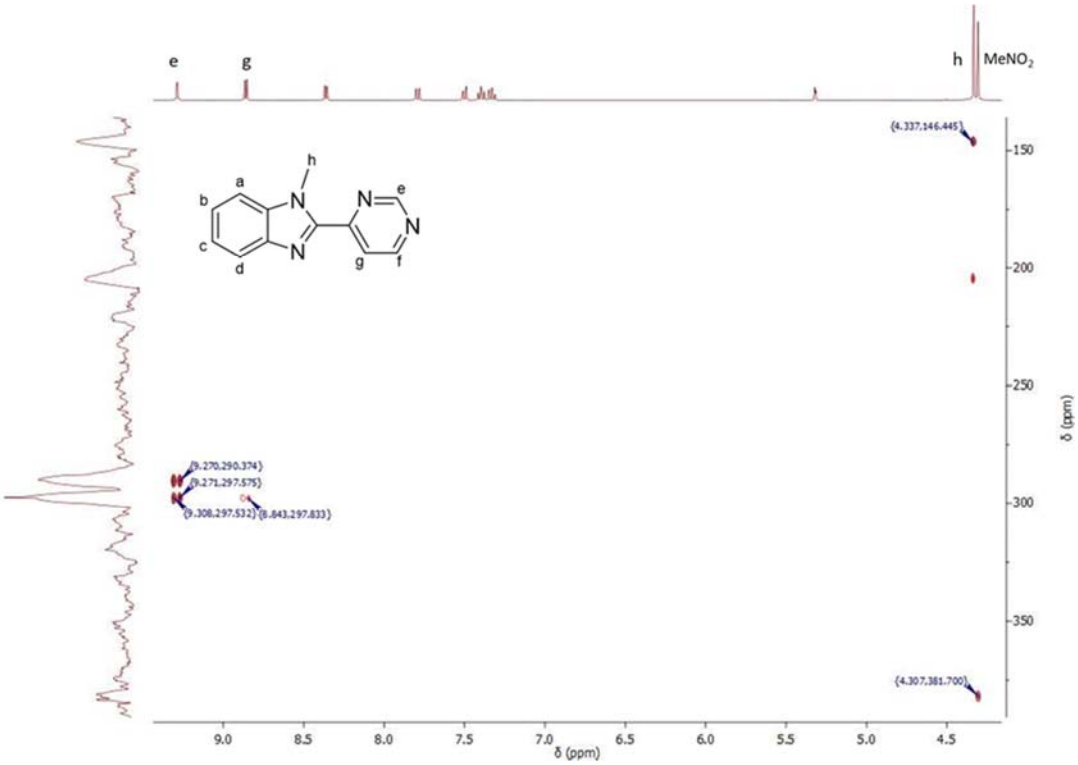

Figure S12 2D-{^{1}H-^{15}N}-HMBC NMR of the ligand 1-methyl-2-(pyrimidin-4-yl)-1H-benzo[d]imidazole (**L7**, CD_2Cl_2, 298 K).

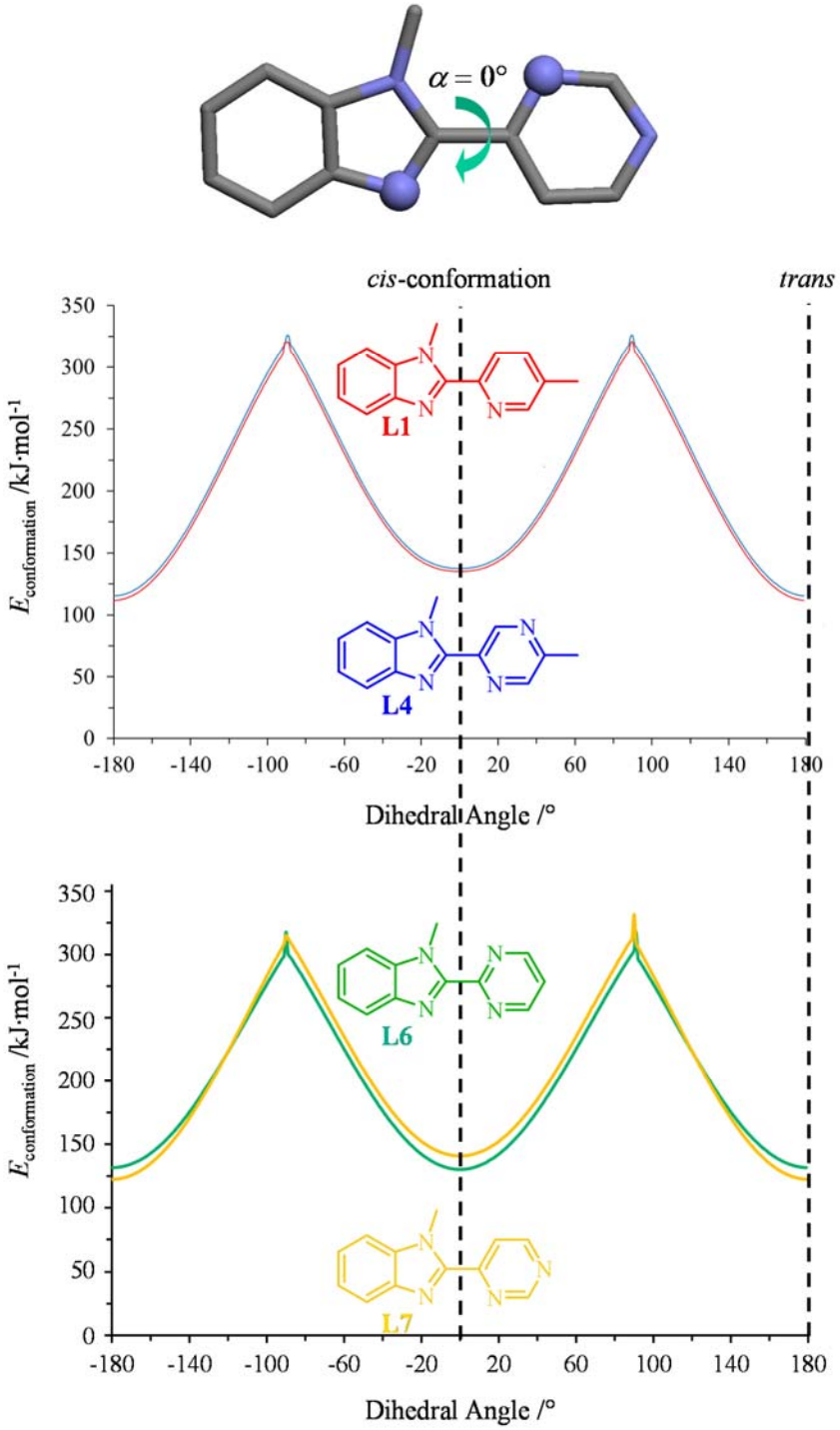

Figure S13 Gas-phase computed energies of ligands **L1** (red), **L4** (blue), **L6** (green) and **L7** (yellow) as a function of the interplanar angle measured between the N-heterocyclic azine ring plane and the benzimidazole ring plane.

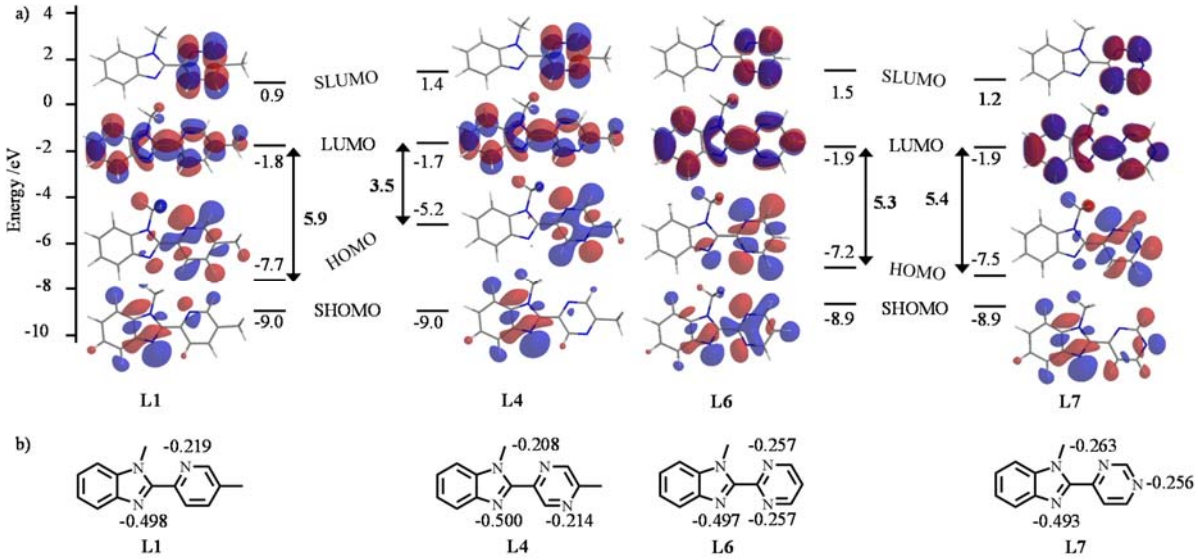

Figure S14 a) Extended Hückel computed frontier orbitals (optimized gas-phase models) and b) computed charges (in electrostatic units) borne by the nitrogen donor atoms for the didentate ligands **L1**, **L4**, **L6** and **L7** (Perkin Elmer Chem3D Pro, version 16.0.1.4, Perkin Elmer Informatics, Inc. 1998-2017. https://www.perkinelmer.com/product/chemoffice-professional-chemofficepro).

Table S1 Crystal data and structure refinement for **L6**.

Compound	**L6**
Empirical formula	$C_{12}H_{10}N_4$
Formula weight	210.24
Temperature	180.01(10) K
Wavelength	1.54184 Å
Crystal system	Orthorhombic
Space group	Pbca
Unit cell dimensions	a = 16.9371(3) Å b = 9.58870(10) Å c = 25.1582(4) Å α= 90° β= 90° γ = 90°
Volume	4085.81(11) Å^3
Z	16
Density (calculated)	1.367 Mg/m^3
Absorption coefficient	0.696 mm^{-1}
F(000)	1760
Crystal size	0.192 x 0.085 x 0.018 mm^3
Theta range for data collection	3.514 to 70.689°
Index ranges	-16≤h≤20, -11≤k≤8, -30≤l≤25
Reflections collected	15128
Independent reflections	3894 [R(int) = 0.0259]
Completeness to theta = 67.684°	100.00%
Absorption correction	Gaussian
Max. and min. transmission	1.000 and 0.838
Refinement method	Full-matrix least-squares on F^2
Data / restraints / parameters	3894 / 0 / 291
Goodness-of-fit on F^2	1.063
Final R indices [I>2sigma(I)]	R1 = 0.0402, wR2 = 0.0964
R indices (all data)	R1 = 0.0518, wR2 = 0.1061
Extinction coefficient	n/a
Largest diff. peak and hole	0.136 and -0.236 e.Å^{-3}

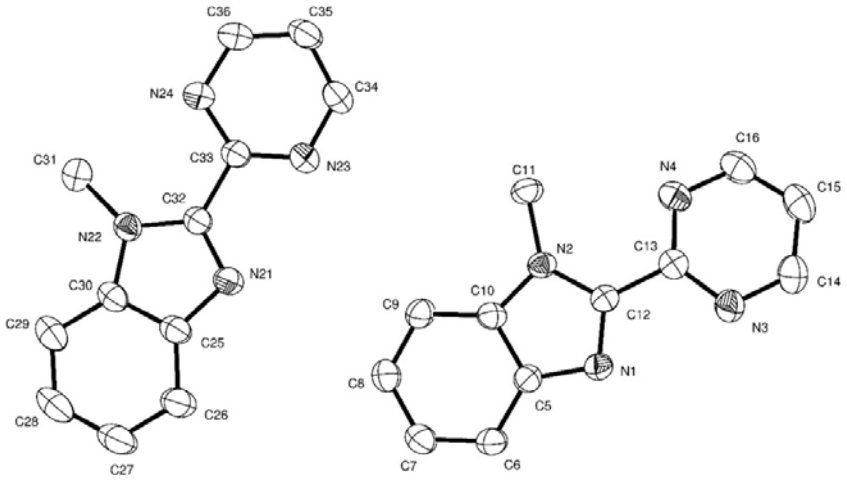

Figure S15 ORTEP view of the two different ligand molecules in the crystal structure of **L6** (ellipsoids are drawn at 40% probability) with numbering scheme. Hydrogen atoms are omitted for clarity.

Table S2 Selected bond distances (Å) and bond angles (°) for ligand **L6**.

Bond Distances (Å)			
C11 - N2	1.4637(17)	C36 - N24	1.343(2)
N1 - C12	1.3180(18)	C36 - C35	1.340(2)
N1 - C5	1.3758(18)	N21 - C32	1.3180(19)
C12 - N2	1.3736(17)	N21 - C25	1.3815(19)
C12 - C13	1.4781(19)	C32 - N22	1.3761(18)
C5 - C6	1.395(2)	C32 - C33	1.4804(19)
C5 - C10	1.4035(19)	C25 - C26	1.398(2)
N2 - C10	1.3821(18)	C25 - C30	1.393(2)
C13 - N4	1.3313(19)	N22 - C30	1.3798(19)
C13 - N3	1.3401(19)	N22 - C31	1.460(2)
C6 - C7	1.372(2)	C33 - N24	1.319(2)
C10 - C9	1.392(2)	C33 - N23	1.320(2)
N4 - C16	1.335(2)	C26 - C27	1.376(3)
N3 - C14	1.335(2)	C30 - C29	1.395(2)
C7 - C8	1.399(2)	N23 - C34	1.334(2)
C9 - C8	1.376(2)	C27 - C28	1.392(3)
C16 - C15	1.366(3)	C29 - C28	1.380(3)
C14 - C15	1.385(3)	C34 - C35	1.360(3)

Bond Angles (°)			
C12-N1-C5	105.11(11)	C35-C36-N24	123.36(17)
N1-C12-N2	113.16(12)	C32-N21-C25	104.70(12)
N1-C12-C13	122.01(12)	N21-C32-N22	113.28(12)
N2-C12-C13	124.83(12)	N21-C32-C33	122.46(13)
N1-C5-C6	129.64(13)	N22-C32-C33	124.25(12)
N1-C5-C10	110.08(12)	N21-C25-C26	129.43(15)
C6-C5-C10	120.27(13)	N21-C25-C30	110.25(13)
C12-N2-C11	129.84(12)	C30-C25-C26	120.32(14)
C12-N2-C10	106.08(11)	C32-N22-C30	105.83(12)
C10-N2-C11	124.06(11)	C32-N22-C31	130.48(12)
N4-C13-C12	118.02(12)	C30-N22-C31	123.62(12)
N4-C13-N3	126.43(13)	N24-C33-C32	117.80(13)
N3-C13-C12	115.55(13)	N24-C33-N23	125.92(14)
C7-C6-C5	118.03(14)	N23-C33-C32	116.28(13)
N2-C10-C5	105.55(12)	C27-C26-C25	117.48(18)
N2-C10-C9	132.68(13)	C25-C30-C29	122.23(15)
C9-C10-C5	121.76(13)	N22-C30-C25	105.94(12)
C13-N4-C16	116.00(14)	N22-C30-C29	131.83(15)
C14-N3-C13	115.75(14)	C33-N24-C36	115.93(15)
C6-C7-C8	121.00(15)	C33-N23-C34	115.30(15)
C8-C9-C10	116.66(14)	C26-C27-C28	121.67(17)
N4-C16-C15	122.76(16)	C28-C29-C30	116.44(17)
N3-C14-C15	122.34(17)	N23-C34-C35	123.91(16)
C9-C8-C7	122.25(14)	C29-C28-C27	121.85(16)
C16-C15-C14	116.73(15)	C36-C35-C34	115.58(15)

Table S3 Selected least-squares planes data for ligand **L6**.

Least-squares planes description	Max. deviation (Å)	Atom	Dihedral Angle (°)
Benzimidazole 1 for N1 C5 C6 C7 C8 C9 C10 N2 C12	0.010	C12	5.93(5)
Pyrimidine 1 N3 C14 C15 C16 N4 C13	0.005	N3	
Benzimidazole 2 N21 C25 C26 C27 C28 C29 C30 N22 C32	0.006	C26-C28	9.71(5)
Pyrimidine 2 N23 C34 C35 C36 N24 C33	0.004	C33C35C34	

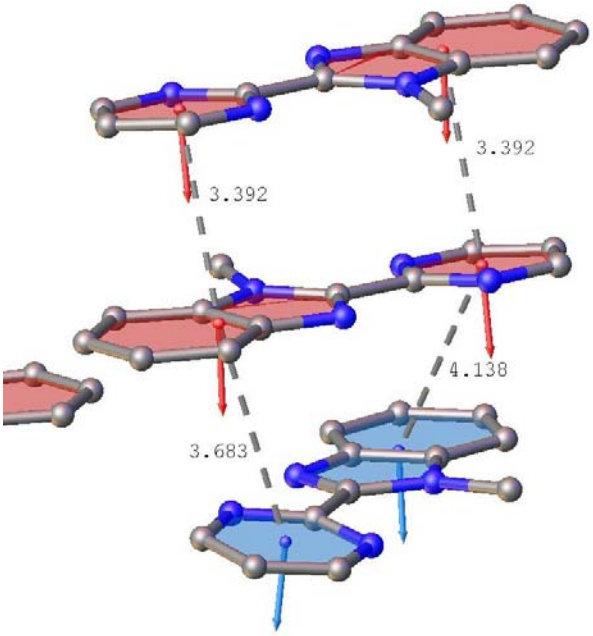

Figure S16 Intermolecular stacking between molecules of ligand **L6** (molecule 1 in red and molecule 2 in blue). Arrows show the normals to planes and grey dotted lines the centroid-centroid distances (Å).

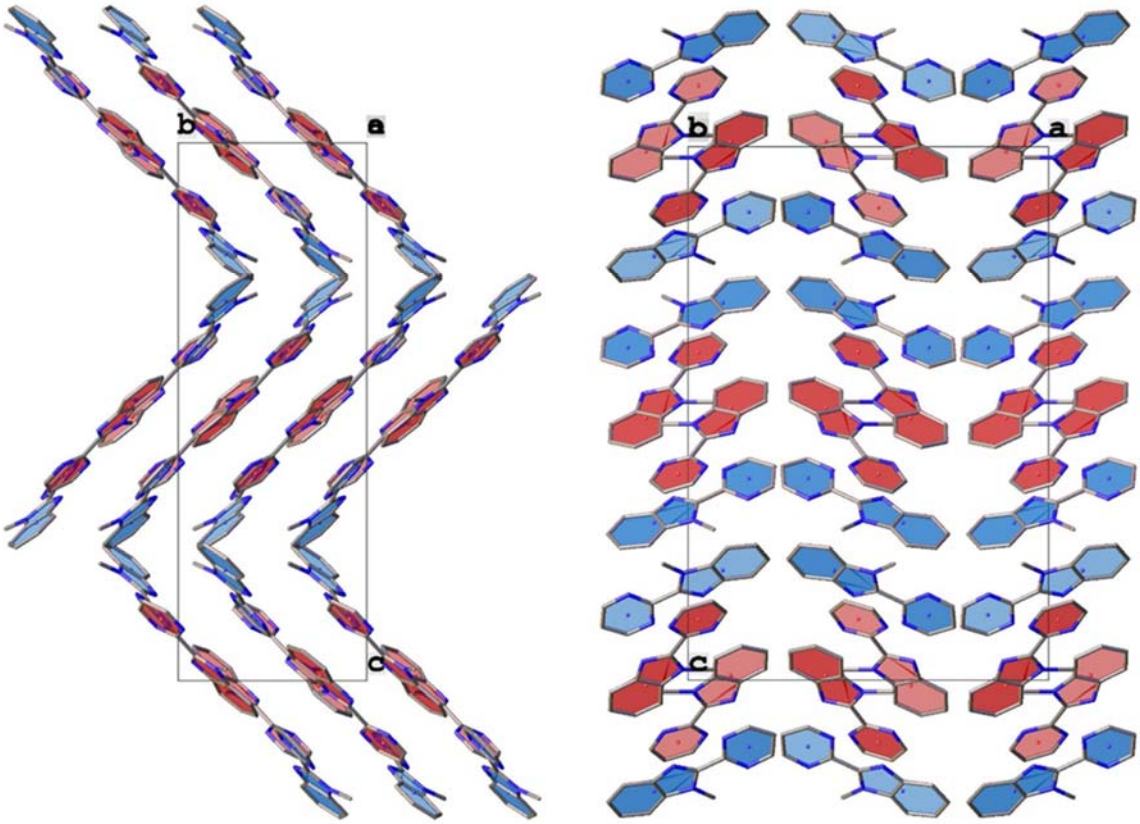

Figure S17 View of the molecular packing along *a* axis (left) and along *b* axis (right).

Table S4 Crystal data and structure refinement for ligand **L7**.

Compound	**L7**
Empirical formula	$C_{12}H_{10}N_4$
Formula weight	210.24
Temperature/K	180.15
Crystal system	monoclinic
Space group	$P2_1/c$
a/Å	7.7949(3)
b/Å	11.6274(5)
c/Å	22.4728(10)
α/°	90
β/°	99.254(4)
γ/°	90
Volume/Å^3	2010.29(14)
Z	8
ρ_{calc}g/cm^3	1.389
μ/mm^{-1}	0.707
F(000)	880.0
Crystal size/mm^3	0.407 × 0.263 × 0.224
Radiation	CuKα (λ = 1.54184)
2Θ range for data collection/°	8.586 to 141.53
Index ranges	$-9 \le h \le 9$, $-14 \le k \le 14$, $-27 \le l \le 26$
Reflections collected	8262
Independent reflections	8262 [R_{sigma} = 0.0270]
Data/restraints/parameters	8262/0/292
Goodness-of-fit on F^2	1.065
Final *R* indexes [$I>=2\sigma(I)$]	R_1 = 0.0521, wR_2 = 0.1511
Final *R* indexes [all data]	R_1 = 0.0595, wR_2 = 0.1592
Largest diff. peak/hole / e Å^{-3}	0.33/-0.26

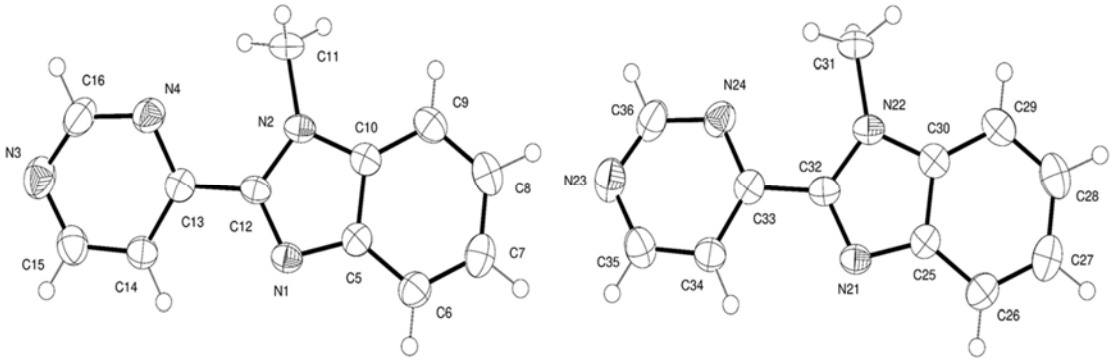

Figure S18 ORTEP view of the two different ligand molecules in its crystal structure of **L7** (ellipsoids are drawn at 50% probability) with numbering scheme.

Table S5 Selected bond distances (Å) and bond angles (°) for ligand **L7**.

Bond Length (Å)			
N1-C5	1.382(3)	N21-C25	1.318(2)
N1-C12	1.320(2)	N21-C32	1.380(3)
N2-C10	1.384(3)	N22-C30	1.461(2)
N2-C11	1.459(2)	N22-C31	1.375(2)
N2-C12	1.374(2)	N22-C32	1.338(3)
N3-C15	1.335(3)	N23-C35	1.320(3)
N3-C16	1.319(3)	N23-C36	1.345(3)
N4-C13	1.349(3)	N24-C33	1.338(3)
N4-C16	1.338(3)	N24-C36	1.398(3)
C5-C6	1.394(3)	C25-C26	1.403(3)
C5-C10	1.400(3)	C25-C30	1.378(3)
C6-C7	1.381(3)	C26-C27	1.415(4)
C7-C8	1.407(3)	C27-C28	1.377(3)
C8-C9	1.379(3)	C28-C29	1.394(3)
C9-C10	1.393(3)	C29-C30	1.468(3)
C12-C13	1.467(3)	C32-C33	1.397(3)
C13-C14	1.390(3)	C33-C34	1.375(3)
C14-C15	1.368(3)	C34-C35	1.318(2)

Bond Angles (°)			
C12-N1-C5	104.83(15)	C32-N21-C25	104.82(15)
C10-N2-C11	123.41(16)	C30-N22-C31	123.40(16)
C12-N2-C10	105.83(15)	C32-N22-C30	105.88(15)
C12-N2-C11	130.73(17)	C32-N22-C31	130.71(16)
C16-N3-C15	114.66(19)	C36-N23-C35	114.69(19)
C16-N4-C13	115.22(19)	C36-N24-C33	115.53(19)
N1-C5-C6	129.57(18)	N21-C25-C26	129.87(18)
N1-C5-C10	110.02(17)	N21-C25-C30	110.03(17)
C6-C5-C10	120.41(19)	C26-C25-C30	120.10(18)
C7-C6-C5	117.8(2)	C27-C26-C25	118.1(2)
C6-C7-C8	121.0(2)	C26-C27-C28	121.1(2)
C9-C8-C7	122.0(2)	C29-C28-C27	121.5(2)
C8-C9-C10	116.57(19)	C28-C29-C30	117.0(2)
N2-C10-C5	105.87(16)	N22-C30-C25	105.82(16)
N2-C10-C9	131.93(18)	N22-C30-C29	131.99(19)
C9-C10-C5	122.20(19)	C29-C30-C25	122.20(19)
N1-C12-N2	113.44(17)	N21-C32-N22	113.45(17)
N1-C12-C13	120.67(16)	N21-C32-C33	120.43(16)
N2-C12-C13	125.88(17)	N22-C32-C33	126.12(16)
N4-C13-C12	119.30(17)	N24-C33-C32	119.64(17)
N4-C13-C14	120.91(18)	N24-C33-C34	120.92(19)
C14-C13-C12	119.76(18)	C34-C33-C32	119.43(17)
C15-C14-C13	117.48(19)	C35-C34-C33	117.24(19)
N3-C15-C14	123.1(2)	N23-C35-C34	123.1(2)
N3-C16-N4	128.6(2)	N23-C36-N24	128.6(2)

Table S6 Selected least-squares planes data for ligand **L7**.

Least-squares planes description	Max. deviation (Å)	Atom	Dihedral Angle (°)
Benzimidazole 1 N1 C5 C6 C7 C8 C9 C10 N2 C12	0.010	N2	12.966)
Pyrimidine 1 N3 C14 C15 C16 N4 C13	0.005	C13	
Benzimidazole 2 N21 C25 C26 C27 C28 C29 C30 N22 C32	0.006	N22	7.58(6)
Pyrimidine 2 N23 C34 C35 C36 N24 C33	0.005	N24	

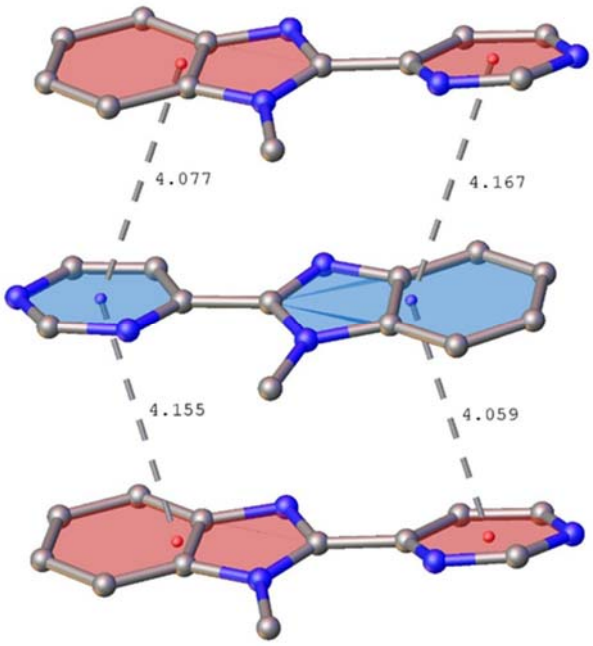

Figure S19 Intermolecular stacking in ligand **L7**. The grey dotted lines show the the centroid-centroid distances (in Å).

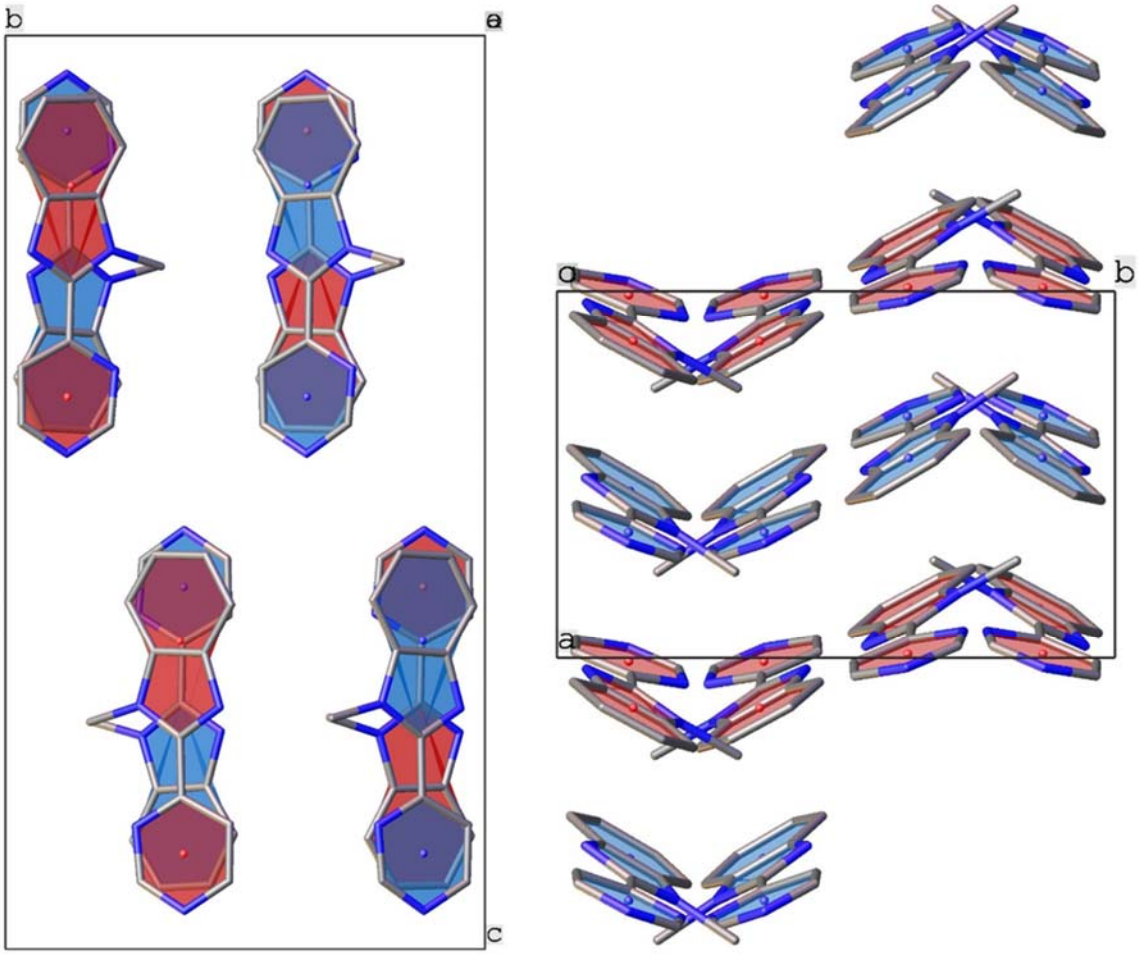

Figure S20 View of the molecular packing along *a* axis (left) and along *c* axis (right) showing the one-dimensional π- π stacking along *a* direction.

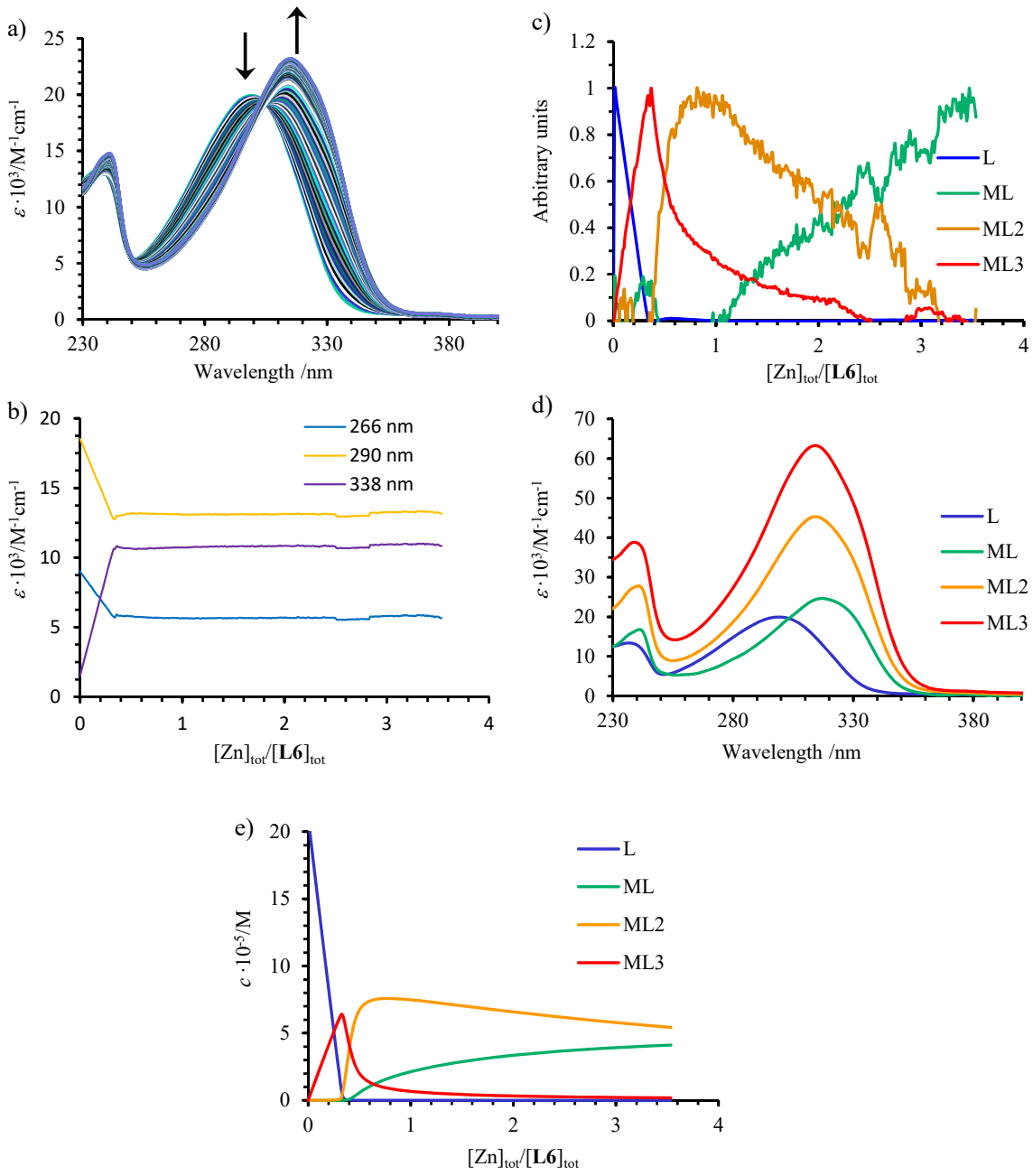

Figure S21 a) Variation of absorption spectra and b) corresponding variation of observed molar extinctions at different wavelengths recorded for the spectrophotometric titration of **L6** with $Zn(CF_3SO_3)_2$ (total ligand concentration: $2.1 \cdot 10^{-4}$ mol.dm^{-3} in acetonitrile, 298 K). c) Evolving factor analysis using four absorbing eigenvectors and d) re-constructed individual electronic absorption spectra. e) Speciation for $[\mathbf{L6}]_{tot} = 2 \cdot 10^{-4}$ M computed by using the stability constants obtained by non-linear least-square fits (Table 1).

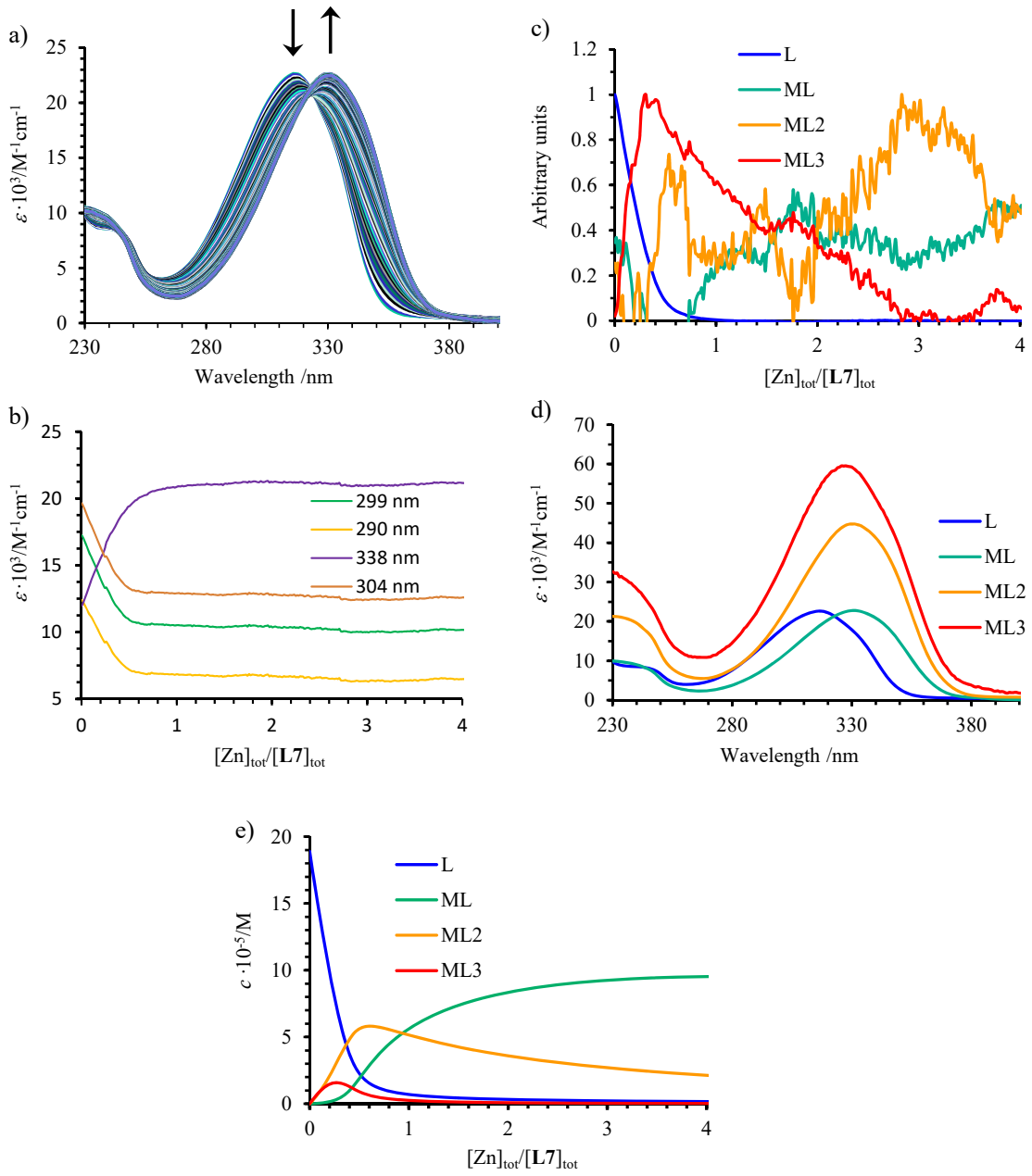

Figure S22 a) Variation of absorption spectra and b) corresponding variation of observed molar extinctions at different wavelengths recorded for the spectrophotometric titration of **L7** with $Zn(CF_3SO_3)_2$ (total ligand concentration: $2.1 \cdot 10^{-4}$ mol.dm^{-3} in acetonitrile, 298 K). c) Evolving factor analysis using four absorbing eigenvectors and d) re-constructed individual electronic absorption spectra. e) Speciation computed for $[\mathbf{L7}]_{tot} = 2 \cdot 10^{-4}$ M by using the stability constants obtained by non-linear least-square fits (Table 1).

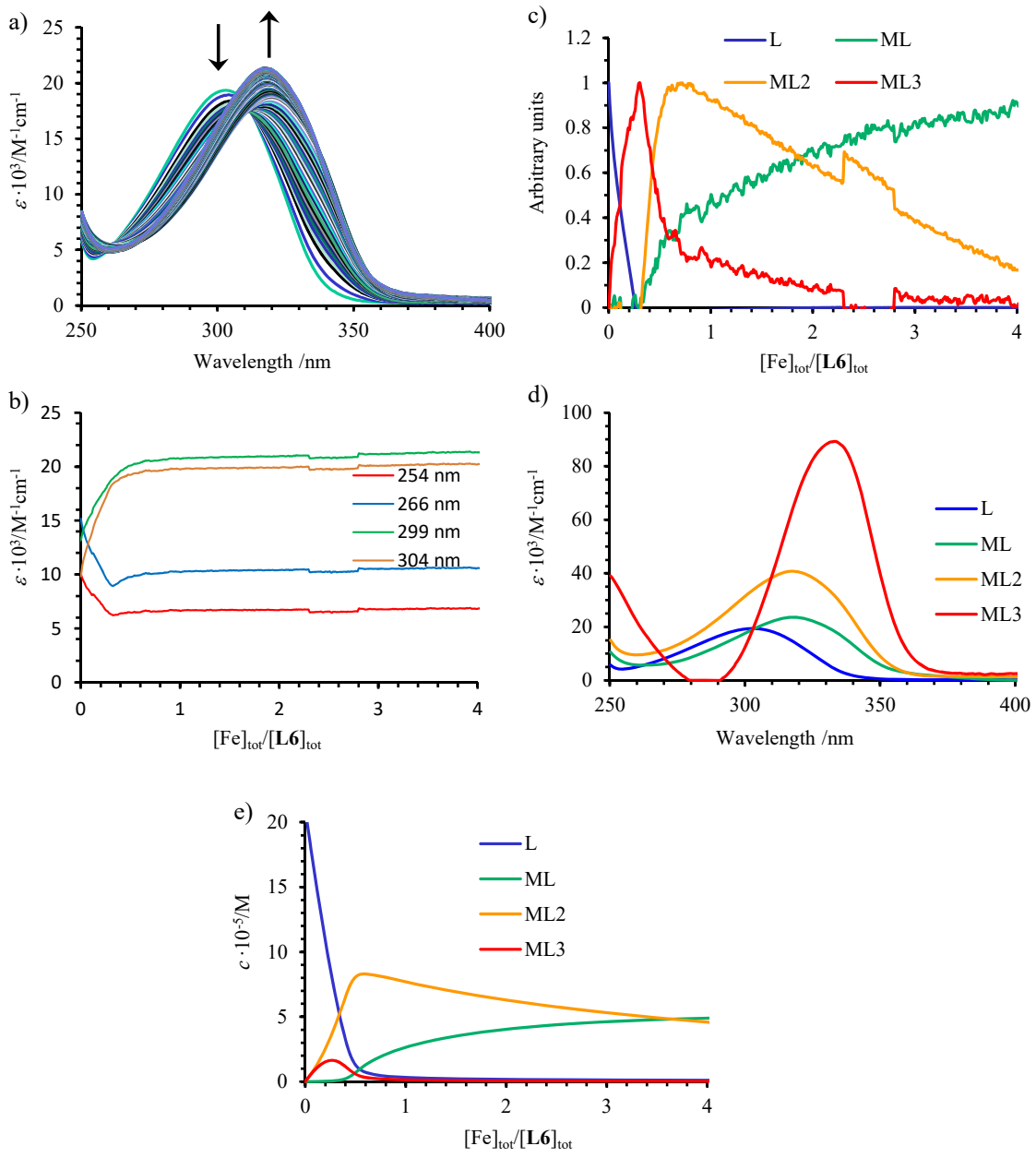

Figure S23 a) Variation of absorption spectra and b) corresponding variation of observed molar extinctions at different wavelengths recorded for the spectrophotometric titration of **L6** with $Fe(CF_3SO_3)_2$ (total ligand concentration: $2.1 \cdot 10^{-4}$ mol.dm^{-3} in acetonitrile, 298 K). c) Evolving factor analysis using four absorbing eigenvectors and d) re-constructed individual electronic absorption spectra. e) Speciation for $[\mathbf{L6}]_{tot} = 2 \cdot 10^{-4}$ M computed by using the stability constants obtained by non-linear least-square fits (Table 1).

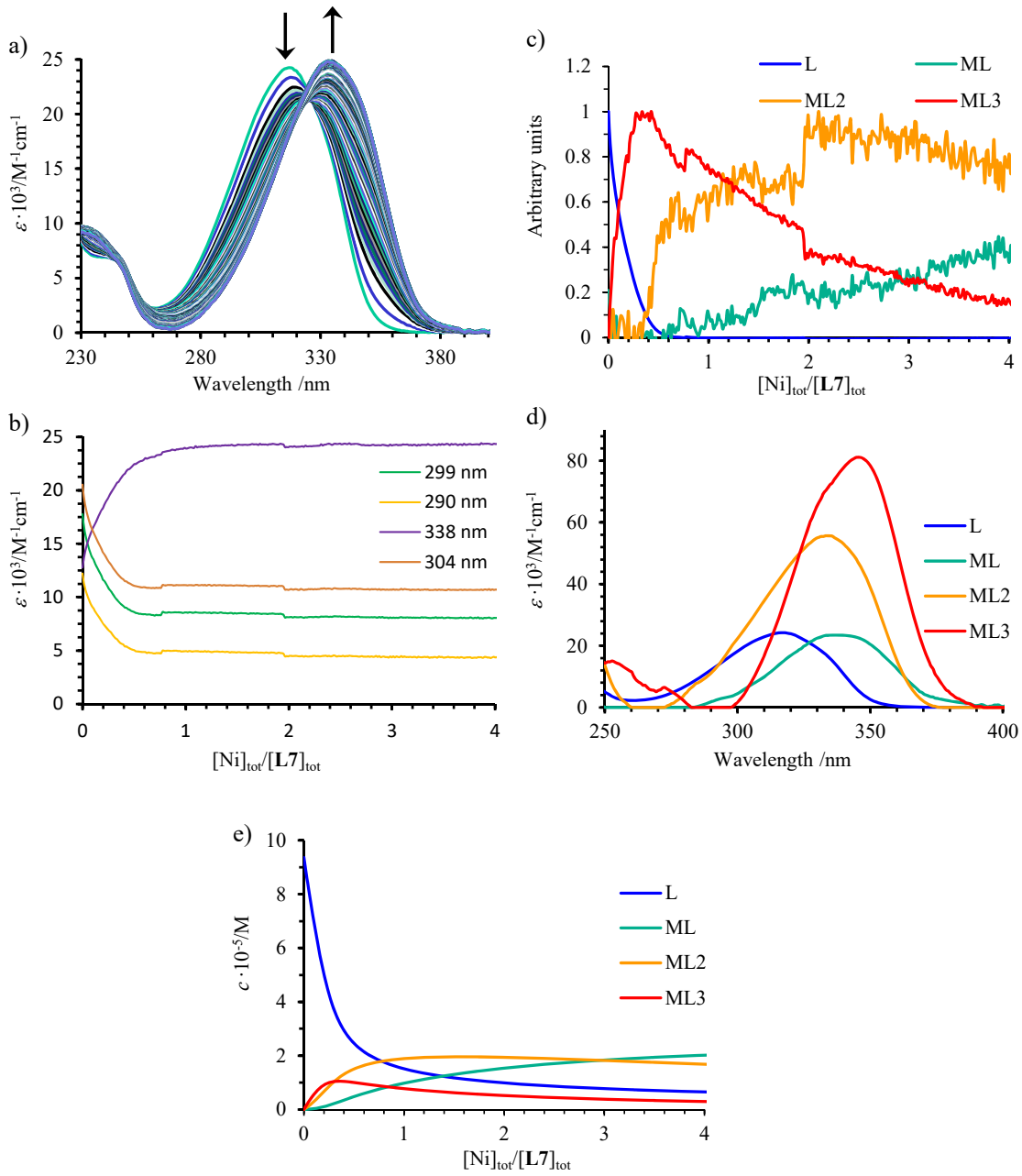

Figure S24 a) Variation of absorption spectra and b) corresponding variation of observed molar extinctions at different wavelengths recorded for the spectrophotometric titration of **L7** with $Ni(BF_4)_2$ (total ligand concentration: $9.4 \cdot 10^{-5}$ mol.dm^{-3} in acetonitrile, 298 K). c) Evolving factor analysis using four absorbing eigenvectors and d) re-constructed individual electronic absorption spectra. e) Speciation for $[\mathbf{L7}]_{tot} = 9.4 \cdot 10^{-5}$ M computed by using the stability constants obtained by non-linear least-square fits (Table 1).

Table S7 Stability constants for the successive formation of $[M(\mathbf{L}\boldsymbol{k})_n]^{2+}$ (M = Zn, Ni, Fe, **L*k*** = **L1**, **L4**, n =1, 2, 3, non-coordinating anions: ClO_4^-, $CF_3SO_3^-$ or BF_4^-) in acetonitrile (293 K), metal-ligand interaction parameter ($f^{M,\mathbf{L}\boldsymbol{k}}$) and inter-ligand interaction parameter ($u^{\mathbf{L}\boldsymbol{k},\mathbf{L}\boldsymbol{k}}$), and associated energies $\Delta G_{affinity} = -RT\ln(f^{M,\mathbf{L}\boldsymbol{k}})$ and $\Delta E_{interaction.} = -RT\ln(u^{\mathbf{L}\boldsymbol{k},\mathbf{L}\boldsymbol{k}})$.

		$\log(f^{M,L})$	$\Delta G_{affinity}$ /kJ·mol^{-1}	$\log(u^{L,L})$	$\Delta E_{interaction}$ /kJ·mol^{-1}
$[Zn(\mathbf{L4})_n]^{2+}$ [a]	$\log(\beta_{1,1}) = 6.89(3)$ [a] $\log(\beta_{1,2}) = 12.76(5)$ [a] $\log(\beta_{1,3}) = 17.64(5)$ [a]	5.46(6)	-31.1(3)	-0.18(7)	1.1(4)
$[Zn(\mathbf{L1})_n]^{2+}$ [a]	$\log(\beta_{1,1}) = 7.7(7)$ [a] $\log(\beta_{1,2}) = 15.0(4)$ [a] $\log(\beta_{1,3}) = 21.9(6)$ [a]	6.32(5)	-36.0(3)	0.40(5)	-2.3(3)
$[Fe(\mathbf{L4})_n]^{2+}$ [b]	$\log(\beta_{1,1}) = 6.045(9)$ [b] $\log(\beta_{1,2}) = 11.49(2)$ [b] $\log(\beta_{1,3}) = 16.88(2)$ [b]	4.5(1)	-25.9(8)	0.5(2)	-2.7(9)
$[Fe(\mathbf{L1})_n]^{2+}$ [b]	$\log(\beta_{1,1}) = 7.0(1)$ [b] $\log(\beta_{1,2}) = 14.7(2)$ [b] $\log(\beta_{1,3}) = 21.9(4)$ [b]	5.8(1)	-32.9(8)	1.0(2)	-5(1)

[a] Reference 74. [b] Reference 61

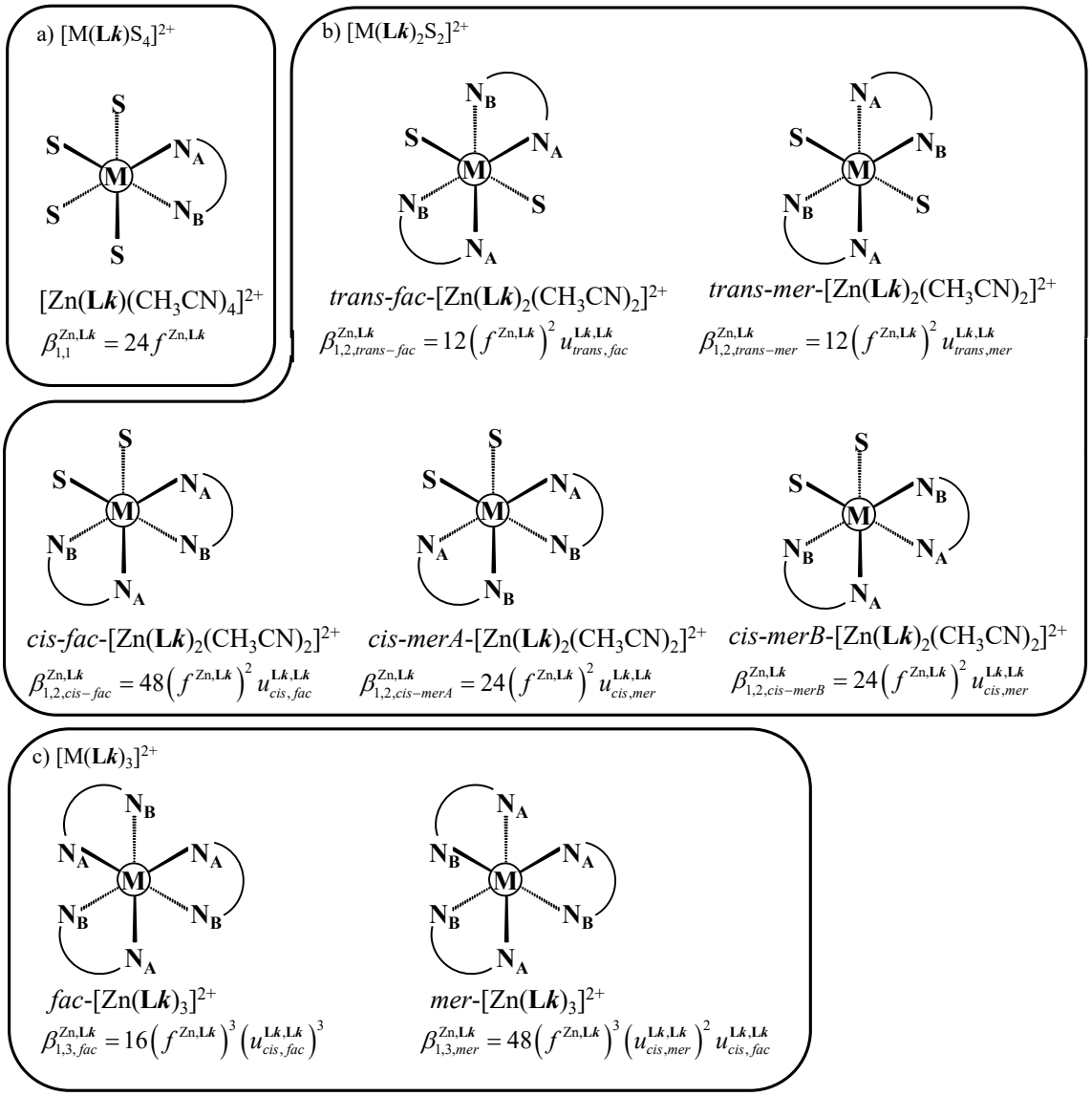

Figure S25 Microspecies and associated microscopic formation constants considered for the complexes a) $[Zn(\mathbf{L}\boldsymbol{k})(CH_3CN)_4]^{2+}$, b) $[Zn(\mathbf{L}\boldsymbol{k})_2(CH_3CN)_2]^{2+}$ and c) $[Zn(\mathbf{L}\boldsymbol{k})_3]^{2+}$. For $[Zn(\mathbf{L}\boldsymbol{k})_2(CH_3CN)_2]^{2+}$, we use the *cis*/*trans* terminology for describing the relative orientation of the two solvent molecules, whereas the additional *mer*/*fac* designation refers to the relative orientation of the two unsymmetrical ligands as defined in the saturated $[Zn(\mathbf{L}\boldsymbol{k})_3]^{2+}$ complex, i.e. a *trans* N_A-Zn-N_A arrangement is noted *merA*, a *trans* N_B-Zn-N_B is noted *merB* and a *trans* N_A-Zn-N_B is noted *fac.*

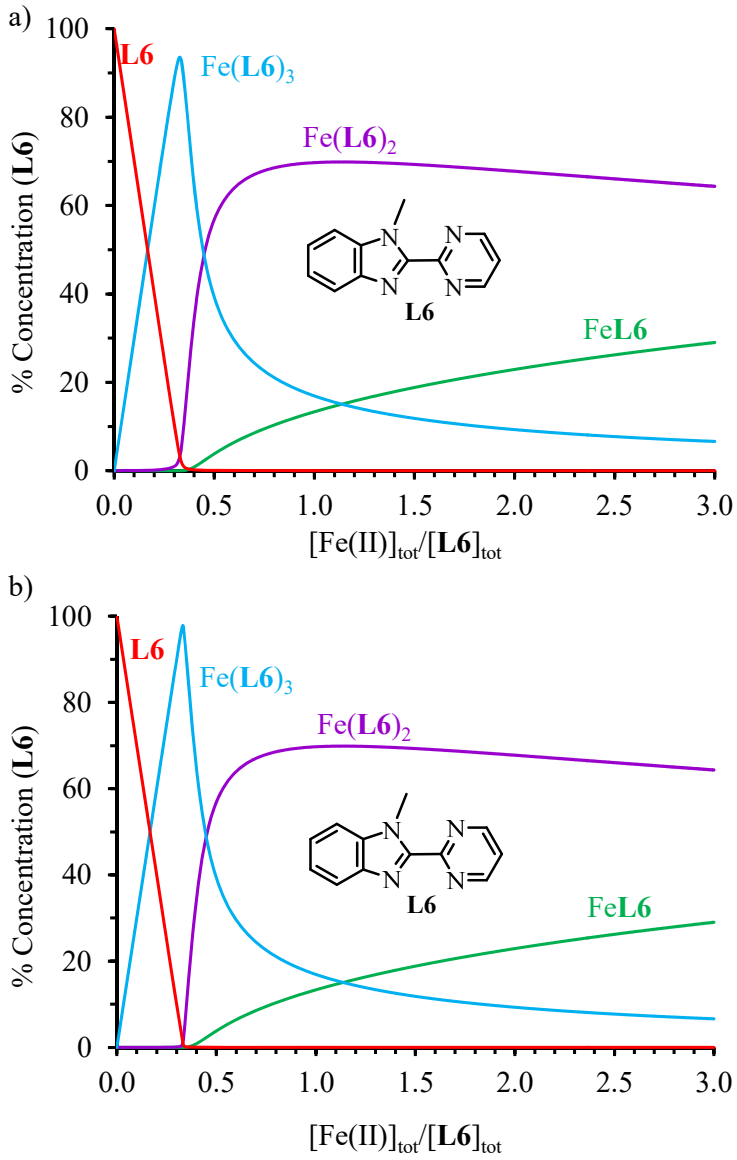

Figure S26 Concentration profiles obtained using HySS2009 simulation[73] and the formation constants collected in Table 1 for the complex species $[Fe(\mathbf{L6})_n]^{2+}$ at a) $|\mathbf{L6}|_{tot}$ = 10 mM, and b) $|\mathbf{L6}|_{tot}$ = 100 mM (acetonitrile, 293 K).

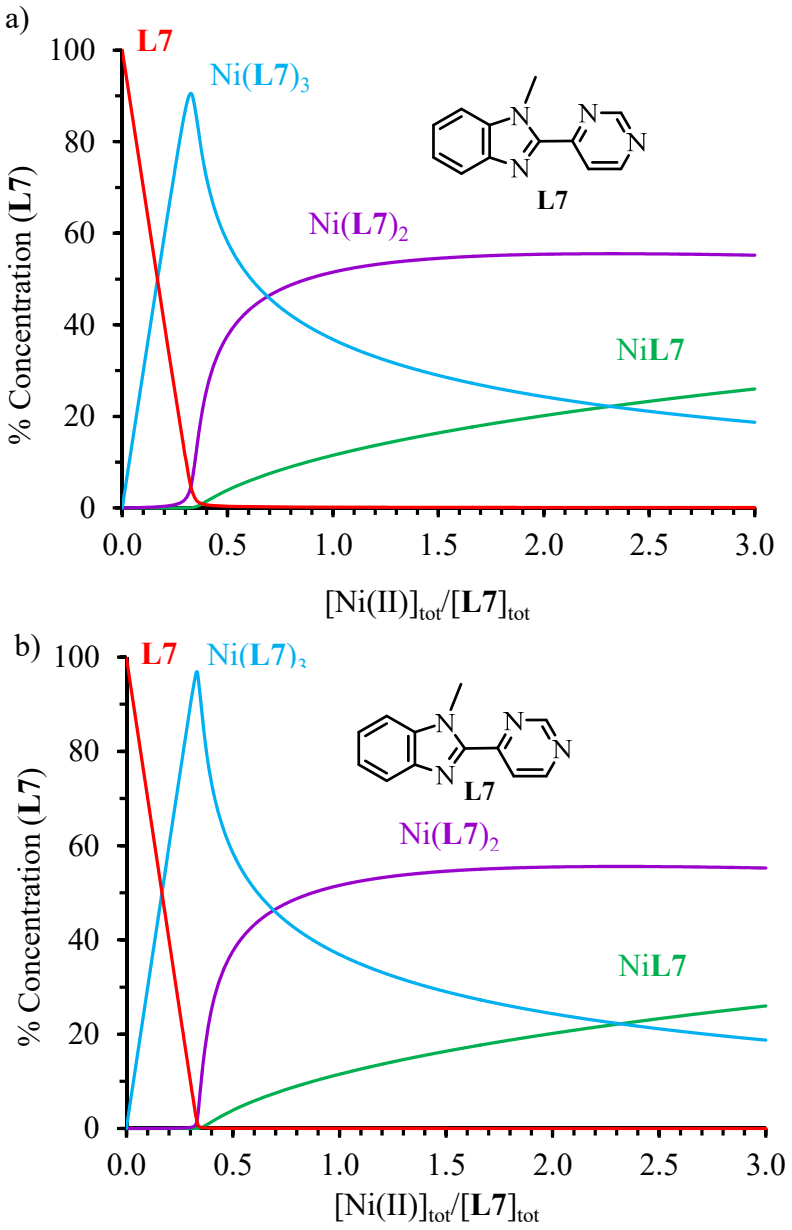

Figure S27 Concentration profiles obtained using HySS2009 simulation[73] and the formation constants collected in Table 1 for the complex species $[Ni(\mathbf{L7})_n]^{2+}$ at a) $|\mathbf{L7}|_{tot}$ = 10 mM, and b) $|\mathbf{L7}|_{tot}$ = 100 mM (acetonitrile, 293 K).

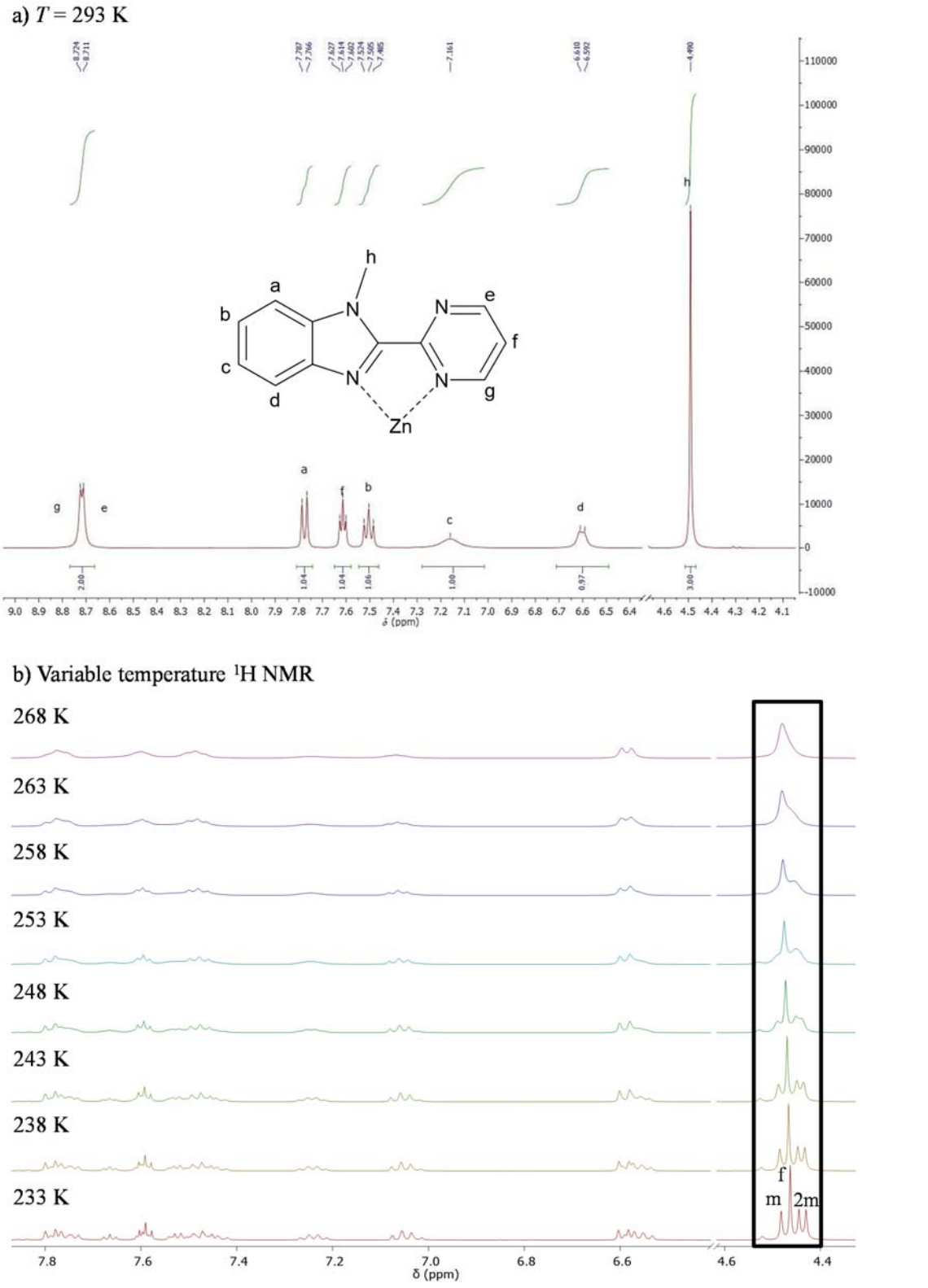

Figure S28 a) Room and b) variable temperature ^{1}H NMR spectra recorded for $[Zn(\mathbf{L6})_3]^{2+}$ using $\left|\mathbf{L6}\right|_{tot}$ = 10 mM in CD_3CN (f = facial, m = meridional).

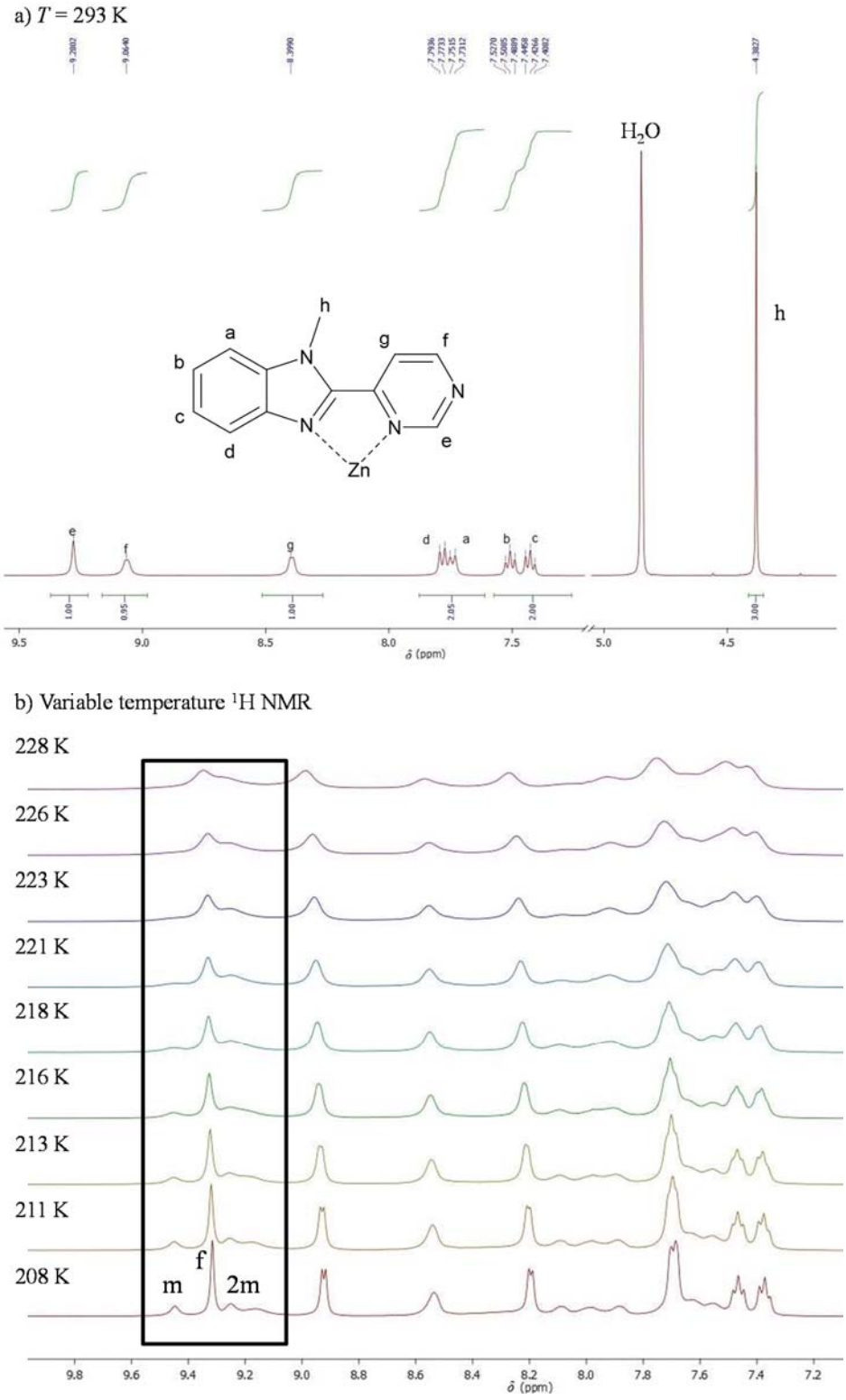

Figure S29 a) Room and b) variable temperature ^{1}H NMR spectra recorded for $[Zn(\mathbf{L7})_3]^{2+}$ using $|\mathbf{L7}|_{tot}$ = 0.1 M in CD_3OD (f = facial, m = meridional).

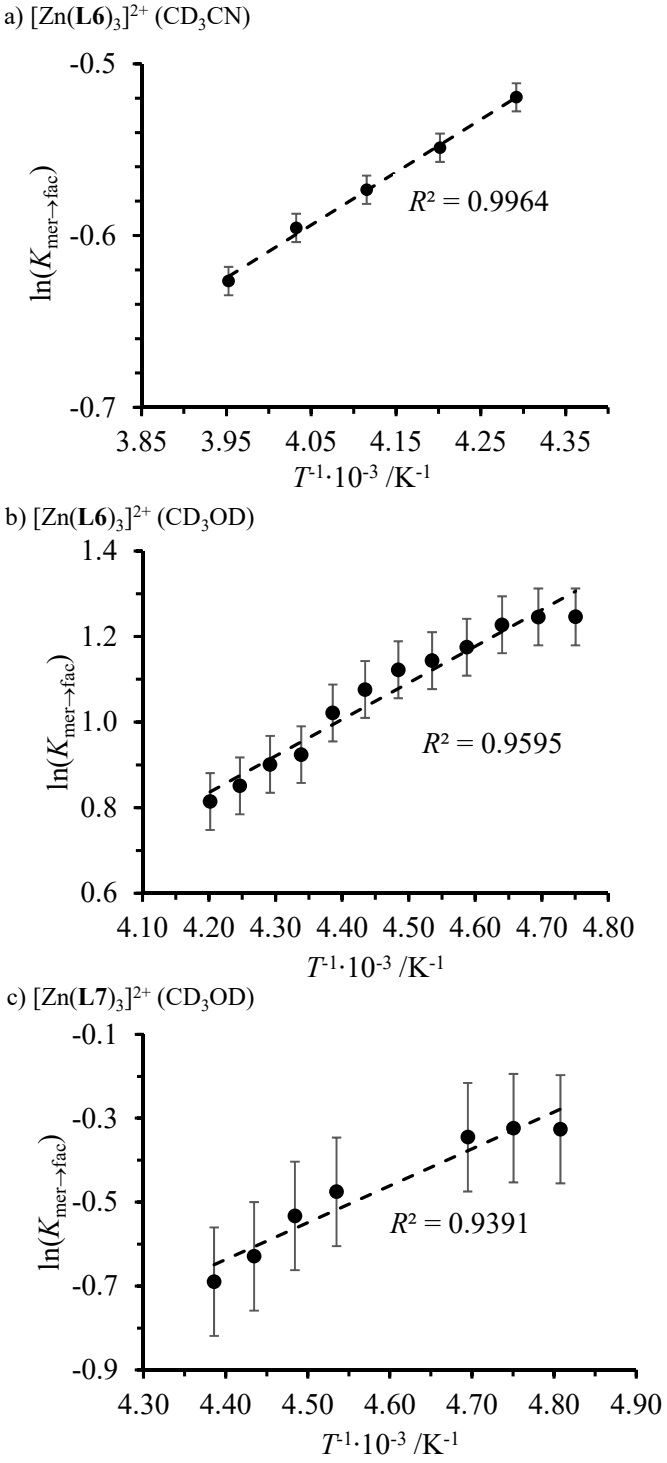

Figure S30 Van't Hoff plots of $\ln(K_{mer\rightarrow fac})$ vs. $1/T$ (equilibrium 14) for a solution of a) 10 mM $[Zn(\mathbf{L6})_3]^{2+}$ in CD_3CN (233–253 K), b) 10 mM $[Zn(\mathbf{L6})_3]^{2+}$ in CD_3OD (210–238 K) and c) 100 mM $[Zn(\mathbf{L7})_3]^{2+}$ in CD_3OD (208–228 K).

Table S8 Thermodynamic enthalpic ($\Delta H^{\mathrm{Zn,L}k}_{mer\rightarrow fac}$) and entropic ($\Delta S^{\mathrm{Zn,L}k}_{mer\rightarrow fac}$) contributions to equilibrium (14) in solution.

Complex	Solvent	ε_r [a]	$\Delta H^{\mathrm{Zn,L}k}_{mer\rightarrow fac}$ /kJ·mol^{-1}	$\Delta S^{\mathrm{Zn,L}k}_{mer\rightarrow fac}$ /J·mol^{-1}·K^{-1}	$\Delta G^{\mathrm{Zn,L}k,\circ}_{mer\rightarrow fac}$ [b] /kJ·mol^{-1}	$T_{1/2}$ /K	Ref.
$[Zn(\mathbf{L1})_3]^{2+}$	CD_3CN	37.5	-1.7(1)	-14(1)	2.5(3)	121(11)	74
$[Zn(\mathbf{L1})_3]^{2+}$	CD_3NO_2	35.9	-7.4(3)	-39(1)	4.2(4)	190(9)	74
$[Zn(\mathbf{L4})_3]^{2+}$	CD_3CN	37.5	-4(1)	-16(4)	0.8(1.6)	250(88)	74
$[Zn(\mathbf{L4})_3]^{2+}$	CD_3NO_2	35.9	-11(1)	-45(4)	2.4(1.5)	244(31)	74

[a] Relative dielectric constants. [b] $\Delta G^{\mathrm{Zn,L}k,\circ}_{mer\rightarrow fac}$ are calculated at T = 298 K.

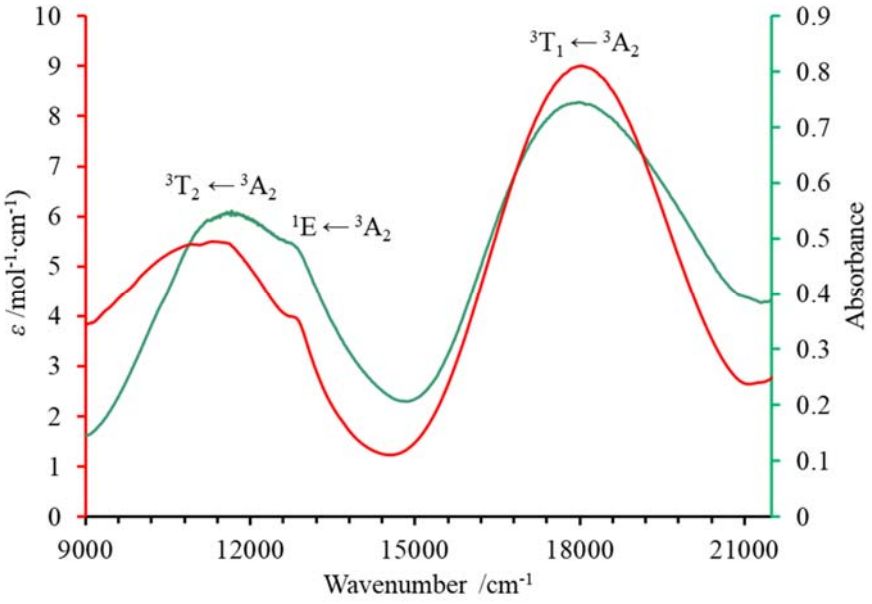

Figure S31 Absorption spectrum of $[Ni(\mathbf{L6})_3]^{2+}$ in acetonitrile (0.1 M, 298 K, red trace, left axis) and solid-state absorption spectrum of $[Ni(\mathbf{L6})_3](BF_4)_2$ (298 K, green trace, right axis) with the d-d transitions labelled on the graph.

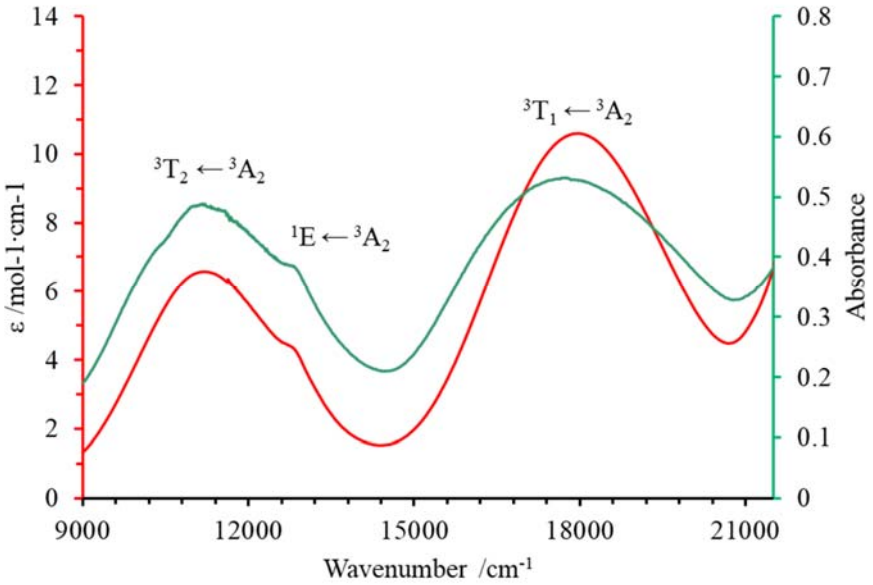

Figure S32 Absorption spectrum of $[Ni(\mathbf{L7})_3]^{2+}$ in acetonitrile (0.1 M, 298 K, , red trace, left axis) and solid-state absorption spectrum of $[Ni(\mathbf{L7})_3](BF_4)_2$ (298 K, green trace, right axis) with the d-d transitions labelled on the graph.

Table S9 Ligand-field strengths (Δ_{oct}) and Racah parameters (B, C) computed[61] for $[Ni(\mathbf{L}\boldsymbol{k})_3]^{2+}$ in 0.1 M acetonitrile solution at 298 K.

	$[Ni(\mathbf{L1})_3]^{2+}$	$[Ni(\mathbf{L4})_3]^{2+}$	$[Ni(\mathbf{L6})_3]^{2+}$	$[Ni(\mathbf{L7})_3]^{2+}$
Δ_{oct} /cm^{-1}	11423	11476	11605	11385
B /cm^{-1}	889	866	865	870
C /cm^{-1}	3096	3149	2995	3068
Δ_{oct}/B	12.9	13.3	13.4	13.1
C/B	3.48	3.64	3.46	3.52
β [a]	0.85	0.83	0.83	0.83
Reference	61	61	This work	This work

[a] Nephelauxetic parameter $\beta = B/B^o$ using B^o = 1042 cm^{-1} for free Ni^{2+} ion.[88]

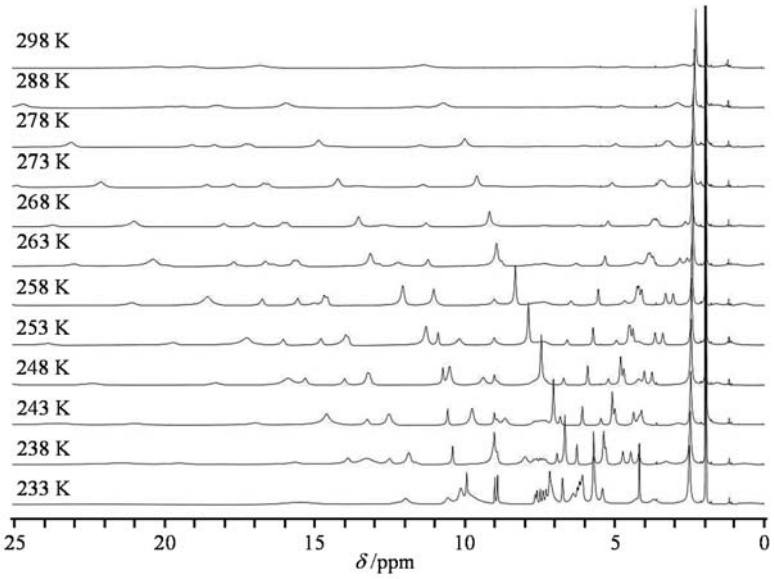

Figure S33 Variable temperature ^{1}H-NMR spectra recorded for 10 mM $[Fe(\mathbf{L6})_3]^{2+}$ in CD_3CN.

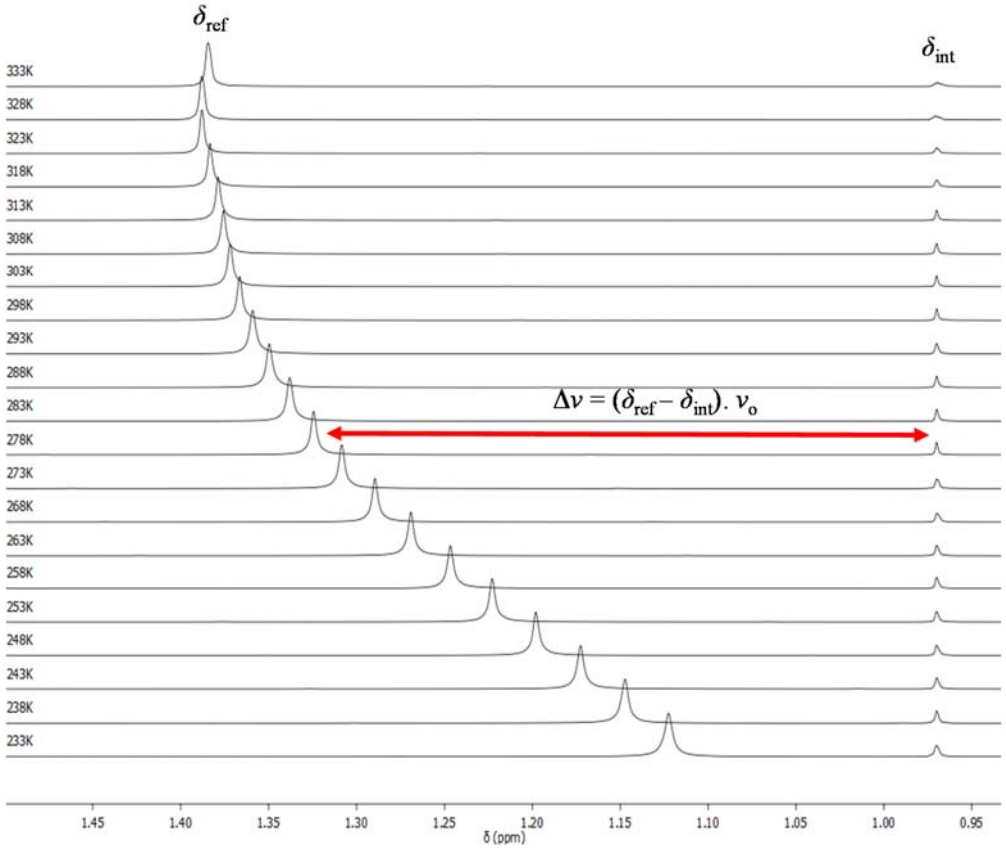

Figure S34 Shift of the ^{1}H-NMR signal of *tert*-butanol outside the coaxial tube (δ_{ref}) to higher frequencies with respect to the signal of *tert*-butanol used as the reference (δ_{int}) in the coaxial tube at temperatures between 233 K – 333 K for the paramagnetic complex $[Fe(\mathbf{L6})_3]^{2+}$ in solution (10.2 mM in CD_3CN).

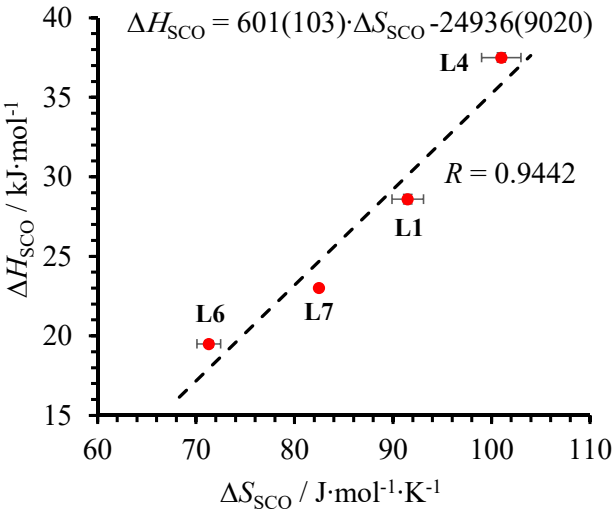

Figure S35 Empirical linear *H*/*S* compensation observed for the spin crossover equilibria observed in $[Fe(\mathbf{L}\boldsymbol{k})_3]^{2+}$ in CD_3CN (**L*k*** = **L1**, **L4**, **L6** and **L7**).

Table S10 Elemental analysis of the primary $[Ni(\mathbf{L6})_3](BF_4)_2{\cdot}1.55CH_3CN{\cdot}0.4H_2O$, $[Zn(\mathbf{L6})_3](CF_3SO_3)_2{\cdot}0.6H_2O$, $[Fe(\mathbf{L6})_3](BF_4)_2{\cdot}0.15CH_3CN{\cdot}1.2H_2O$, $[Ni(\mathbf{L7})_3](BF_4)_2{\cdot}0.85H_2O$, $[Zn(\mathbf{L7})_3](PF_6)_2{\cdot}1.25H_2O$ and $[Fe(\mathbf{L7})_3](PF_6)_{1.76}(BF_4)_{0.24}{\cdot}0.6H_2O$ complexes.

Complex		%C	%H	%N	Mol. Wt.
$[Ni(\mathbf{L6})_3](BF_4)_2{\cdot}1.55CH_3CN\ 0.4H_2O$ η =66%	*Calculated*	50.29	3.83	20.32	933.865
	Found	50.19	3.7	20.46	
	Deviation	0.1	0.13	0.14	
$[Zn(\mathbf{L6})_3](CF_3SO_3)_2{\cdot}0.6H_2O$ η =72%	*Calculated*	45.41	3.13	16.72	1005.42
	Found	45.38	3.07	16.76	
	Deviation	0.03	0.06	0.04	
$[Fe(\mathbf{L6})_3](BF_4)_2{\cdot}0.15CH_3CN{\cdot}1.2H_2O$ η =79%	*Calculated*	49.1	3.73	19.17	887.951
	Found	49.17	3.82	19.54	
	Deviation	0.07	0.09	0.08	
$[Ni(\mathbf{L7})_3](BF_4)_2{\cdot}0.85H_2O$ η =52%	*Calculated*	49.23	3.64	19.14	878.32
	Found	49.05	3.41	18.93	
	Deviation	0.18	0.23	0.21	
$[Zn(\mathbf{L7})_3](PF_6)_2{\cdot}1.25H_2O$ η = 51%	*Calculated*	42.87	3.25	16.67	1008.52
	Found	42.78	3.16	16.76	
	Deviation	0.09	0.09	0.09	
$[Fe(\mathbf{L7})_3](PF_6)_{1.76}(BF_4)_{0.24}{\cdot}0.6H_2O$ η =46%	*Calculated*	44.42	3.23	17.27	973.34
	Found	44.09	3.25	17.06	
	Deviation	0.33	0.02	0.21	

Table S11 Crystal data and structure refinement for $[Zn(\mathbf{L6})_3](ClO_4)_2(C_2H_3N)_{2.5}$ (**1**), $[Zn(\mathbf{L6})_3](BF_4)_2\cdot(CH_3CN)_2$ (**2**), $[Ni(\mathbf{L6})_3](ClO_4)_2$ (**3**) and $[Ni(\mathbf{L6})_3](ClO_4)_2\cdot CH_3CN$ (**4**).

	$[Zn(\mathbf{L6})_3](ClO_4)_2\cdot(CH_3CN)_{2.5}$ **(1)**	$[Zn(\mathbf{L6})_3](BF_4)_2\cdot(CH_3CN)_2$ **(2)**	$[Ni(\mathbf{L6})_3](ClO_4)_2$ **(3)**	$[Ni(\mathbf{L6})_3](ClO_4)_2\cdot CH_3CN$ **(4)**
Empirical formula	$C_{41.01}H_{37.51}Cl_2N_{14.50}O_8Zn$	$C_{40}H_{36}B_2F_8N_{14}Zn$	$C_{36}H_{30}Cl_2N_{12}NiO_8$	$C_{38}H_{33}Cl_2N_{13}NiO_8$
Formula Unit	$C_{36}H_{30}Cl_2N_{12}ZnO_8.\ (C_2H_3N)_{2.5}$	$C_{36}H_{30}B_2F_8N_{12}Zn\ (C_2H_3N)_2$	$C_{36}H_{30}Cl_2N_{12}NiO_8$	$C_{36}H_{30}Cl_2N_{12}NiO_8\cdot C_2H_3N$
Formula weight	997.69	951.82	888.33	929.38
Temperature	180.00(10) K	180.01(10) K	100.00(10) K	180.00(10) K
Wavelength	1.54184 Å	1.54184 Å	1.54184 Å	1.54184 Å
Crystal system	Triclinic	Triclinic	Triclinic	Monoclinic
Space group	P-1	P-1	P-1	$P12_1/c1$
Unit cell dimensions	a = 12.7622(7) Å b = 14.6333(6) Å c = 14.8701(5) Å α= 62.805(4)° β= 69.432(4)° γ = 70.165(4)°	a = 11.8497(5) Å b = 13.0576(5) Å c = 14.6652(5) Å α= 77.910(3)° β= 83.652(3)° γ = 73.048(4)°	a = 14.6645(6) Å b = 14.5548(6) Å c = 17.0631(6) Å α= 90.232(3)° β= 93.788(3)° γ = 90.093(3)°	a = 9.51580(10) Å b = 22.5839(2) Å c = 19.1174(2) Å α= 90° β= 96.5810(10)° γ = 90°
Volume	2258.7(2) $Å^3$	2119.42(15) $Å^3$	3634.0(2) $Å^3$	4081.33(7) $Å^3$
Z	2	2	4	4
Density (calculated)	1.467 Mg/m^3	1.491 Mg/m^3	1.624 Mg/m^3	1.513 Mg/m^3
Absorption coefficient	2.428 mm^{-1}	1.547 mm^{-1}	2.752 mm^{-1}	2.485 mm^{-1}
F(000)	1026	972	1824	1912
Crystal size	0.354 x 0.281 x 0.232 mm^3	0.495 x 0.162 x 0.127 mm^3	0.186 x 0.114 x 0.076 mm^3	0.234 x 0.218 x 0.18 mm^3
Theta range for data collection	3.477 to 68.893°.	3.602 to 68.837°.	2.595 to 68.975°	3.040 to 68.897°.

Index ranges	-15≤h≤15, -17≤k≤16, -17≤l≤13	-14≤h≤14, -15≤k≤15, -16≤l≤17	-17≤h≤15, -17≤k≤17, -19≤l≤20	-11≤h≤10, -27≤k≤27, -17≤l≤23
Reflections collected	17217	16019	32057	33472
Independent reflections	8247 [R(int) = 0.0154]	7730 [R(int) = 0.0312]	13338 [R(int) = 0.0420]	7537 [R(int) = 0.0197]
Completeness to theta (67.5°)	99.70%	99.80%	99.90%	100.00%
Absorption correction	Gaussian	Analytical	Analytical	Analytical
Max. and min. transmission	1.000 and 0.470	0.883 and 0.679	0.868 and 0.726	0.699 and 0.638
Refinement method	Full-matrix least-squares on F^2	Full-matrix least-squares on F^2	Full-matrix least-squares on F^2	Full-matrix least-squares on F^2
Data / restraints / parameters	8245 / 10 / 610	7730 / 0 / 535	13338 / 254 / 1247	7537 / 62 / 609
Goodness-of-fit on F2	1.053	1.048	1.110	1.044
Final R indices [I>2sigma(I)]	R1 = 0.0689, wR2 = 0.1910	R1 = 0.0564, wR2 = 0.1545	R1 = 0.0841, wR2 = 0.1817	R1 = 0.0468, wR2 = 0.1301
R indices (all data)	R1 = 0.0751, wR2 = 0.1970	R1 = 0.0686, wR2 = 0.1657	R1 = 0.0905, wR2 = 0.1860	R1 = 0.0484, wR2 = 0.1316
Extinction coefficient	n/a	n/a	n/a	n/a
Largest diff. peak and hole	0.710 and -0.821 e.Å^{-3}	0.933 and -0.559 e.Å^{-3}	0.646 and -0.881 e.Å^{-3}	0.821 and -0.669 e.Å^{-3}

Comments on the models:

$[Zn(\mathbf{L6})_3](BF_4)_2 \cdot (CH_3CN)_2$ (**2**)**:** The acetonitrile solvent molecules were found to be highly disordered in voids (V=387 Å^3) and their contribution to the scattering was masked using the solvent-masking routine smtbx.mask in OLEX2 [B. Rees, L. Jenner and M. Yusupov, *Acta Cryst. D*, 2005, **61**, 1299-1301.]. The electron count and voids volume correspond to about two acetonitrile molecules per formula unit, which were added in the given chemical formula and other crystal data.

$[Ni(\mathbf{L6})_3](ClO4)_2$ (**3**): The structure is based on twinned data and refined with two components of ratio 0.664/0.336 and twin law -1 0 0 0 1 0 0 0 -1.

Table S12 Crystal data and structure refinement for $[Ni(\mathbf{L6})_3](BF_4)_2{\cdot}C_2H_3N$ (**5**), $[Fe(\mathbf{L6})_3](ClO_4)_2$ (**6**), and $[Fe(\mathbf{L6})_3](BF_4)_2{\cdot}(C_5H_{12}O)_{0.5}$ (**7**).

	$[Ni(\mathbf{L6})_3](BF_4)_2.CH_3CN$ **(5)**	$[Fe(\mathbf{L6})_3](ClO_4)_2$ **(6)**	$[Fe(\mathbf{L6})_3](BF_4)_2{\cdot}(C_5H_{12}O)_{0.5}{\cdot}(C_2H_3N)_{0.5}$ **(7)**
Empirical formula	$C_{38}H_{33}B_2F_8N_{13}Ni$	$C_{36}H_{30}Cl_2FeN_{12}O_8$	$C_{39.50}H_{36.6}B_2F_8FeN_{12.5}O_{0.50}$
Formula Unit	$C_{36}H_{30}B_2F_8N_{12}Ni.\ C_2H_3N$	$C_{36}H_{30}Cl_2FeN_{12}O_8$	$C_{36}H_{30}B_2F_8FeN_{12}{\cdot}(C_5H_{12}O)_{0.5}{\cdot}(C_2H_3N)_{0.5}$
Formula weight	904.1	885.47	923.88
Temperature	180.00(10) K	100.01(10) K	180.00(10) K
Wavelength	1.54184 Å	1.54184 Å	1.54184 Å
Crystal system	Monoclinic	Monoclinic	Triclinic
Space group	$P12_1/c1$	$P12_1/c1$	P-1
Unit cell dimensions	a = 9.42950(10) Å b = 22.5937(3) Å c = 18.8708(2) Å α= 90° β= 94.9100(10)° γ = 90°	a = 14.8236(2) Å b = 14.3119(2) Å c = 16.9607(3) Å α= 90° β= 94.4286(13)° γ = 90°	a = 11.8247(6) Å b = 12.9758(6) Å c = 14.7202(6) Å α= 77.760(4)° β= 83.510(4)° γ = 74.276(4)°
Volume	4005.62(8) $Å^3$	3587.54(10) $Å^3$	2120.94(17) $Å^3$
Z	4	4	2
Density (calculated)	1.499 Mg/m^3	1.639 Mg/m^3	1.447 Mg/m^3
Absorption coefficient	1.449 mm^{-1}	5.379 mm^{-1}	3.579 mm^{-1}
F(000)	1848	1816	946
Crystal size	0.308 x 0.215 x 0.172 mm^3	0.265 x 0.199 x 0.077 mm^3	0.329 x 0.128 x 0.051 mm^3
Theta range for data collection	3.058 to 68.802°	2.990 to 68.807°	3.077 to 69.825°

Index ranges	-11≤h≤11, -23≤k≤27, -15≤l≤22	-12≤h≤17, -17≤k≤16, -20≤l≤20	-14≤h≤14, -12≤k≤15, -17≤l≤17
Reflections collected	17683	16165	16085
Independent reflections	7352 [R(int) = 0.0170]	6553 [R(int) = 0.0190]	7746 [R(int) = 0.0291]
Completeness to theta = 67.500°	99.80%	99.80%	99.70%
Absorption correction	Analytical	Analytical	Analytical
Max. and min. transmission	0.830 and 0.746	0.681 and 0.392	0.852 and 0.558
Refinement method	Full-matrix least-squares on F^2	Full-matrix least-squares on F^2	Full-matrix least-squares on F^2
Data / restraints / parameters	7352 / 75 / 637	6553 / 42 / 581	7746 / 14 / 624
Goodness-of-fit on F2	1.056	1.033	1.028
Final R indices [I>2sigma(I)]	R1 = 0.0413, wR2 = 0.1084	R1 = 0.0372, wR2 = 0.0964	R1 = 0.0590, wR2 = 0.1660
R indices (all data)	R1 = 0.0452, wR2 = 0.1109	R1 = 0.0411, wR2 = 0.0992	R1 = 0.0724, wR2 = 0.1819
Extinction coefficient	n/a	n/a	n/a
Largest diff. peak and hole	0.652 and -0.567 e.$Å^{-3}$	0.715 and -0.570 e.$Å^{-3}$	0.502 and -0.396 e.$Å^{-3}$

Table S13 Crystal data and structure refinement for $[Zn(\mathbf{L7})_3](ClO_4)_2$ (**8**) $[Zn(\mathbf{L7})_3](PF_6)_2$ (**9**) and $[Ni(\mathbf{L7})_3](ClO_4)_{1.48}(PF_6)_{0.52}$ (**10**).

	$[Zn(\mathbf{L7})_3](ClO_4)_2$ (**8**)	$[Zn(\mathbf{L7})_3](PF_6)_2$ (**9**)	$[Ni(\mathbf{L7})_3](PF_6)_{0.52}(ClO_4)_{1.48}$ (**10**)
Empirical formula	$C_{36}H_{30}Cl_2N_{12}O_8Zn$	$C_{36}H_{30}F_{12}N_{12}P_2Zn$	$C_{72}H_{60}Cl_{2.96}F_{6.24}N_{24}Ni_2O_{11.84}P_{1.04}$
Formula Unit	$C_{36}H_{30}Cl_2N_{12}O_8Zn$	$C_{36}H_{30}F_{12}N_{12}P_2Zn$	$(C_{36}H_{30}N_{12}NiO_{5.92}Cl_{6.48}F_{3.12}P_{0.52})_2$
Formula weight	894.99	986.03	1824
Temperature	180.00(10) K	149.99(10) K	120.01(12) K
Wavelength	1.54184 Å	1.54184 Å	1.54184 Å
Crystal system	Trigonal	Monoclinic	Monoclinic
Space group	P-3c1	$P12_1/c1$	$P12_1/n1$
Unit cell dimensions	a = 10.1894(3) Å b = 10.1894(3) Å c = 20.0955(10) Å α= 90° β= 90° γ = 120°	a = 13.58526(12) Å b = 10.68649(11) Å c = 27.0840(3) Å α= 90° β= 91.9320(9)° γ = 90°	a = 18.9538(2) Å b = 21.5853(3) Å c = 19.0060(3) Å α= 90° β= 98.5966(14)° γ = 90°
Volume	1806.86(14) $Å^3$	3929.78(7) $Å^3$	7688.46(19) $Å^3$
Z	2	4	4
Density (calculated)	1.645 Mg/m^3	1.667 Mg/m^3	1.576 Mg/m^3
Absorption coefficient	2.937 mm^{-1}	2.581 mm^{-1}	2.570 mm^{-1}
F(000)	916	1992	3731
Crystal size	0.126 x 0.102 x 0.063 mm^3	0.236 x 0.062 x 0.059 mm^3	0.092 x 0.073 x 0.043 mm^3
Theta range for data collection	4.400 to 68.876°	3.255 to 74.472°	3.071 to 71.738°

Index ranges	-12≤h≤11, -12≤k≤12,-24≤l≤23	-16≤h≤14, -13≤k≤13, -33≤l≤33	-23≤h≤19, -25≤k≤26, -21≤l≤23
Reflections collected	6333	52508	67327
Independent reflections	1125 [R(int) = 0.0250]	8009 [R(int) = 0.0299]	14753 [R(int) = 0.0279]
Completeness to theta = 67.500°	100.00%	99.90%	99.90%
Absorption correction	Analytical	Gaussian	Gaussian
Max. and min. transmission	0.856 and 0.787	1.000 and 0.384	1.000 and 0.729
Refinement method	Full-matrix least-squares on F^2	Full-matrix least-squares on F^2	Full-matrix least-squares on F^2
Data / restraints / parameters	1125 / 0 / 164	8008 / 806 / 724	14753 / 980 / 1219
Goodness-of-fit on F^2	1.125	1.058	1.048
Final R indices [I>2sigma(I)]	R1 = 0.0658, wR2 = 0.1578	R1 = 0.0505, wR2 = 0.1400	R1 = 0.0536, wR2 = 0.1396
R indices (all data)	R1 = 0.0708, wR2 = 0.1609	R1 = 0.0539, wR2 = 0.1429	R1 = 0.0635, wR2 = 0.1454
Largest diff. peak and hole	0.490 and -0.798 e.Å^{-3}	0.92 and -0.75 e.Å^{-3}	1.121 and -0.697 e.Å^{-3}

Comments on the models:

$[Zn(\mathbf{L7})_3](ClO_4)_2$ (**8**): Zn atom is located onto a 3-fold axis and nearby a 2-fold axis perpendicular to it. There is only 1/3 of the complex in the asymmetric unit which is disordered around the 2-fold axis (occupancies fixed to 0.5).

$[Zn(\mathbf{L7})_3](PF_6)_2$ (**9**)**:** Two disordered hexafluorophosphate anion were refined using two components. Restraints were used on P-F and F-F distances as well as on anisotropic displacement parameters. The displacement parameters of the phosphor atoms were constrained to be identical. One part of the ligand is also disordered and was refined using 2 components and restraints on the geometry (FLAT and SADI) and on the displacement parameters (RIGU SIMU). EADP restraints were used on very close atoms.

$[Ni(\mathbf{L7})_3](PF_6)_{0.52}(ClO_4)_{1.48}$ (**10**) **:** Two of the counterions were disordered and could not be satisfactorily modelled using only hexafluorophosphate. Since perchlorate were also present in the solution, a mixed perchlorate and hexafluoroborate model were used. One other counterion was fitted using two perchlorate molecules. Restraints were used on distances and displacement parameters. The displacement parameters of some central atoms were constrained to be identical. Finally, a disordered solvent molecule could not be fitted properly in our hands. The squeeze/bypass method was used. The R before applying the solvent correction were R1=0.0751 and wR2 0.2194. Four holes were located per unit-cell containing each about 24 electrons. This is almost the electron count of an acetonitrile molecule.

Table S14 Crystal data and structure refinement for $Ni(\mathbf{L7})_3](BF_4)_2{\cdot}CH_3OH{\cdot}(CH_3CN)_{0.5}$ (**11**), $[Fe(\mathbf{L7})_3](PF_6)(BF_4){\cdot}CH_3OH$ (**12**) and $[Fe(\mathbf{L7})_3](PF_6)_{1.72}(ClO_4)_{0.28}{\cdot}CH_3OH$ (**13**).

	$[Ni(\mathbf{L7})_3](BF_4)_2{\cdot}CH_3OH(CH_3CN)_{0.5}$ (**11**)	$[Fe(\mathbf{L7})_3]0.75(PF_6)1.25(BF_4){\cdot}CH_3OH$ (**12**)	$[Fe(\mathbf{L7})_3](PF_6)_{1.72}(ClO_4)_{0.28}\ CH_3OH$ (**13**)
Empirical formula	$C_{38}H_{35.50}B_2F_8N_{12.50}NiO$	$C_{73}H_{64}B_{2.5}F_{19}Fe_2N_{24}OP_{1.5}$	$C_{73}H_{64}Cl_{0.56}F_{20.63}Fe_2N_{24}O_{3.25}P_{3.44}$
Formula Unit	$(C_{36}H_{30}N_{12}NiB_2F_8)$ $(CH_3OH)(CH_3CN)_{0.5}$	$(C_{36}H_{30}N_{12}FeB_{1.25}P_{0.75}F_9)_2$ (CH_3OH)	$(C_{36}H_{30}N_{12}Fe_2Cl_{0.28}F_{10.36}O_{1.12}P_{1.72})_2$ (CH_3OH)
Formula weight	915.62	1839.80	1959.46
Temperature	150.00(10) K	150.00(10) K	150.15 K
Wavelength	1.54184 Å	1.54184 Å	1.54184 Å
Crystal system	Triclinic	Monoclinic	Monoclinic
Space group	P-1	$P12_1/n1$	$P12_1/n1$
Unit cell dimensions	a = 11.6311(2) Å b = 12.8430(2) Å c = 14.99232(18) Å α= 94.6407(12)° β= 100.7070(12)° γ = 113.7978(17)°	a = 18.82600(10) Å b = 21.23850(10) Å c = 18.88290(10) Å α= 90° β= 98.0140(10)° γ = 90°	a = 19.0452(4) Å b = 21.4963(4) Å c = 19.0632(5) Å α= 90° β= 98.075(2)° γ = 90°
Volume	1982.93(6) $Å^3$	7476.33(7) $Å^3$	7727.1(3) $Å^3$
Z	2	4	4
Density (calculated)	1.534 Mg/m^3	1.635 Mg/m^3	1.684 Mg/m^3
Absorption coefficient	1.486 mm^{-1}	4.412 mm^{-1}	4.911 mm^{-1}
F(000)	938	3800	3979

Crystal size	0.232 x 0.153 x 0.049 mm^3	0.217 x 0.056 x 0.031 mm^3	0.082 x 0.037 x 0.022 mm^3
Theta range for data collection	3.046 to 74.466°	3.105 to 74.447°	3.116 to 70.252°
Index ranges	-14≤h≤14, -16≤k≤15,-15≤l≤18	-23≤h≤20, -26≤k≤26, -23≤l≤23	-22≤h≤23, -25≤k≤25, -20≤l≤22
Reflections collected	34638	96589	56784
Independent reflections	7887 [R(int)=0.0360]	14949 [R(int)=0.0268]	14030 [R(int)=0.0572]
Completeness to theta = 67.5°	99.00%	99.20%	97.3 %
Absorption correction	Analytical	Gaussian	Gaussian
Max. and min. transmission	0.934 and 0.788	1.000 and 0.429	0.948 and 0.708
Refinement method	Full-matrix least-squares on F^2	Full-matrix least-squares on F^2	Full-matrix least-squares on F^2
Data / restraints / parameters	7887/0/567	14949/395/1253	14030/207/1227
Goodness-of-fit on F2	1.121	1.038	1.035
Final R indices [I>2sigma(I)]	R1=0.0506, wR2=0.1424	R1=0.0379, wR2=0.1023	R1=0.0764, wR2=0.2007
R indices (all data)	R1=0.0550, wR2=0.1457	R1=0.0430, wR2=0.1056	R1=0.1190, wR2=0.2256
Largest diff. peak	0.796 and -0.775 e.$Å^{-3}$	1.136 and -0.416 e.$Å^{-3}$	1.204 and -0.710 e.$Å^{-3}$

Comments on the models:

$[Fe(\mathbf{L7})_3](PF_6)(BF_4)\cdot CH_3OH$ (**12**)**:** One disordered tetrafluoroborate anion was refined using two components. Restraints were used on B-F and F-F distances as well as on anisotropic displacement parameters. The displacement parameters of the boron atoms were constrained to be identical. A disordered solvent methanol molecule was also modelled with two components, using restraints on C-O distances and displacement parameters. Two sites are mixed tetrafluorobarate/ hexafluorophospate sites and were refined using two components with restraints on the geometry (SADI) and restraints and constraints on the displacement parameters (RIGU and EADP)

$[Fe(\mathbf{L7})_3](PF_6)_{1.72}(ClO_4)_{0.28}\cdot CH_3OH$ (**13**): One of the counterions was disordered and could not be satisfactorily modelled using only hexafluorophosphate. Since perchlorate were also present in the solution, a mixed perchlorate and hexafluorophosphate model was used, giving a better fit to the electronic density. Restraints were used on distances and displacement parameters. A disordered solvent methanol molecule was also modelled using two components, with restraints on distances and displacement parameters.

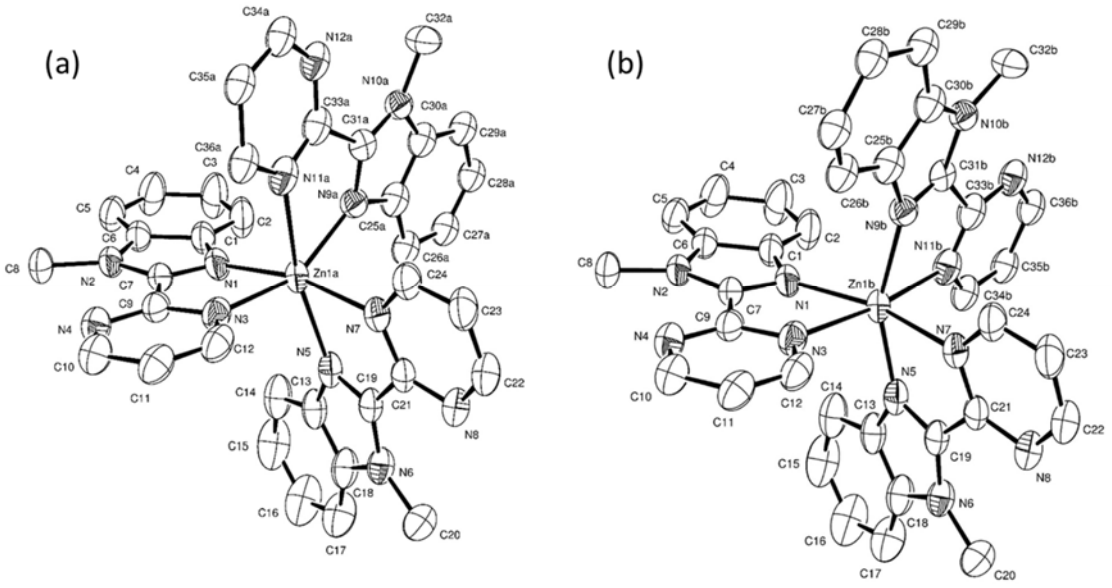

Figure S36 ORTEP view of $[Zn(\mathbf{L6})_3]^{2+}$ in the crystal structure of $[Zn(\mathbf{L6})_3](ClO_4)_2 \cdot (C_2H_3N)_{2.5}$ (**1**) (a) *fac* isomer (b) *mer* isomer (ellipsoids are drawn at 40% probability) with numbering scheme. Hydrogen atoms and ClO_4^- counter anions are omitted for clarity.

Table S15 Selected bond distances (Å) and bond angles (°) for $[Zn(\mathbf{L6})_3](ClO_4)_2 \cdot (C_2H_3N)_{2.5}$ (**1**).

Bond Distances (Å)			
Zn(1A)-N(1)	2.183(4)	Zn(1B)-N(1)	2.062(4)
Zn(1A)-N(3)	2.055(4)	Zn(1B)-N(3)	2.430(4)
Zn(1A)-N(5)	2.248(4)	Zn(1B)-N(5)	1.972(4)
Zn(1A)-N(7)	2.173(4)	Zn(1B)-N(7)	2.373(4)
Zn(1A)-N(9A)	2.065(6)	Zn(1B)-N(9B)	2.111(7)
Zn(1A)-N(11A)	2.497(7)	Zn(1B)-N(11B)	2.206(8)
Bond Angles (°)			
N(1)-Zn(1A)-N(5)	94.23(14)	N(1)-Zn(1B)-N(3)	72.36(14)
N(1)-Zn(1A)-N(11A)	102.01(18)	N(1)-Zn(1B)-N(7)	154.67(17)
N(3)-Zn(1A)-N(1)	77.95(14)	N(1)-Zn(1B)-N(9B)	96.6(2)
N(3)-Zn(1A)-N(5)	98.28(14)	N(1)-Zn(1B)-N(11B)	104.5(2)
N(3)-Zn(1A)-N(7)	96.76(15)	N(5)-Zn(1B)-N(1)	107.21(17)
N(3)-Zn(1A)-N(9A)	153.7(2)	N(5)-Zn(1B)-N(3)	94.89(15)
N(3)-Zn(1A)-N(11A)	83.41(19)	N(5)-Zn(1B)-N(7)	75.40(15)
N(5)-Zn(1A)-N(11A)	163.65(18)	N(5)-Zn(1B)-N(9B)	155.5(2)
N(7)-Zn(1A)-N(1)	166.89(16)	N(5)-Zn(1B)-N(11B)	92.1(2)
N(7)-Zn(1A)-N(5)	74.50(13)	N(7)-Zn(1B)-N(3)	82.33(13)
N(7)-Zn(1A)-N(11A)	89.15(17)	N(9B)-Zn(1B)-N(3)	97.8(2)
N(9A)-Zn(1A)-N(1)	96.47(18)	N(9B)-Zn(1B)-N(7)	85.6(2)
N(9A)-Zn(1A)-N(5)	107.80(18)	N(9B)-Zn(1B)-N(11B)	76.1(3)
N(9A)-Zn(1A)-N(7)	93.42(18)	N(11B)-Zn(1B)-N(3)	173.0(3)
N(9A)-Zn(1A)-N(11A)	72.5(2)	N(11B)-Zn(1B)-N(7)	100.5(2)

Table S16 Selected least-squares planes data for $[Zn(\mathbf{L6})_3](ClO_4)_2 \cdot (C_2H_3N)_{2.5}$ (**1**)

Least-squares planes description	Max. deviation (Å)	Atom	Dihedral Angle (°)
Benzimidazole 1 N1 C1 C2 C3 C4 C5 C6 N2 C7	0.016	C2	4.7(2)
Pyrimidine 1 C9 N3 C12 C11 C10 N4	0.009	C11	
Benzimidazole 2 C19 N5 C13 C14 C15 C16 C17 C18 N6	0.021	C19	11.3(2)
Pyrimidine 2 C21 N8 C22 C23 C24 N7	0.008	N8	
Benzimidazole 3A C31A N9A C25A C26A C27A C28A C29A C30A N10A	0.055	C31A	8.5(2)
Pyrimidine 3A C33A N12A C34A C35A C36A N11A	0.036	C36A-C34A	
Benzimidazole 3B C31B N9B C25B C26B C27B C28B C29B C30B N10B	0.110	C27B	3.1(3)
Pyrimidine 3B C33B N12B C36B C35B C34B N11B	0.041	C36B	

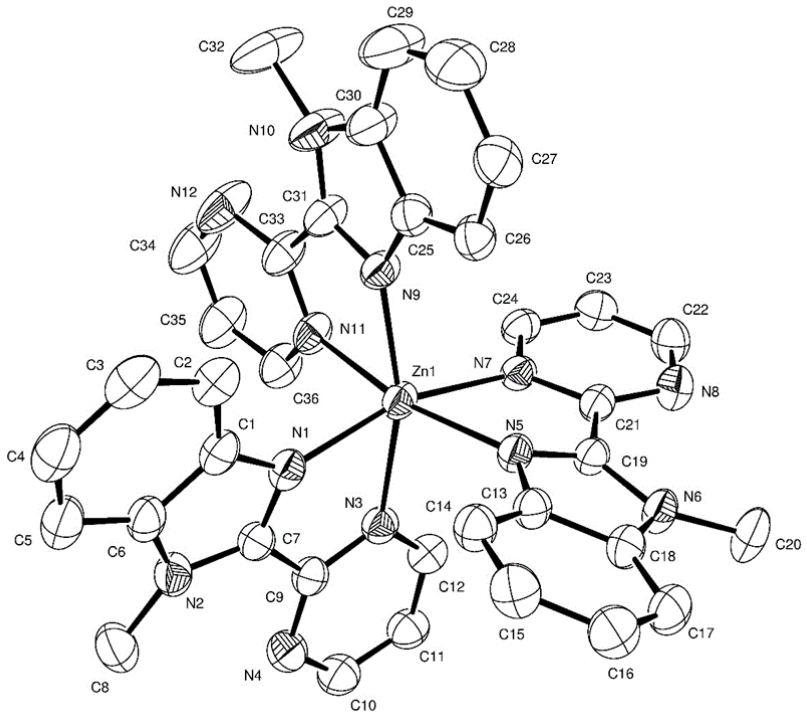

Figure S37 ORTEP view of *fac*-$[Zn(\mathbf{L6})_3]^{2+}$ in the crystal structure of $[Zn(\mathbf{L6})_3](BF_4)_2.(CH_3CN)_2$ (**2**) (ellipsoids are drawn at 40% probability) with numbering scheme. Hydrogen atoms and BF_4^- counter anions are omitted for clarity

Table S17 Selected bond distances (Å) and bond angles (°) for $[Zn(\mathbf{L6})_3](BF_4)_2 \cdot (CH_3CN)_2$ (**2**).

Bond Distances (Å)			
Zn(1)-N(1)	2.130(3)		
Zn(1)-N(3)	2.248(3)		
Zn(1)-N(5)	2.127(2)		
Zn(1)-N(7)	2.261(3)		
Zn(1)-N(9)	2.069(3)		
Zn(1)-N(11)	2.234(3)		
Bond Angles (°)			
N(1)-Zn(1)-N(3)	75.46(10)	N(9)-Zn(1)-N(1)	98.03(11)
N(1)-Zn(1)-N(7)	162.32(10)	N(9)-Zn(1)-N(3)	162.31(10)
N(1)-Zn(1)-N(11)	93.53(10)	N(9)-Zn(1)-N(5)	102.55(10)
N(3)-Zn(1)-N(7)	87.61(9)	N(9)-Zn(1)-N(7)	99.64(10)
N(5)-Zn(1)-N(1)	100.78(10)	N(9)-Zn(1)-N(11)	76.26(10)
N(5)-Zn(1)-N(3)	94.87(9)	N(11)-Zn(1)-N(3)	87.61(10)
N(5)-Zn(1)-N(7)	75.32(9)	N(11)-Zn(1)-N(7)	90.69(10)
N(5)-Zn(1)-N(11)	165.64(10)		

Table S18 Selected least-squares planes data for $[Zn(\mathbf{L6})_3](BF_4)_2$ (**2**).

Least-squares planes description	Max. deviation (Å)	Atom	Dihedral Angle (°)
Benzimidazole 1 N1 C1 C2 C3 C4 C5 C6 N2 C7	0.016	C1	9.7(1)
Pyrimidine 1 C9 N3 C12 C11 C10 N4	0.001	N4-C9-C11-C12	
Benzimidazole 2 C19 N5 C13 C14 C15 C16 C17 C18 N6	0.032	C19	17.2(1)
Pyrimidine 2 C21 N8 C22 C23 C24 N7	0.011	C21	
Benzimidazole 3 C31 N9 C25 C26 C27 C28 C29 C30 N10	0.014	N10	8.73(14)
Pyrimidine 3 C33 N12 C34 C35 C36 N11	0.016	C33	

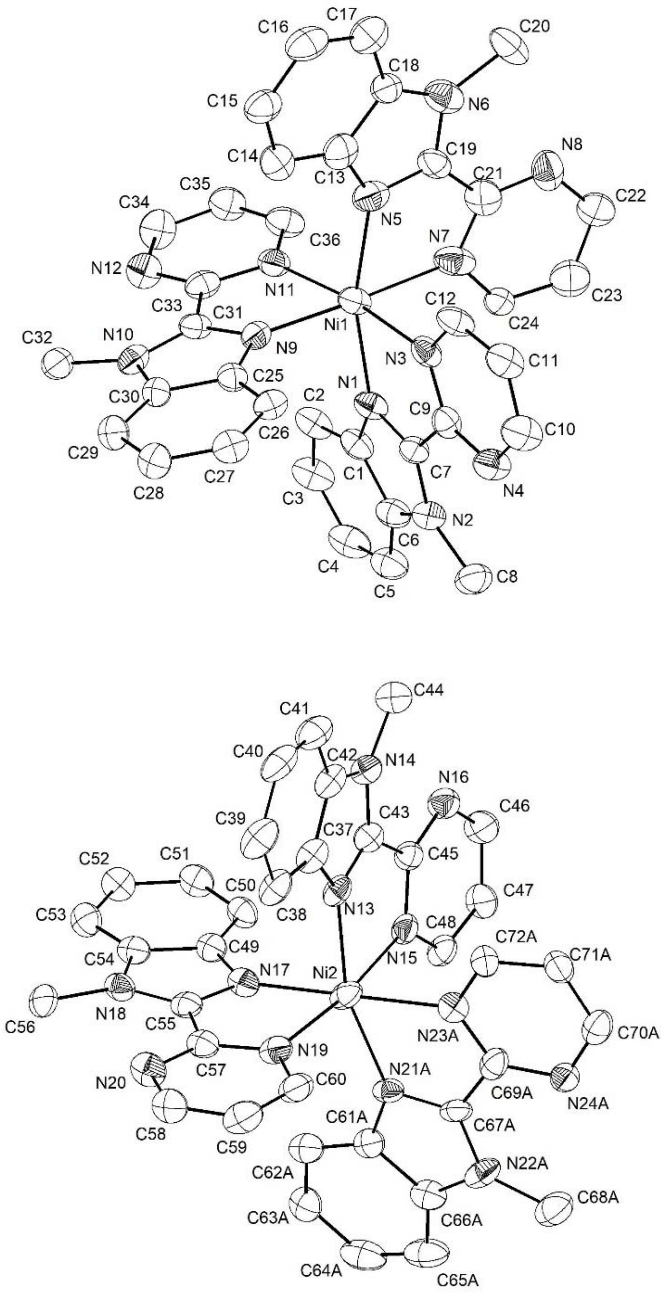

Figure S38 ORTEP view of the two different *mer*-$[Ni(\mathbf{L6})_3]^{2+}$ cations in the crystal structure of $[Ni(\mathbf{L6})_3](ClO_4)_2$ (**3**) (ellipsoids are drawn at 40% probability) with numbering scheme. Hydrogen atoms, and ClO_4^- counter anions are omitted for clarity.

Table S19 Selected bond distances (Å) and bond angles (°) of $[Ni(\mathbf{L6})_3](ClO_4)_2$ (**3**).

Bond Distances (Å)			
Ni(1)-N(1)	2.073(6)	Ni(2)-N(15)	2.111(6)
Ni(1)-N(3)	2.112(7)	Ni(2)-N(17)	2.089(7)
Ni(1)-N(5)	2.061(6)	Ni(2)-N(19)	2.110(6)
Ni(1)-N(7)	2.188(7)	Ni(2)-N(21A)	2.010(12)
Ni(1)-N(9)	2.079(7)	Ni(2)-N(23A)	2.250(13)
Ni(1)-N(11)	2.088(7)	Ni(2)-N(21B)	1.895(16)
Ni(2)-N(13)	2.072(6)	Ni(2)-N(23B)	2.264(16)

Bond Angles (°)			
N(1)-Ni(1)-N(3)	77.8(3)	N(15)-Ni(2)-N(23A)	87.6(4)
N(1)-Ni(1)-N(7)	90.0(3)	N(15)-Ni(2)-N(23B)	91.3(5)
N(1)-Ni(1)-N(11)	91.0(3)	N(17)-Ni(2)-N(15)	95.6(2)
N(3)-Ni(1)-N(7)	97.2(3)	N(17)-Ni(2)-N(19)	79.0(3)
N(5)-Ni(1)-N(1)	87.6(3)	N(17)-Ni(2)-N(23A)	175.8(4)
N(5)-Ni(1)-N(3)	163.9(3)	N(17)-Ni(2)-N(23B)	87.6(4)
N(5)-Ni(1)-N(7)	92.2(3)	N(19)-Ni(2)-N(15)	172.3(2)
N(5)-Ni(1)-N(9)	76.9(3)	N(19)-Ni(2)-N(23A)	97.6(4)
N(5)-Ni(1)-N(11)	102.7(3)	N(19)-Ni(2)-N(23B)	93.8(5)
N(9)-Ni(1)-N(1)	94.0(3)	N(21A)-Ni(2)-N(13)	162.8(4)
N(9)-Ni(1)-N(3)	95.6(3)	N(21A)-Ni(2)-N(15)	93.2(4)
N(9)-Ni(1)-N(7)	176.8(2)	N(21A)-Ni(2)-N(17)	104.3(4)
N(9)-Ni(1)-N(11)	77.8(3)	N(21A)-Ni(2)-N(19)	93.3(4)
N(11)-Ni(1)-N(3)	171.8(3)	N(21A)-Ni(2)-N(23A)	78.3(5)
N(11)-Ni(1)-N(7)	99.1(3)	N(21B)-Ni(2)-N(13)	102.3(5)
N(13)-Ni(2)-N(15)	78.3(2)	N(21B)-Ni(2)-N(15)	92.4(5)
N(13)-Ni(2)-N(17)	91.5(2)	N(21B)-Ni(2)-N(17)	165.2(5)
N(13)-Ni(2)-N(19)	96.4(2)	N(21B)-Ni(2)-N(19)	94.1(5)
N(13)-Ni(2)-N(23A)	86.3(4)	N(21B)-Ni(2)-N(23B)	79.8(6)
N(13)-Ni(2)-N(23B)	169.4(5)		

Table S20 Selected least-squares planes data for $[Ni(\mathbf{L6})_3](ClO_4)_2$ (**3**).

Least-squares planes description	Max. deviation (Å)	Atom	Dihedral Angle (°)
Benzimidazole 1 N1 C1 C2 C3 C4 C5 C6 N2 C7	0.023	C2	9.2(3)
Pyrimidine 1 N3 C9 N4 C10 C11 C12	0.012	C12	
Benzimidazole 2 N5 C19 N6 C18 C17 C16 C15 C14 C13	0.027	C18	9.8(2)
Pyrimidine 2 N7 C24 C23 C22 N8 C21	0.023	N8	
Benzimidazole 3 N9 C25 C26 C27 C28 C29 C30 N10 C31	0.028	C29	3.9(3)
Pyrimidine 3 N11 C36 C35 C34 N12 C33	0.009	N12	
Benzimidazole 1' C43 N13 C37 C38 C39 C40 C41 C42 N14	0.022	C40	8.7(2)
Pyrimidine 1' N15 C48 C47 C46 N16 C45	0.010	N16	
Benzimidazole 2' N17 C49 C50 C51 C52 C53 C54 N18 C55	0.018	C53	1.5(2)
Pyrimidine 2' N19 C57 N20 C58 C59 C60	0.019	N19	
Benzimidazole 3'A N21A C67A N22A C66A C65A C64A C63A C62A C61A	0.034	N21A	11.0(5)
Pyrimidine 3'A C69A N24A C70A C71A C72A N23A	0.020	N24A	
Benzimidazole 3'B N9 C25 C26 C27 C28 C29 C30 N10 C31	0.091	C67B	20.1(6)
Pyrimidine 3'B C69B N24B C70B C71B C72B N23B	0.026	N23B-C72B	

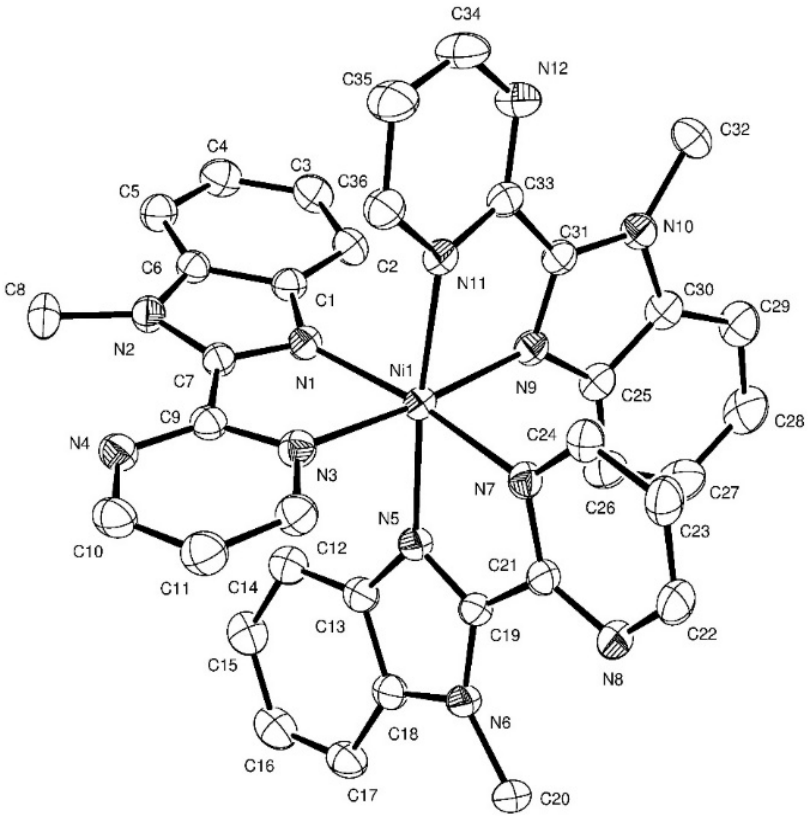

Figure S39 ORTEP view of *fac*-$[Ni(\mathbf{L6})_3]^{2+}$ in the crystal structure of $[Ni(\mathbf{L6})_3](ClO_4)_2 \cdot C_2H_3N$ (**4**) (ellipsoids are drawn at 40% probability) with numbering scheme. Hydrogen atoms, and ClO_4^- counter anions are omitted for clarity.

Table S21 Selected bond distances (Å) and bond angles (°) for $[Ni(\mathbf{L6})_3](ClO_4)_2 \cdot C_2H_3N$ (**4**).

Bond Distances (Å)			
Ni(1)-N(1)	2.062(2)		
Ni(1)-N(3)	2.140(2)		
Ni(1)-N(5)	2.067(2)		
Ni(1)-N(7)	2.093(2)		
Ni(1)-N(9)	2.077(2)		
Ni(1)-N(11)	2.120(2)		
Bond Angles (°)			
N(1)-Ni(1)-N(3)	78.27(7)	N(5)-Ni(1)-N(11)	173.84(8)
N(1)-Ni(1)-N(5)	99.14(8)	N(7)-Ni(1)-N(3)	92.75(7)
N(1)-Ni(1)-N(7)	170.87(8)	N(7)-Ni(1)-N(11)	96.06(7)
N(1)-Ni(1)-N(9)	100.54(7)	N(9)-Ni(1)-N(3)	174.19(7)
N(1)-Ni(1)-N(11)	86.60(7)	N(9)-Ni(1)-N(7)	88.56(7)
N(5)-Ni(1)-N(3)	87.38(7)	N(9)-Ni(1)-N(11)	78.20(7)
N(5)-Ni(1)-N(7)	78.62(8)	N(11)-Ni(1)-N(3)	96.03(7)
N(5)-Ni(1)-N(9)	98.43(7)		

Table S22 Selected least-squares planes data for [Ni(**L6**)$_3$](ClO$_4$)$_2$·C$_2$H$_3$N (**4**).

Least-squares planes description	Max. deviation (Å)	Atom	Dihedral Angle (°)
Benzimidazole 1 N1 C1 C2 C3 C4 C5 C6 N2 C7	0.012	C3	7.39(8)
Pyrimidine 1 N3 C9 N4 C10 C11 C12	0.006	C9-N3	
Benzimidazole 2 0N5 C13 C14 C15 C16 C17 C18 N6 C19	0.042	C19	10.96(8)
Pyrimidine 2 N7 C24 C23 C22 N8 C21	0.006	C21-C23	
Benzimidazole 3 N9 C25 C26 C27 C28 C29 C30 N10 C31	0.041	C31	16.34(10)
Pyrimidine 3 N11 C36 C35 C34 N12 C33	0.008	C33	

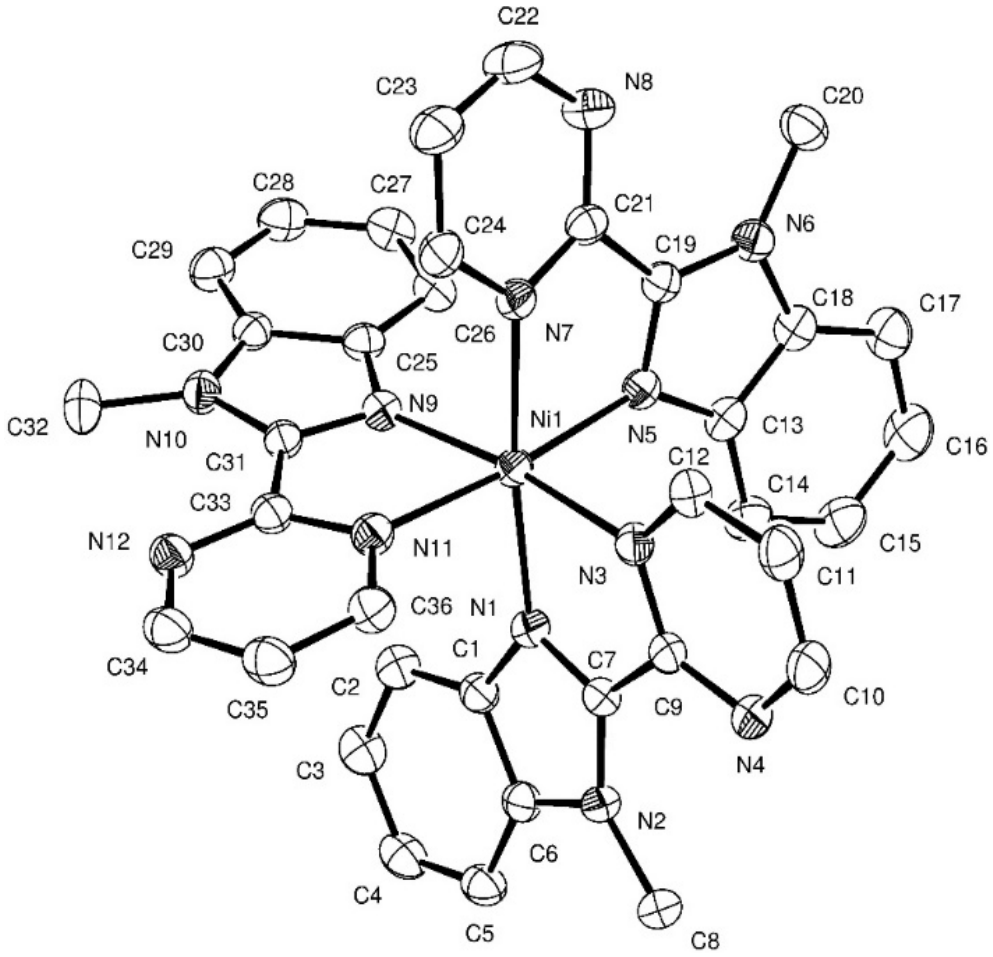

Figure S40 ORTEP view of *fac*-[Ni(**L6**)$_3$]$^{2+}$ in the crystal structure of [Ni(**L6**)$_3$](BF$_4$)$_2$·CH$_3$CN (**5**) (ellipsoids are drawn at 40% probability) with numbering scheme. Hydrogen atoms, acetonitrile solvent molecules and BF_4^- counter anions are omitted for clarity.

Table S23 Selected bond distances (Å) and bond angles (°) for [Ni(**L6**)$_3$](BF$_4$)$_2$·CH$_3$CN (**5**).

Bond Distances (Å)			
Ni(1)-N(1)	2.066(2)		
Ni(1)-N(3)	2.098(2)		
Ni(1)-N(5)	2.075(2)		
Ni(1)-N(7)	2.121(2)		
Ni(1)-N(9)	2.063(2)		
Ni(1)-N(11)	2.135(2)		
Bond Angles (°)			
N(1)-Ni(1)-N(3)	78.61(9)	N(5)-Ni(1)-N(11)	174.13(6)
N(1)-Ni(1)-N(5)	98.24(6)	N(7)-Ni(1)-N(11)	96.14(6)
N(1)-Ni(1)-N(7)	173.35(6)	N(9)-Ni(1)-N(1)	99.60(6)
N(1)-Ni(1)-N(11)	87.57(6)	N(9)-Ni(1)-N(3)	170.80(6)
N(3)-Ni(1)-N(7)	95.67(6)	N(9)-Ni(1)-N(5)	100.05(6)
N(3)-Ni(1)-N(11)	92.76(6)	N(9)-Ni(1)-N(7)	86.58(6)
N(5)-Ni(1)-N(3)	89.15(6)	N(9)-Ni(1)-N(11)	78.12(6)
N(5)-Ni(1)-N(7)	78.14(6)		

Table S24 Selected least-squares planes data for [Ni(**L6**)$_3$](BF$_4$)$_2$·CH$_3$CN (**5**).

Least-squares planes description	Max. deviation (Å)	Atom	Dihedral Angle (°)
Benzimidazole 1 N1 C7 N2 C6 C5 C4 C3 C2 C1	0.040	C7	10.94(8)
Pyrimidine 1 N3 C12 C11 C10 N4 C9	0.008	N4-C9	
Benzimidazole 2 N5 C19 N6 C18 C17 C16 C15 C14 C13	0.04	C19	16.39(9)
Pyrimidine 2 N7 C24 C23 C22 N8 C21	0.009	N7-C21	
Benzimidazole 3 N9 C25 C26 C27 C28 C29 C30 N10 C31	0.010	C31	7.54(8)
Pyrimidine 3 N11 C33 N12 C34 C35 C36	0.008	N11	

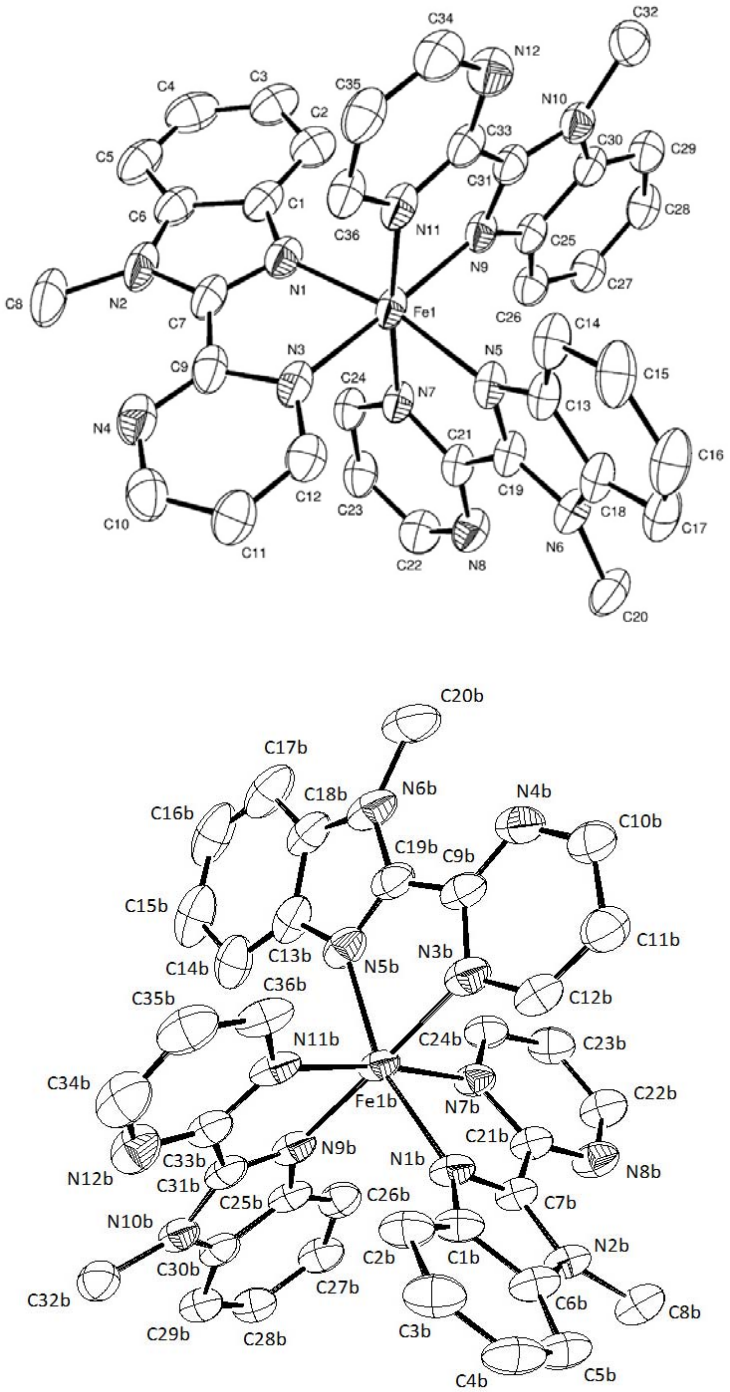

Figure S41 ORTEP view of the two different *mer*-$[Fe(\mathbf{L6})_3]^{2+}$ cations in the crystal structure of $[Fe(\mathbf{L6})_3](ClO_4)_2$ (**6**) (ellipsoids are drawn at 40% probability) at 180 K with numbering scheme. Hydrogen atoms and counter anions are omitted for clarity.

Table S25 Selected bond distances (Å) and bond angles (°) for $[Fe(\mathbf{L6})_3](ClO_4)_2$ (**6**) at 180 K.

Bond Distances (Å)			
Fe(1)-N(1)	1.989(4)	Fe(1B)-N(1B)	2.071(4)
Fe(1)-N(3)	2.018(5)	Fe(1B)-N(3B)	2.164(5)
Fe(1)-N(5)	1.999(4)	Fe(1B)-N(5B)	2.054(4)
Fe(1)-N(7)	2.003(4)	Fe(1B)-N(7B)	2.095(4)
Fe(1)-N(9)	2.005(4)	Fe(1B)-N(9B)	2.078(5)
Fe(1)-N(11)	1.998(4)	Fe(1B)-N(11B)	2.088(5)
Bond Angles (°)			
N(1)-Fe(1)-N(3)	80.47(19)	N(1B)-Fe(1B)-N(3B)	87.81(18)
N(1)-Fe(1)-N(5)	168.95(19)	N(1B)-Fe(1B)-N(7B)	77.52(16)
N(1)-Fe(1)-N(7)	93.05(17)	N(1B)-Fe(1B)-N(9B)	92.04(17)
N(1)-Fe(1)-N(9)	99.30(18)	N(1B)-Fe(1B)-N(11B)	97.32(17)
N(1)-Fe(1)-N(11)	91.77(17)	N(5B)-Fe(1B)-N(1B)	162.2(2)
N(5)-Fe(1)-N(3)	90.47(18)	N(5B)-Fe(1B)-N(3B)	76.9(2)
N(5)-Fe(1)-N(7)	80.23(17)	N(5B)-Fe(1B)-N(7B)	92.56(17)
N(5)-Fe(1)-N(9)	90.04(17)	N(5B)-Fe(1B)-N(9B)	103.76(19)
N(7)-Fe(1)-N(3)	87.91(18)	N(5B)-Fe(1B)-N(11B)	93.96(17)
N(9)-Fe(1)-N(3)	94.71(17)	N(7B)-Fe(1B)-N(3B)	87.70(18)
N(9)-Fe(1)-N(7)	177.38(17)	N(9B)-Fe(1B)-N(3B)	176.46(17)
N(11)-Fe(1)-N(3)	96.96(19)	N(9B)-Fe(1B)-N(7B)	95.73(18)
N(11)-Fe(1)-N(5)	95.62(17)	N(9B)-Fe(1B)-N(11B)	78.22(19)
N(11)-Fe(1)-N(7)	173.65(16)	N(11B)-Fe(1B)-N(3B)	98.28(19)
N(11)-Fe(1)-N(9)	80.43(18)	N(11B)-Fe(1B)-N(7B)	172.01(17)

Table S26 Selected least-squares planes data for $[Fe(\mathbf{L6})_3](ClO_4)_2$ (**6**).

Least-squares planes description	Max. deviation (Å)	Atom	Dihedral Angle (°)
Benzimidazole 1 C7 N2 C6 C5 C4 C3 C2 C1 N1	0.031	C6	8.9(2)
Pyrimidine 1 C9 N3 C12 C11 C10 N4	0.017	C12	
Benzimidazole 2 C19 N5 C13 C14 C15 C16 C17 C18 N6	0.032	C18	9.9(2)
Pyrimidine 2 N7 C21 N8 C22 C23 C24	0.003	C23	
Benzimidazole 3 N9 C31 N10 C30 C29 C28 C27 C26 C25	0.020	C27	1.8(2)
Pyrimidine 3 N11 C36 C35 C34 N12 C33	0.014	C33	
Benzimidazole 1B C7B N2B C6B C5B C4B C3B C2B C1B N1B	0.028	C2B	11.6(2)
Pyrimidine 1B N7B C21B N8B C22B C23B C24B	0.009	C24B	
Benzimidazole 2B C19B N5B C13B C14B C15B C16B C17B C18B N6B	0.034	C18B	8.2(2)
Pyrimidine 2B C9B N3B C12B C11B C10B N4B	0.018	C12B	
Benzimidazole 3B N9B C31B N10B C30B C29B C28B C27B C26B C25B	0.024	C30B	2.6(2)
Pyrimidine 3B N11B C36B C35B C34B N12B C33B	0.020	C33B	

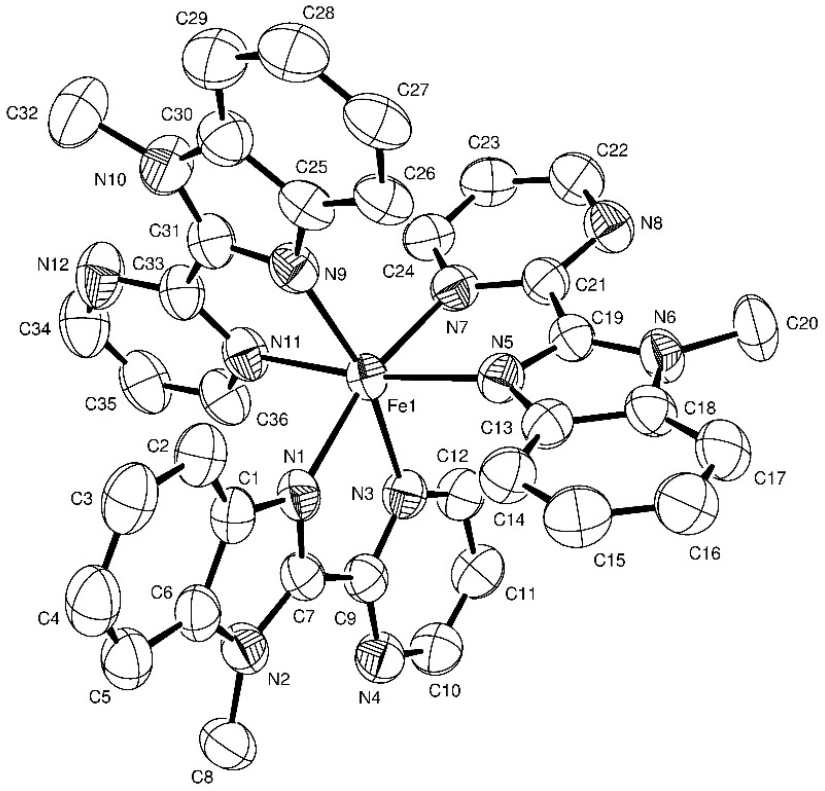

Figure S42 ORTEP view of *fac*-$[Fe(\mathbf{L6})_3]^{2+}$ cations in the crystal structure of $[Fe(\mathbf{L6})_3](BF_4)_2\cdot(C_5H_{12}O)_{0.5}.(C_2H_5N)_{0.5}$ (**7**) (ellipsoids are drawn at 40% probability) with numbering scheme. Hydrogen atoms and counter anions are omitted for clarity.

Table S27 Selected bond distances (Å) and bond angles (°) for $[Fe(\mathbf{L6})_3](BF_4)_2 \cdot (C_5H_{12}O)_{0.5} \cdot (C_2H_5N)_{0.5}$ (**7**).

Bond Distances (Å)			
Fe(1)-N(14)	2.101(3)		
Fe(1)-N(3)	2.143(3)		
Fe(1)-N(5)	2.102(3)		
Fe(1)-N(7)	2.150(4)		
Fe(1)-N(9)	2.063(4)		
Fe(1)-N(11)	2.150(3)		
Bond Angles (°)			
N(14)-Fe(1)-N(3)	76.61(11)	N(5)-Fe(1)-N(11)	170.21(11)
N(1)-Fe(1)-N(7)	165.93(11)	N(7)-Fe(1)-N(11)	93.82(11)
N(1)-Fe(1)-N(11)	91.15(11)	N(9)-Fe(1)-N(1)	96.38(11)
N(3)-Fe(1)-N(7)	90.21(11)	N(9)-Fe(1)-N(3)	165.48(11)
N(3)-Fe(1)-N(11)	90.08(11)	N(9)-Fe(1)-N(5)	100.37(11)
N(5)-Fe(1)-N(1)	98.56(10)	N(9)-Fe(1)-N(7)	97.56(11)
N(5)-Fe(1)-N(3)	93.30(10)	N(9)-Fe(1)-N(11)	77.23(11)
N(5)-Fe(1)-N(7)	77.00(10)		

Table S28 Selected least-squares planes data for $[Fe(\mathbf{L6})_3](BF_4)_2 \cdot (C_5H_{12}O)_{0.5} \cdot (C_2H_5N)_{0.5}$ (**7**).

Least-squares planes description	Max. deviation (Å)	Atom	Dihedral Angle (°)
Benzimidazole 1 C7 N1 C1 C2 C3 C4 C5 C6 N2	0.022	C3	8.7(1)
Pyrimidine 1 N3 C12 C11 C10 N4 C9	0.009	C10	
Benzimidazole 2 N5 C13 C14 C15 C16 C17 C18 N6 C19	0.034	C19	14.5(2)
Pyrimidine 2 N7 C24 C23 C22 N8 C21	0.009	C21	
Benzimidazole 3 N9 C25 C26 C27 C28 C29 C30 N10 C31	0.011	N9-C30	7.6(2)
Pyrimidine 3 N11 C33 N12 C34 C35 C36	0.013	C33	

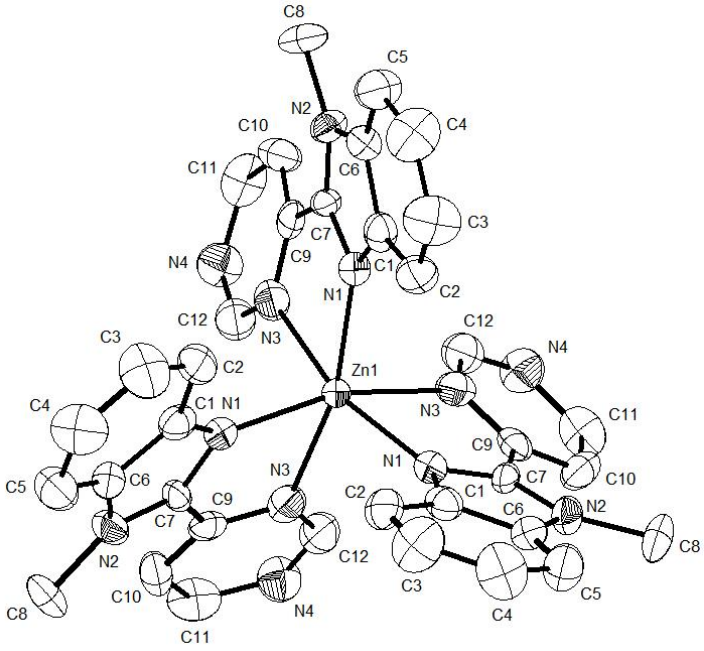

Figure S43 ORTEP view of *fac*-$[Zn(\mathbf{L7})_3]^{2+}$ cations in the crystal structures of $[Zn(\mathbf{L7})_3](ClO_4)_2$ (**8**) (ellipsoids are drawn at 40% probability) with numbering scheme. Hydrogen atoms and counter anions are omitted for clarity. The cation is located on a crystallographic threefold axis and near a twofold axis (therefore all ligands are disordered but the conformation stays facial).

Table S29 Selected bond distances (Å) and bond angles (°) of $[Zn(\mathbf{L7})_3](ClO_4)_2$ (**8**).

Bond Distances (Å)			
Zn(1)-N(1)	2.083(6)	Zn(1)-N(3)	2.307(13)
Bond Angles (°)			
N(1)-Zn(1)-N(3)			74.5(5)

Table S30 Selected least-squares planes data for $[Zn(\mathbf{L3})_3](ClO_4)_2$ (**8**).

Least-squares planes description	Max. deviation (Å)	Atom	Dihedral Angle (°)
Benzimidazole 1 N1 C1 C2 C3 C4 C5 N2 C6 C7	0.032	C1	20.2(4)
Pyrimidine 1 N3 C9 C10 C11 C12 N4	0.036	C11	

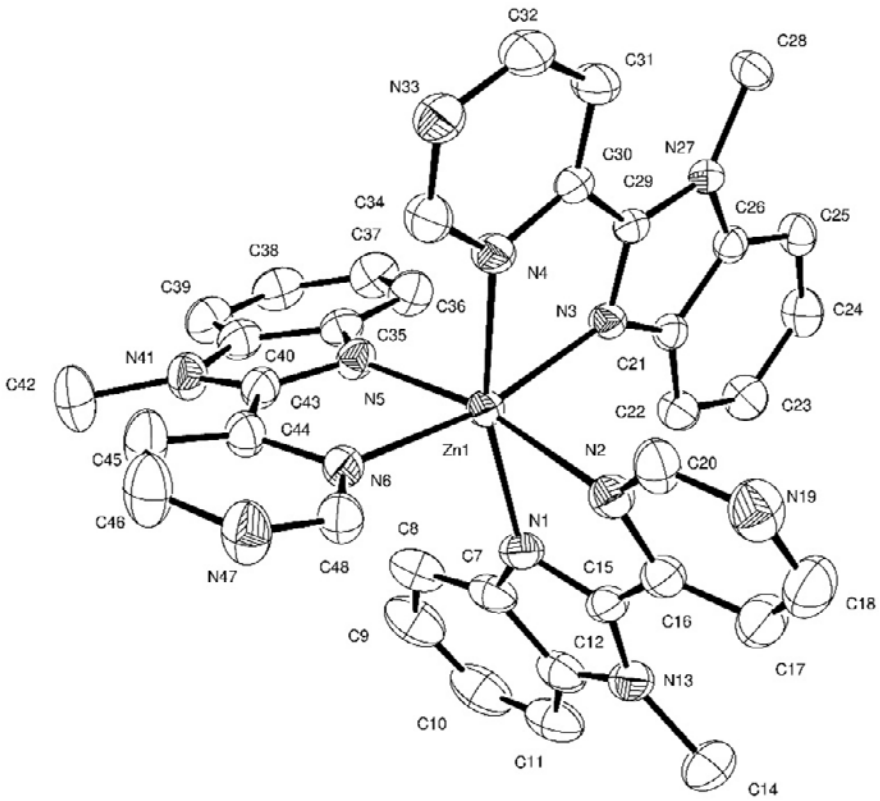

Figure S44 ORTEP view of *fac*-$[Zn(\mathbf{L7})_3]^{2+}$ cations in the crystal structure of $[Zn(\mathbf{L7})_3](PF_6)_2$ (**8**) (ellipsoids are drawn at 40% probability) with numbering scheme. Hydrogen atoms and counter anions are omitted for clarity.

Table S31 Selected bond distances (Å) and bond angles (°) of $[Zn(\mathbf{L7})_3](PF_6)_2$ (**9**).

Bond Distances (Å)			
Zn(1)-N(1)	2.084(2)	Zn(1)-N(4)	2.241(2)
Zn(1)-N(2)	2.334(2)	Zn(1)-N(5)	2.110(2)
Zn(1)-N(3)	2.108(2)	Zn(1)-N(6)	2.156(18) and 2.179(3)
Bond Angles (°)			
N(1)-Zn(1)-N(2)	74.77(9)	N(3)-Zn(1)-N(6)	165.79(11) and 172.1(9)
N(1)-Zn(1)-N(3)	96.24(8)	N(4)-Zn(1)-N(2)	90.42(8)
N(1)-Zn(1)-N(4)	163.37(9)	N(5)-Zn(1)-N(2)	167.61(8)
N(1)-Zn(1)-N(5)	101.13(9)	N(5)-Zn(1)-N(4)	94.89(9)
N(1)-Zn(1)-N(6)	97.96(12) and 91.4(9)	N(5)-Zn(1)-N(6)	76.57(12) and 75.5(8)
N(3)-Zn(1)-N(2)	90.94(8)	N(6)-Zn(1)-N(2)	92.28(12) and 92.8(8)
N(3)-Zn(1)-N(4)	76.12(8)	N(6)-Zn(1)-N(4)	90.01(11) and 96.9(9)
N(3)-Zn(1)-N(5)	101.19(8)		

Table S32 Selected least-squares planes data for $[Zn(\mathbf{L7})_3](PF_6)_2$ (**9**).

Least-squares planes description	Max. deviation (Å)	Atom	Dihedral Angle (°)
Benzimidazole 1 N1 C7 C8 C9 C10 C11 N13 C12 C15	0.035	N1	5.0(1)
Pyrimidine 1 N2 C20 N19 C18 C17 C16	0.027	N19	
Benzimidazole 2 N3 C21 C22 C23 C24 C25 C26 N27 C29	0.009	C23-25	4.68(9)
Pyrimidine 2 C30 C31 C32 N33 C34 N4	0.019	N4	
Benzimidazole 3 N5 C35 C36 C37 C38 C39 C40 N41 C43	0.02	C38-N5	21.2(1) and 15.8(3)
Pyrimidine 3 C44 C45 C46 N47 C48 N6	0.03 (N6A) 0.01(N6B)	N6A C48B	

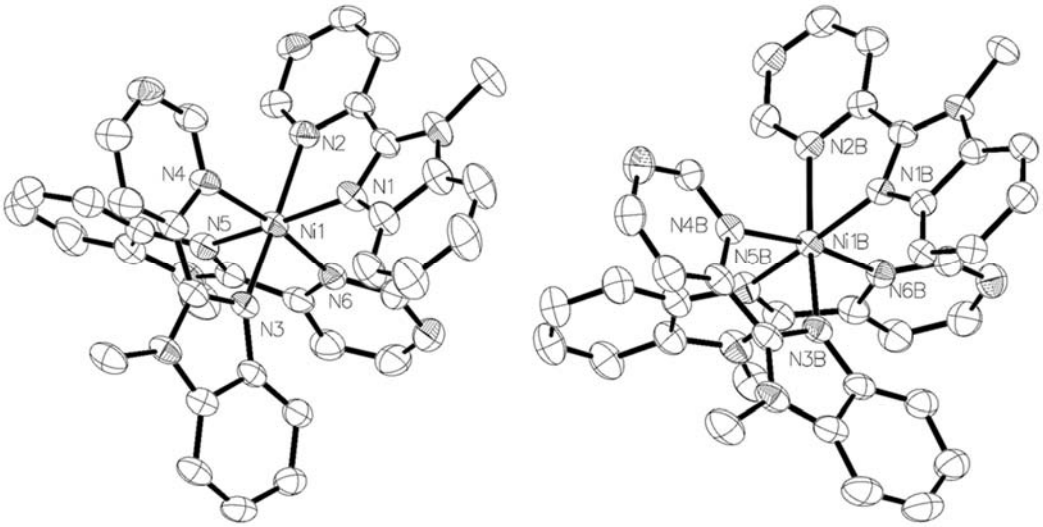

Figure S45 ORTEP view of *mer*-$[Ni(\mathbf{L7})_3]^{2+}$ cations in the crystal structure of $[Ni(\mathbf{L7})_3](PF_6)_{0.52}(ClO_4)_{1.48}$ (**10**) (ellipsoids are drawn at 50% probability) with numbering scheme. Hydrogen atoms and counter anions are omitted for clarity.

Table S33 Selected bond distances (Å) and bond angles (°) of $[Ni(\mathbf{L7})_3](PF_6)_{0.52}(ClO_4)_{1.48}$ (**10**)

Bond Distances (Å)			
Ni(1)-N(1)	2.047(2)	Ni(1B)-N(1B)	2.072(2)
Ni(1)-N(2)	2.119(2)	Ni(1B)-N(2B)	2.113(2)
Ni(1)-N(3)	2.064(2)	Ni(1B)-N(3B)	2.046(2)
Ni(1)-N(4)	2.110(2)	Ni(1B)-N(4B)	2.085(2)
Ni(1)-N(5)	2.090(2)	Ni(1B)-N(5B)	2.093(2)
Ni(1)-N(6)	2.116(2)	Ni(1B)-N(6B)	2.124(2)
Bond Angles (°)			
N(1)-Ni(1)-N(2)	77.69(10)	N(1B)-Ni(1B)-N(2B)	77.54(9)
N(1)-Ni(1)-N(3)	97.85(10)	N(1B)-Ni(1B)-N(4B)	93.79(9)
N(1)-Ni(1)-N(4)	91.61(10)	N(1B)-Ni(1B)-N(5B)	170.75(9)
N(1)-Ni(1)-N(5)	170.30(10)	N(1B)-Ni(1B)-N(6B)	95.65(9)
N(1)-Ni(1)-N(6)	95.55(10)	N(2B)-Ni(1B)-N(6B)	87.96(9)
N(3)-Ni(1)-N(2)	172.86(9)	N(3B)-Ni(1B)-N(1B)	92.66(9)
N(3)-Ni(1)-N(4)	78.14(9)	N(3B)-Ni(1B)-N(2B)	169.55(9)
N(3)-Ni(1)-N(5)	90.51(9)	N(3B)-Ni(1B)-N(4B)	78.68(10)
N(3)-Ni(1)-N(6)	96.58(9)	N(3B)-Ni(1B)-N(5B)	94.69(9)
N(4)-Ni(1)-N(2)	96.29(9)	N(3B)-Ni(1B)-N(6B)	96.72(9)
N(4)-Ni(1)-N(6)	171.64(9)	N(4B)-Ni(1B)-N(2B)	98.13(9)
N(5)-Ni(1)-N(2)	94.45(10)	N(4B)-Ni(1B)-N(5B)	93.15(9)
N(5)-Ni(1)-N(4)	94.93(10)	N(4B)-Ni(1B)-N(6B)	169.69(9)
N(5)-Ni(1)-N(6)	78.53(10)	N(5B)-Ni(1B)-N(2B)	95.43(9)
N(6)-Ni(1)-N(2)	89.45(9)	N(5B)-Ni(1B)-N(6B)	77.93(9)

Table S34 Selected least-squares planes data for $[Ni(\mathbf{L7})_3](PF_6)_{0.52}(ClO_4)_{1.48}$ (**10**).

Least-squares planes description	Max. deviation/Å	Atom	Dihedral Angle (°)
Benzimidazole 1 N1 C1 C2 C3 C4 C5 C6 N7 C8	0.024	C1	7.70(9)
Pyrimidine 1 N2 C12 N8 C11 C10 C9	0.015	C12	
Benzimidazole 2 N3 C13 C14 C15 C16 C17 C18 N9 C19	0.030	C16-18	9.68(10)
Pyrimidine 2 N4 C23 N10 C22 C21 C20	0.012	C23	
Benzimidazole 3 N5 C25 C26 C27 C28 C29 C30 N11 C32	0.037	N5	18.04(11)
Pyrimidine 3 N6 C36 N12 C35 C34 C33	0.029	C33	
Benzimidazole 1B N1B C8B N7B C6B C5B C4B C3B C2B C1B	0.032	C8B	13.01(8)
Pyrimidine 1B N2B C9B C10B C11B N8B C12B	0.015	C9B	
Benzimidazole 2B N3B C13B C14B C15B C16B C17B C18B N9B C19B	0.038	C19B	9.53(8)
Pyrimidine 2B N4B C23B N10B C22B C21B C20B	0.013	C20B	
Benzimidazole 3B N5B C25B C26B C27B C28B C29B C30B N11B C32B	0.014	C30B	4.74(9)
Pyrimidine 3B N6B C36B N12B C35B C34B C33B	0.025	C33B	

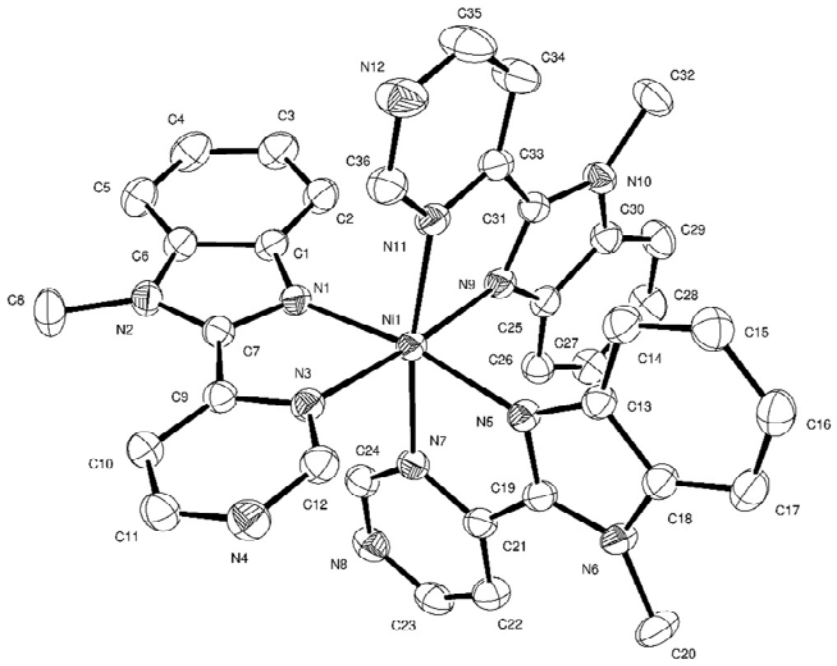

Figure S46 ORTEP view of *mer*-[Ni(**L7**)$_3$]$^{2+}$ cations in the crystal structure of [Ni(**L7**)$_3$](BF$_4$)$_2$·(CH$_3$OH)·(CH$_3$CN)$_{0.5}$ (**11**) (ellipsoids are drawn at 40% probability) with numbering scheme. Hydrogen atoms and counter anions are omitted for clarity.

Table S35 Selected bond distances (Å) and bond angles (°) of $[Ni(\mathbf{L7})_3](BF_4)_2\cdot(CH_3OH)\cdot(CH_3CN)_{0.5}$ (**11**).

Bond Distances (Å)			
Ni(1)-N(1)	2.0595(18)	Ni(1)-N(7)	2.0936(18)
Ni(1)-N(3)	2.1161(18)	Ni(1)-N(9)	2.0799(18)
Ni(1)-N(5)	2.0894(18)	Ni(1)-N(11)	2.0950(18)

Bond Angles (°)			
N(1)-Ni(1)-N(3)	78.13(7)	N(7)-Ni(1)-N(3)	89.05(7)
N(1)-Ni(1)-N(5)	170.87(7)	N(7)-Ni(1)-N(11)	170.89(7)
N(1)-Ni(1)-N(7)	94.79(7)	N(9)-Ni(1)-N(3)	175.31(7)
N(1)-Ni(1)-N(9)	98.11(7)	N(9)-Ni(1)-N(5)	88.61(7)
N(1)-Ni(1)-N(11)	91.91(7)	N(9)-Ni(1)-N(7)	94.08(7)
N(5)-Ni(1)-N(3)	95.44(7)	N(9)-Ni(1)-N(11)	78.84(7)
N(5)-Ni(1)-N(7)	78.49(7)	N(11)-Ni(1)-N(3)	98.38(7)
N(5)-Ni(1)-N(11)	95.46(7)		

Table S36 Selected least-squares planes data for $[Ni(\mathbf{L7})_3](BF_4)_2\cdot(CH_3OH)\cdot(CH_3CN)_{0.5}$ (**11**).

Least-squares planes description	Max. deviation/Å	Atom	Dihedral Angle (°)
Benzimidazole 1 C7 N1 C1 C2 C3 C4 C5 C6 N2	0.018	C3	10.09(9)
Pyrimidine 1 N3 C12 C11 C10 N4 C9	0.017	C9	
Benzimidazole 2 N5 C13 C14 C15 C16 C17 C18 N6 C19	0.022	C19	8.72(5)
Pyrimidine 2 N7 C24 C23 C22 N8 C21	0.014	C24	
Benzimidazole 3 N9 C25 C26 C27 C28 C29 C30 N10 C31	0.006	C26	7.52(8)
Pyrimidine 3 N11 C33 N12 C34 C35 C36	0.005	C36	

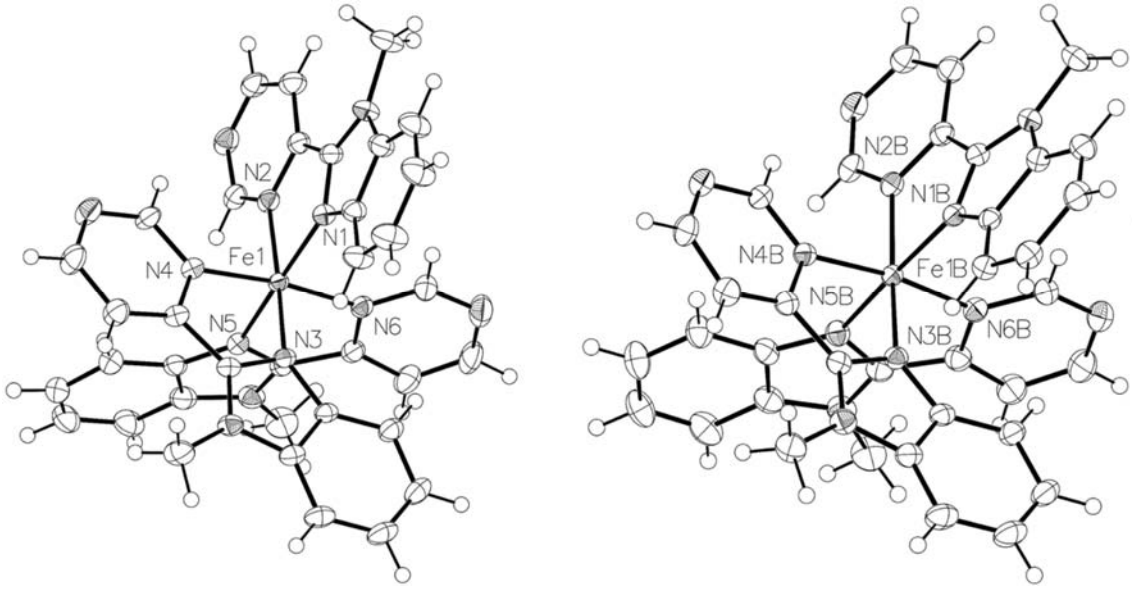

Figure S47 ORTEP view of the two different *mer*-$[Fe(\mathbf{L7})_3]^{2+}$ cations in the crystal structure of $[Fe(\mathbf{L7})_3](PF_6)(BF_4)\cdot CH_3OH$ (**12**) (ellipsoids are drawn at 50% probability) with numbering scheme. Hydrogen atoms and counter anions are omitted for clarity.

Table S37 Selected bond distances (Å) and bond angles (°) of [Fe(**L7**)$_3$](PF$_6$)(BF$_4$)·CH$_3$OH (**12**).

Bond Distances (Å)			
Fe(1)-N(1)	1.9645(16)	Fe(1B)-N(1B)	1.9715(16)
Fe(1)-N(2)	1.9970(16)	Fe(1B)-N(2B)	1.9799(16)
Fe(1)-N(3)	1.9791(16)	Fe(1B)-N(3B)	1.9635(16)
Fe(1)-N(4)	1.9828(16)	Fe(1B)-N(4B)	1.9655(16)
Fe(1)-N(5)	1.9892(16)	Fe(1B)-N(5B)	1.9950(16)
Fe(1)-N(6)	1.9970(16)	Fe(1B)-N(6B)	2.0026(16)
Bond Angles (°)			
N(1)-Fe(1)-N(2)	80.26(7)	N(1B)-Fe(1B)-N(2B)	80.75(6)
N(1)-Fe(1)-N(3)	96.78(7)	N(1B)-Fe(1B)-N(5B)	173.31(7)
N(1)-Fe(1)-N(4)	90.86(7)	N(1B)-Fe(1B)-N(6B)	94.14(7)
N(1)-Fe(1)-N(5)	172.11(7)	N(2B)-Fe(1B)-N(5B)	95.17(7)
N(1)-Fe(1)-N(6)	94.46(7)	N(2B)-Fe(1B)-N(6B)	88.38(7)
N(3)-Fe(1)-N(2)	174.91(7)	N(3B)-Fe(1B)-N(1B)	92.50(6)
N(3)-Fe(1)-N(5)	80.48(6)	N(3B)-Fe(1B)-N(2B)	172.74(6)
N(3)-Fe(1)-N(6)	89.82(6)	N(3B)-Fe(1B)-N(4B)	80.69(7)
N(4)-Fe(1)-N(2)	95.12(6)	N(3B)-Fe(1B)-N(5B)	91.80(7)
N(4)-Fe(1)-N(3)	95.36(6)	N(3B)-Fe(1B)-N(6B)	94.81(7)
N(4)-Fe(1)-N(5)	94.50(7)	N(4B)-Fe(1B)-N(1B)	92.26(6)
N(4)-Fe(1)-N(6)	173.48(6)	N(4B)-Fe(1B)-N(2B)	96.81(6)
N(5)-Fe(1)-N(2)	93.46(7)	N(4B)-Fe(1B)-N(5B)	93.49(7)
N(5)-Fe(1)-N(6)	80.60(7)	N(4B)-Fe(1B)-N(6B)	172.34(7)
N(6)-Fe(1)-N(2)	89.27(6)	N(5B)-Fe(1B)-N(6B)	80.39(7)

Table S38 Selected least-squares planes data for [Fe(**L7**)$_3$](PF$_6$)(BF$_4$)·CH$_3$OH (**12**).

Least-squares planes description	Max. deviation/Å	Atom	Dihedral Angle (°)
Benzimidazole 1 C8 N1 C1 C2 C3 C4 C5 C6 N7	0.03	C8	9.79(8)
Pyrimidine 1 C9 C10 C11 N8 C12 N2	0.02	N2	
Benzimidazole 2 C13 C14 C15 C16 C17 C18 N9 C19	0.03	C18	4.79(9)
Pyrimidine 2 N4 C20 C21 C22 N10 C23	0.01	C23	
Benzimidazole 3 N5 C25 C26 C27 C28 C29 C30 N11 C32	0.05	C27	15.53(10)
Pyrimidine 3 N6 C36 N12 C35 C34 C33	0.03	N6	
Benzimidazole 1B N1B C1B C2B C3B C4B C5B C6B N7B C8B	0.03	C8B	12.45(7)
Pyrimidine 1B C9B C10B C11B N8B C12B N2B	0.01	C9-N8B	
Benzimidazole 2B N3B C13B C14B C15B C16B C17B C18B N9B C19B	0.04	C19B	9.47(7)
Pyrimidine 2B N4B C23B N10B C22B C21B C20B	0.01	N4B	
Benzimidazole 3B N5B C32B N11B C30B C29B C28B C27B C26B C25B	0.01	C32B-C28B	6.21(8)
Pyrimidine 3B N6B C36B N12B C35B C34B C33B	0.02	C33B	

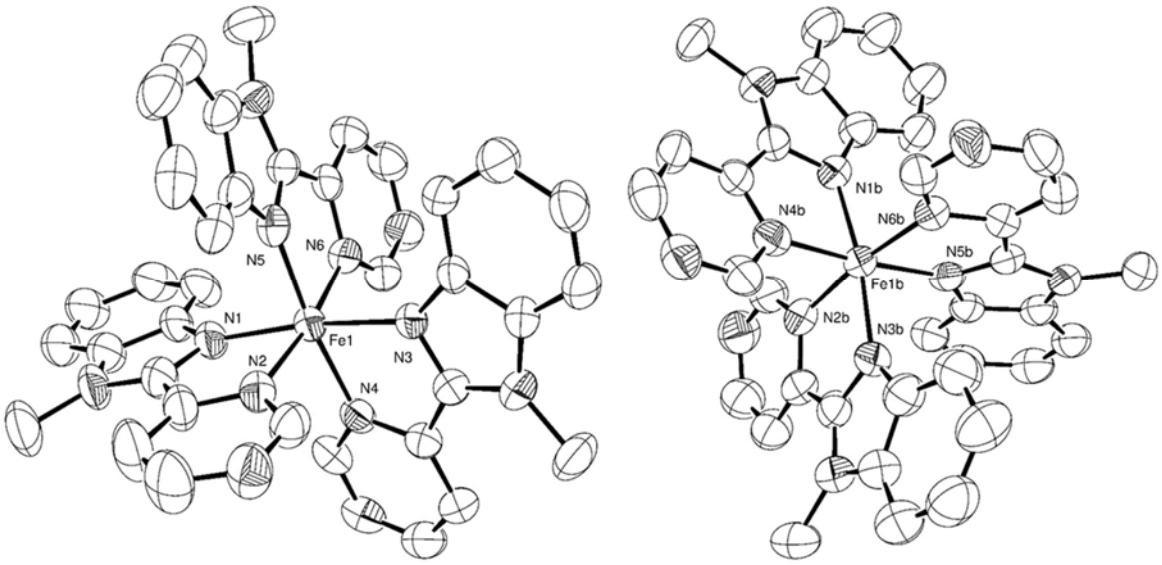

Figure S48 ORTEP view of the two different *mer*-$[Fe(\mathbf{L7})_3]^{2+}$ cations in the crystal structure of $[Fe(\mathbf{L7})_3](PF_6)_{1.72}(ClO_4)_{0.28}\cdot CH_3OH$ (**13**) (ellipsoids are drawn at 50% probability) with numbering scheme. Hydrogen atoms and counter anions are omitted for clarity.

Table S39 Selected bond distances (Å) and bond angles (°) of $[Fe(\mathbf{L7})_3](PF_6)_{1.72}(ClO_4)_{0.28}\cdot CH_3OH$ (**13**).

Bond Distances (Å)			
Fe(1)-N(1)	1.989(4)	Fe(1B)-N(1B)	1.950(4)
Fe(1)-N(2)	2.009(5)	Fe(1B)-N(2B)	2.015(5)
Fe(1)-N(3)	1.977(4)	Fe(1B)-N(3B)	1.991(5)
Fe(1)-N(4)	1.991(4)	Fe(1B)-N(4B)	2.008(5)
Fe(1)-N(5)	1.966(5)	Fe(1B)-N(5B)	1.983(5)
Fe(1)-N(6)	1.970(4)	Fe(1B)-N(6B)	1.995(5)

Bond Angles (°)			
N(1)-Fe(1)-N(2)	80.31(18)	N(1B)-Fe(1B)-N(2B)	94.02(19)
N(1)-Fe(1)-N(4)	95.27(18)	N(1B)-Fe(1B)-N(3B)	171.94(19)
N(3)-Fe(1)-N(1)	172.60(18)	N(1B)-Fe(1B)-N(4B)	80.12(19)
N(3)-Fe(1)-N(2)	93.71(18)	N(1B)-Fe(1B)-N(5B)	97.51(18)
N(3)-Fe(1)-N(4)	80.23(17)	N(1B)-Fe(1B)-N(6B)	91.10(19)
N(4)-Fe(1)-N(2)	89.37(18)	N(3B)-Fe(1B)-N(2B)	80.92(19)
N(5)-Fe(1)-N(1)	90.85(18)	N(3B)-Fe(1B)-N(4B)	93.58(19)
N(5)-Fe(1)-N(2)	94.54(19)	N(3B)-Fe(1B)-N(6B)	94.52(19)
N(5)-Fe(1)-N(3)	93.98(17)	N(4B)-Fe(1B)-N(2B)	90.53(19)
N(5)-Fe(1)-N(4)	173.22(17)	N(5B)-Fe(1B)-N(2B)	94.19(18)
N(5)-Fe(1)-N(6)	80.48(19)	N(5B)-Fe(1B)-N(3B)	89.16(18)
N(6)-Fe(1)-N(1)	93.79(18)	N(5B)-Fe(1B)-N(4B)	174.86(18)
N(6)-Fe(1)-N(2)	172.28(18)	N(5B)-Fe(1B)-N(6B)	80.09(19)
N(6)-Fe(1)-N(3)	92.54(17)	N(6B)-Fe(1B)-N(2B)	172.79(18)
N(6)-Fe(1)-N(4)	96.17(18)	N(6B)-Fe(1B)-N(4B)	95.35(19)

Table S40 Selected least-squares planes data for $[Fe(\mathbf{L7})_3](PF_6)_{1.72}(ClO_4)_{0.28}\cdot CH_3OH$ (**13**).

Least-squares planes description	Max. deviation/Å	Atom	Dihedral Angle (°)
Benzimidazole 1 N1 C1 C2 C3 C4 C5 C6 N7 C39	0.02	C4	7.5(2)
Pyrimidine 1 N2 C11 N8 C10 C9 C8	0.032	C8	
Benzimidazole 2 N3 C19 N9 C17 C16 C15 C14 C13 C12	0.02	C12-C19	9.8(2)
Pyrimidine 2 C20 C21 C22 N10 C23 N4	0.014	C22	
Benzimidazole 3 N5 C24 C25 C26 C27 C28 C29 N11 C31	0.038	C26	9.3(1)
Pyrimidine 3 C32 C33 C34 N12 C35 N6	0.005	C32	
Benzimidazole 1B C39B N1B C1B C2B C3B C4B C5B C6B N7B	0.025	C1B	8.03(16)
Pyrimidine 1B N4B C20B C21B C22B N10B C23B	0.02	N4B	
Benzimidazole 2B C19B N9B C17B C16B C15B C14B C13B C12B N3B	0.061	C14B	15.5(2)
Pyrimidine 2B N2B C11B N8B C10B C9B C8B	0.027	C8B	
Benzimidazole 3B C24B C25B C26B C27B C28B C29B N11B C31B	0.025	N5B	4.0(2)
Pyrimidine 3B N6B C32B C33B C34B N12B C35B	0.008	C34B	

Table S41 Structural data of complexes **1**-**7** incorporating ligand **L6** in the solid-state.[a]

	$[Zn(\mathbf{L6})_3](ClO_4)_2$ $(CH_3CN)_{2.5}$ (**1**)		$[Zn(\mathbf{L6})_3](BF_4)_2$. $(CH_3CN)_2$ (**2**)	$[Ni(\mathbf{L6})_3](ClO_4)_2$ (**3**)	$[Ni(\mathbf{L6})_3](ClO_4)_2$ CH_3CN (**4**)	$[Ni(\mathbf{L6})_3](BF_4)_2$ CH_3CN (**5**)	$[Fe(\mathbf{L6})_3](ClO_4)_2$ (**6**)	$[Fe(\mathbf{L6})_3](BF_4)_2$ $(C_5H_{12}O)_{0.5}$ $(C_2H5N)_{0.5}$(**7**)
T/ K	180		180	100	180	180	180	180
Crystal System	Triclinic		Triclinic	Triclinic	Monoclinic	Monoclinic	Triclinic	Triclinic
Configuration.	56% facial	44% meridional	facial	meridional	facial	facial	meridional	facial
d (M-N_{bz}) [b]	2.16(8)	2.04(6)	2.10(3)	2.04(7) [e]	2.069(7)	2.068(5)	2.03(3) [e]	2.09(2)
d (M-N_{py}) [c]	2.24(18)	2.33(9)	2.24(1)	2.15(8) [e]	2.11(2)	2.12(2)	2.06(5) [e]	2.148(5)
α / °	8.2(2.7)	6.4(3.5)	11.9(4.6)	8.2(5.5) [e]	11.6(4.5)	11.6(4.5)	7.2(3.9) [e]	10.3(3.7)
β / °	83.1(1.9)	83.7(1.6)	83.6(3.1)	88.0(1.4) [e]	86.6(1.2)	86. 9(1.5)	88.6(8) [e]	86.1(3.1)
γ / °	75.0(2.3)	74.6(1.6)	75.7(5)	78.3(9) [e]	78.4(2)	78.3(3)	83.3(5.7) [d]	77.0(4)
Octahedron [d]	3.13	3.126	1.91	1.377 [e]	1.142	1.15	1.067 [e]	1.443

[a] α = interannular intraligand angles, β = interchelate angles and γ = chelate bite angles. [b] bz= benzimidazole. [c] py= pyrimidine. [d] SHAPE's scores as compared to an ideal octahedron or trigonal prismatic geometry.[115] [e] Average value for more than two complexes in the asymmetric unit.

Table S42 Structural data of complexes **8**-**13** incorporating ligand **L7** in the solid-state.[a]

	$[Zn(\mathbf{L7})_3](ClO_4)_2$ (**8**)	$[Zn(\mathbf{L7})_3](PF_6)_2$ (**9**)	$[Ni(\mathbf{L7})_3](PF_6)_{0.52}(ClO_4)_{1.48}\cdot CH_3CN$ **(10)**	$[Ni(\mathbf{L7})_3](BF_4)_2CH_3OH(CH_3CN)_{0.5}$ (**11**)	$[Fe(\mathbf{L7})_3](PF_6)(BF_4)\ CH_3OH$ (**12**)	$[Fe(\mathbf{L7})_3](PF_6)_{1.72}(ClO_4)_{0.28}\ CH_3OH$ (**13**)
T /K	180	150	120	150	150	150
Crystal System	Trigonal	Monoclinic	Monoclinic	Triclinic	Monoclinic	Monoclinic
Configuration	facial	facial	meridional	meridional	meridional	meridional
d (M-N_{bz}) [b]	2.083(6)	2.101(14)	2.068(20) [e]	2.076(15)	1.980(12) [e]	1.975(15) [e]
d (M-N_{py}) [c]	2.307(13)	2.227(77)	2.111(13) [e]	2.101(12)	1.984(13) [e]	1.991(24) [e]
α / °	20.2(4)	10.4(7.8)	10.5(4.6) [e]	8.8(1.0)	9.8(4.0) [e]	9.0(3.8) [e]
β / °	83.8(3)	85.6(2.6)	89.9(1.7) [e]	88.7(4)	88.7(8) [e]	89.1(7) [e]
γ / °	74.5(3)	75.8(7)	78.1(5) [e]	78.5(4)	80.5(2) [e]	80.4(3) [e]
Octahedron [d]	2.131	1.727	1.143 [e]	1.040	0.706 [e]	0.727 [e]

[a] α = interannular intraligand angles, β = interchelate angles and γ = chelate bite angles. [b] bz= benzimidazole. [c] py= pyrimidine. [d] SHAPE's scores as compared to an ideal octahedron or trigonal prismatic geometry.[115] [e] Average value for more than two complexes in the asymmetric unit.

Table S43 Comparison of the structural data for hexa-coordinate Fe^{II} centers in the complexes $[Fe(\mathbf{L6})_3](ClO_4)_2$ (**6**) and $[Fe(\mathbf{L6})_3](BF_4)_2\cdot(C_5H_{12}O)_{0.5}\cdot(C_2H_5N)_{0.5}$ (**7**) in the solid-state at 100 K and 180 K.[a]

	mer-$[Fe(\mathbf{L6})_3](ClO_4)_2$		*fac*-$[Fe(\mathbf{L6})_3](BF_4)_2$	
T / K	100K	180K	100K	180K
Crystal System	Monoclinic	Triclinic	Triclinic	Triclinic
d (M-N_{bz})[b]	1.988(7)	2.03(3) [e]	1.99(2)	2.09(2)
d (M-N_{py})[c]	1.994(16)	2.06(5) [e]	1.99(1)	2.148(5)
α / °	7.4(4.7)	7.2(3.9) [e]	8.2(4.2)	10.3(3.7)
β / °	88.9(2)	88.58(82) [e]	88.8(7)	86.1(3.1)
γ / °	80.7(2)	83.3(5.7) [e]	80.4(2)	77.0(4)
Octahedron[d]	0.75	1.067 [e]	0.728	1.443

[a] α = interannular intraligand angles, β = interchelate angles and γ = chelate bite angles. [b] bz= benzimidazole. [c] py= pyrimidine. [d] SHAPE's scores as compared to an ideal octahedron or trigonal prismatic geometry.[115] [e] Average value for more than two complexes in the asymmetric unit.

Table S44 Crystal data, structure refinement and Fe-N distances for variable-temperature X-ray diffraction of [Fe(**L6**)$_3$](ClO$_4$)$_2$ (**6**) (heating rate 4K/min).

Temperature (K)	100.0(2)	130.0(1)	160.2(4)	170.2(3)	180.0(1)	190.1(2)	200.2(3)
Crystal system	Monoclinic	Monoclinic	Monoclinic	Triclinic	Triclinic	Triclinic	Triclinic
Space group	$P2_1/c$	$P2_1/c$	$P2_1/c$	P-1	P-1	P-1	P-1
Cell dimensions							
a (Å)	14.7997(4)	14.8156(2)	14.8371(4)	14.8301(10)	14.8446(7)	14.8537(5)	14.8683(5)
b (Å)	14.3249(4)	14.3681(3)	14.4044(4)	14.4509(8)	14.4714(7)	14.5135(7)	14.5298(6)
c (Å)	16.9540(4)	16.9875(3)	17.0101(4)	17.0059(9)	17.0415(6)	17.0261(8)	17.0382(8)
α (°)	90	90	90	90.327(5)	90.483(3)	89.144(4)	90.938(4)
β (°)	94.392(2)	94.4281(16)	94.413(2)	94.189(5)	94.246(3)	94.348(3)	94.310(3)
γ (°)	90	90	90	89.740(5)	89.407(4)	90.793(3)	89.116(3)
Volume (Å^3)	3583.77(16)	3605.35(12)	3624.60(16)	3634.7(4)	3650.5(3)	3659.2(3)	3669.5(3)
Z	4	4	4	4	4	4	4
d_{calc} (g/cm^3)	1.641	1.631	1.623	1.618	1.611	1.607	1.603
μ (mm^{-1})	5.385	5.352	5.324	5.309	5.286	5.274	5.259
Crystal size (mm^3)	0.272 x 0.245 x 0.171	0.277 x 0.231 x 0.202	0.272 x 0.245 x 0.171	0.272 x 0.245 x 0.171	0.357 x 0.22 x 0.194	0.277 x 0.231 x 0.202	0.277 x 0.231 x 0.202
θ range for data collection (°)	2.995 - 68.868	2.992 - 68.784-	2.987 - 68.748	2.605 - 68.962	2.600 - 69.000	2.603 - 69.354	2.601 - 69.276
Index ranges	-14≤h≤17, -16≤k≤17, -18≤l≤20	-17≤h≤13, -17≤k≤17, -20≤l≤19	-14≤h≤17, -16≤k≤17, -17≤l≤20	-14≤h≤17, -16≤k≤17, -17≤l≤20	-17≤h≤17, -17≤k≤16, -17≤l≤20	-14≤h≤17, -16≤k≤17, -20≤l≤20	-17≤h≤14, -16≤k≤17, -20≤l≤20
Nref collected	15691	15670	15821	16251	30197	29441	29431

Independent reflections / R_{int}	6510 / 0.0261	6587 / 0.0232	6588 / 0.0261	10644 / 0.0310	13344 / 0.0335	13340 / 0.0426	13379 / 0.0418
Completeness (to θ = 67.5°)°	99.4 %	99.9 %	99.4 %	80.4 %	99.8 %	99.6 %	99.6 %
Data / restraints / parameters	6510 / 0 / 535	6587 / 0 / 535	6588 / 0 / 535	10644 / 0 / 1072	13344 / 6 / 1073	13340 / 0 / 1062	13379 / 0 / 1097
GOF on F^2	1.051	1.040	1.046	1.060	1.041	1.055	1.044
R_1, wR_2 (I>2σ(I))	0.0506, 0.1361	0.0553, 0.1504	0.0623, 0.1708	0.0692, 0.1768	0.0754, 0.2104	0.0902, 0.2540	0.0891, 0.2501
R_1, wR_2 (all data)	0.0541, 0.1390	0.0592, 0.1544	0.0680, 0.1769	0.0796, 0.1863	0.0890, 0.2307	0.1049, 0.2694	0.1055, 0.2674
Largest diff. peak / hole (e-.$Å^{-3}$)	1.110 / -0.575	1.433 / -0.587	1.504 / -0.633	0.729 / -0.764	1.286 / -0.799	1.739 / -0.717	1.848 / -0.547
dFe – N (Å)							
Fe1 N1	1.985(3)	1.985(3)	1.991(3)	1.991(4)	1.995(4)	2.063(5)	1.993(5)
Fe1 N3	2.020(3)	2.024(3)	2.041(3)	2.060(5)	2.036(5)	2.194(6)	2.025(5)
Fe1 N5	1.982(2)	1.986(3)	1.999(3)	2.009(4)	2.009(4)	2.088(4)	2.002(5)
Fe1 N7	1.984(2)	1.994(3)	2.006(3)	1.997(4)	2.013(4)	2.124(5)	2.004(4)
Fe1 N9	1.999(3)	2.000(3)	2.009(3)	2.011(5)	2.012(4)	2.096(5)	2.004(5)
Fe1 N11	1.982(2)	1.988(3)	1.997(3)	1.998(4)	2.006(4)	2.114(5)	1.994(5)
Fe1B N1B				2.029(4)	2.065(4)	2.002(5)	2.101(4)
Fe1B N3B				2.098(5)	2.145(5)	2.026(5)	2.215(5)
Fe1B N5B				2.007(4)	2.043(4)	1.992(5)	2.083(5)
Fe1B N7B				2.039(4)	2.083(4)	2.007(5)	2.142(5)
Fe1B N9B				2.035(5)	2.068(5)	2.004(5)	2.110(5)
Fe1B N11B				2.023(5)	2.075(5)	1.994(5)	2.133(5)

Temperature (K)	210.2(4)	230.2(3)	240.2(3)	250.2(3)	265.2(3)	281(8)
Crystal system	Triclinic	Triclinic	Triclinic	Monoclinic	Monoclinic	Monoclinic
Space group	*P*-1	*P*-1	*P*-1	$P2_1/c$	$P2_1/c$	$P2_1/c$
Cell dimensions						
a (Å)	14.8681(9)	14.8989(6)	14.8958(7)	14.9289(3)	14.9377(4)	14.9848(3)
b (Å)	14.5584(8)	14.5767(7)	14.6045(7)	14.6273(4)	14.6510(4)	14.7075(3)
c (Å)	17.0585(9)	17.0816(8)	17.1060(6)	17.1269(3)	17.1339(4)	17.1641(3)
α (°)	90.879(4)	90.775(4)	90.341(3)	90	90°	90
β (°)	94.097(5)	94.220(3)	94.040(3)	94.0683(18)	94.087(2)	93.9532(15)
γ (°)	88.911(5)	89.272(3)	89.554(4)	90	90	90
V ($Å^3$)	3681.9(4)	3699.1(3)	3711.9(3)	3730.57(13)	3740.26(18)	3773.78(11)
Z	4	4	4	4	4	4
d_{calc} (g/cm^3)	1.597	1.590	1.584	1.577	1.572	1.558
μ (mm^{-1})	5.241	5.217	5.199	5.173	5.159	5.114
Crystal size	0.272 x 0.245 x 0.171	0.277 x 0.231 x 0.202	0.272 x 0.245 x 0.171	0.277 x 0.231 x 0.202	0.272 x 0.245 x 0.171	0.364 x 0.222 x 0.194
θ range for data collection (°)	2.597 - 68.903	2.594 - 69.417	2.590 - 69.101	2.968 - 68.777	2.966 - 68.969	2.956 - 68.760
Index ranges	-14<=h<=17, -16<=k<=17, -17<=l<=20	-18<=h<=14, -16<=k<=17, -20<=l<=20	-15<=h<=18, -16<=k<=17, -17<=l<=20	-17<=h<=14, -17<=k<=17, -20<=l<=19	-14<=h<=18, -16<=k<=17, -17<=l<=20	-17<=h<=17, -12<=k<=17, -13<=l<=20
Nref collected	16417	29803	16690	16305	14806	17075
Independent reflections / R_{int}	10747 / 0.034	13475 / 0.0424	10877 / 0.0309	6813 / 0.0256	6783 / 0.0323	6891 / 0.0187
Completeness (θ = 67.5°)	80.2 %	99.6 %	80.5 %	99.6 %	98.9 %	99.7 %
Data / restraints / parameters	10747 / 0 / 1097	13475 / 0 / 1097	10877 / 0 / 1097	6813 / 0 / 535	6783 / 0 / 535	6891 / 0 / 535

GOF on F^2	1.060	1.028	1.054	1.054	1.172	1.054
R_1, wR_2 ($I>2\sigma(I)$)	0.0870, 0.2370	0.0852, 0.2333	0.0688, 0.1868	0.0539, 0.1510	0.0730, 0.2093	0.0528, 0.1516
R_1, wR_2 (all data)	0.1041, 0.2576	0.1038, 0.2522	0.0854, 0.2028	0.0623, 0.1594	0.1008, 0.2793	0.0603, 0.1603
Largest diff. peak / hole ($e\text{-}.Å^{-3}$)	1.574 / -0.687	1.490 / -0.530	0.766 / -0.527	0.940 / -0.406	0.665 / -1.328	0.743 / -0.484
dFe – N (Å)						
Fe1 N1	1.999(5)	2.021(5)	2.051(4)	2.085(3)	2.067(5)	2.110(3)
Fe1 N3	2.040(6)	2.085(5)	2.159(5)	2.215(3)	2.237(5)	2.263(3)
Fe1 N5	2.013(5)	2.038(4)	2.069(4)	2.100(2)	2.097(4)	2.130(2)
Fe1 N7	1.994(5)	2.045(4)	2.088(4)	2.155(3)	2.167(5)	2.195(2)
Fe1 N9	2.012(6)	2.033(5)	2.069(5)	2.107(3)	2.120(5)	2.131(3)
Fe1 N11	1.991(5)	2.036(5)	2.074(5)	2.136(3)	2.155(5)	2.175(3)
Fe1B N1B	2.115(5)	2.111(4)	2.106(4)			
Fe1B N3B	2.243(6)	2.231(5)	2.223(5)			
Fe1B N5B	2.095(5)	2.084(5)	2.075(4)			
Fe1B N7B	2.156(5)	2.160(5)	2.152(4)			
Fe1B N9B	2.123(6)	2.119(5)	2.115(5)			
Fe1B N11B	2.142(6)	2.150(5)	2.134(5)			

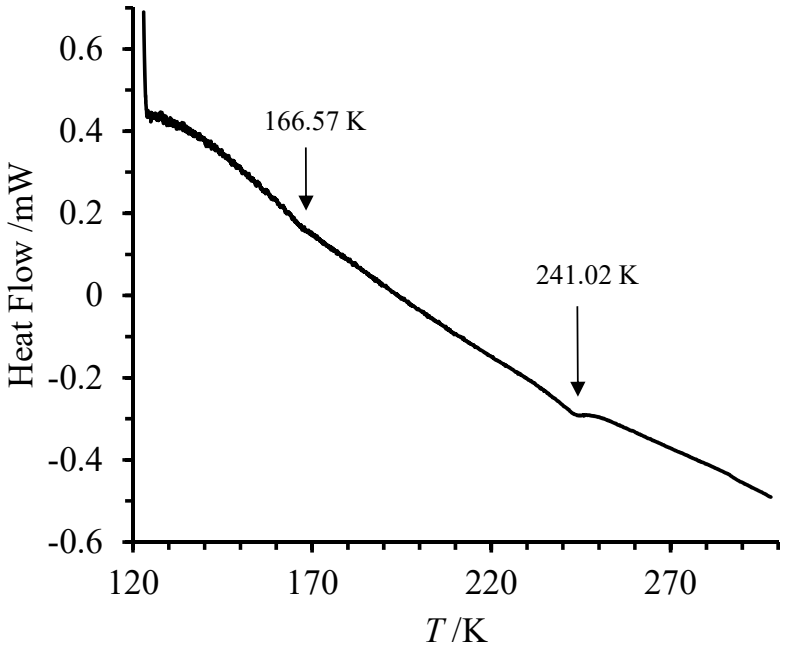

Figure S49 Differential scanning calorimetric (DSC) trace recorded for [Fe(**L6**)$_3$](ClO$_4$)$_2$ (**5**) under an inert atmosphere.

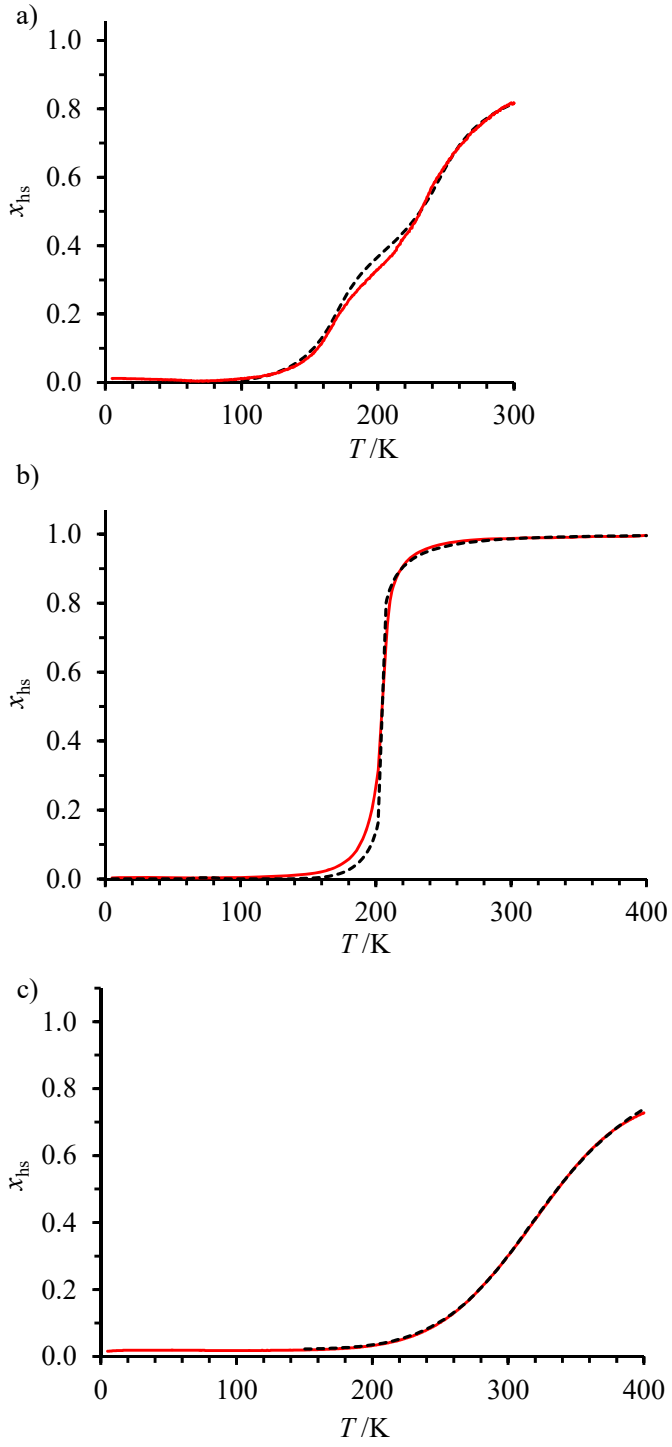

Figure S50 Plots of high-spin mole fractions (x_{hs}) versus temperature (T) between 5-300 K for a) [Fe(**L6**)$_3$](ClO$_4$)$_2$ (**6**, facial isomers) and 4-400 K for b) [Fe(**L6**)$_3$](BF$_4$)$_2$·(C$_5$H$_{12}$O)$_{0.5}$ (**7**, meridional isomers) and c) [Fe(**L7**)$_3$](PF$_6$)(BF$_4$)·CH$_3$OH (**12**, meridional isomers). The red points represents the experimentally measured values while the dashed black traces are built by using the fitted values of ΔH_{sco}, ΔS_{sco}, and γ (Table 4, see text).

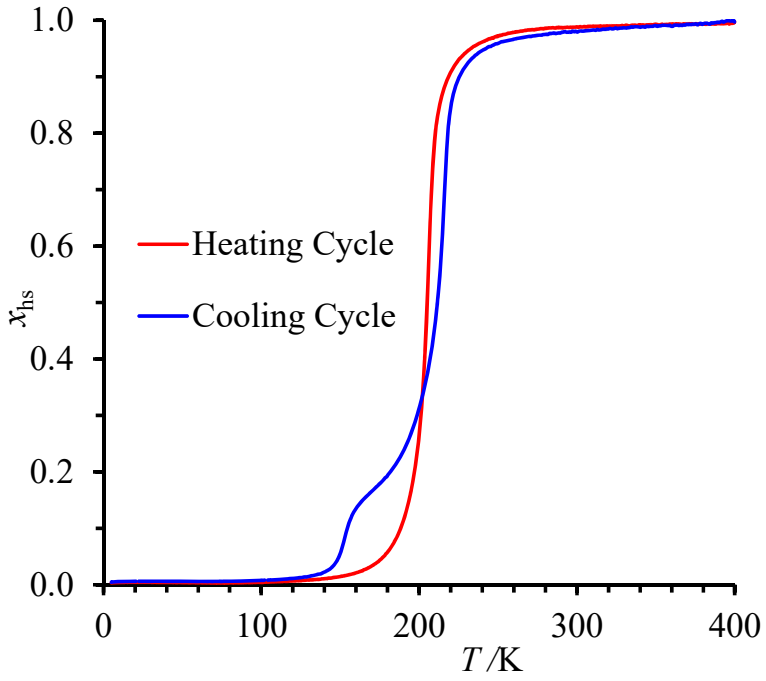

Figure S51 Plots of high-spin mole fractions (x_{hs}) versus temperature (T) in the 4-400 K range computed from the plots of molar paramagnetic susceptibility ($\chi_M T$) versus temperature (T) with eq. (17) for a complete heating/cooling cycle for [Fe(**L6**)$_3$](BF$_4$)$_2$·(C$_5$H$_{12}$O)$_{0.5}$ (**7**). The bump during the cooling cycle between 200-150 K is probably the result of the loss of interstitial tert-butyl-methylether during the heating process.